AD-A130 072 SCANNING STRATEGIES FOR NEXT GENERATION WEATHER RADARS 1/1
A STUDY BASED ON L..(U) NATIONAL OCEANIC AND
ATMOSPHERIC ADMINISTRATION NORMAN OK NAT..
UNCLASSIFIED P R MAHAPATRA ET AL. JUL 82 F/G 17/9 NL

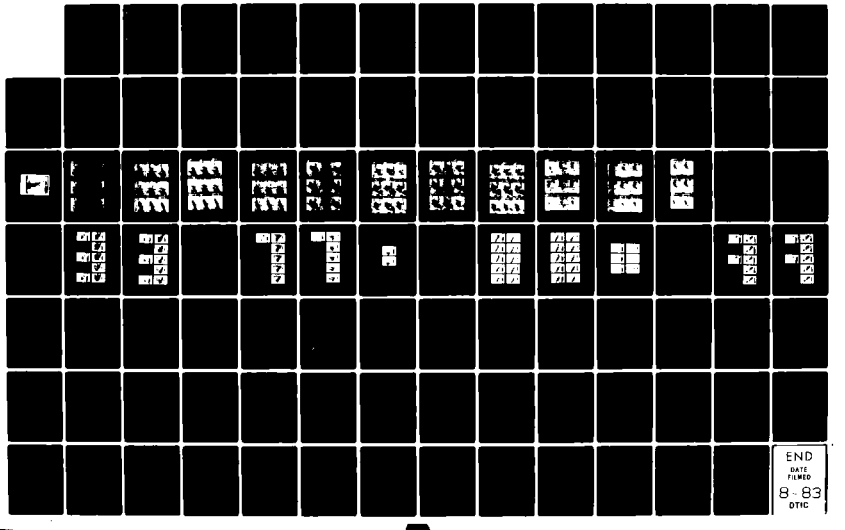

END
DATE FILMED
8-83
DTIC

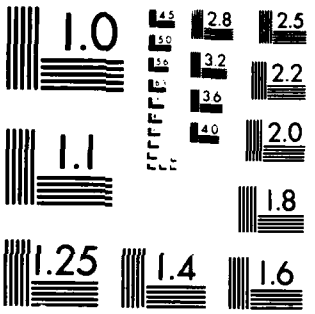

DOT/FAA/RD-82/69

Program Engineering &
Maintenance Service
Washington, D.C. 20591

Scanning Strategies for Next Generation Weather Radars

A Study Based on Lifetimes of Convective Atmospheric Phenomena Hazardous to Aviation

July 1982

Final Report

U.S. Department of Transportation
Federal Aviation Administration

NOTICE

This document is disseminated under the sponsorship of the Department of Transportation in the interest of information exchange. The United States Government assumes no liability for its contents or use thereof.

Technical Report Documentation Page

1. Report No.	2. Government Accession No.	3. Recipient's Catalog No.
DOT/FAA/RD-82/69	AD-A130 072	

4. Title and Subtitle	5. Report Date
Scanning Strategies for Next Generation Weather Radars A Study Based on Lifetimes of Convective Atmospheric Phenomena Hazardous to Aviation	July 1982
	6. Performing Organization Code RT0000
7. Author(s) P. R. Mahapatra and D. S. Zrnic'	8. Performing Organization Report No.
9. Performing Organization Name and Address U.S. Dept. of Commerce National Oceanic & Atmospheric Administration National Severe Storms Lab. 1313 Halley Circle, Norman, OK 73069	10. Work Unit No. (TRAIS)
	11. Contract or Grant No. DTFA01-80-Y-10524
12. Sponsoring Agency Name and Address U.S. Department of Transportation Federal Aviation Administration Systems Research and Development Service Washington, D.C. 20591	13. Type of Report and Period Covered Final Report
	14. Sponsoring Agency Code FAA/ARD-230

15. Supplementary Notes

Prepared under sections of FAA Interagency Agreement No. DTFA01-80-Y-10524 managed by the Surveillance Systems Branch, ARD-230.

16. Abstract

This report presents the methodology and results of a study to estimate the lifetimes of significant features in typical storm phenomena. These results are expected to help in deciding the scan strategy of NEXRAD radars. In particular, the question of the adequacy of a 5-minute information update rate for NEXRAD in its aviation weather surveillance role has been addressed. Two methods are used for the lifetime study: photo-interpretive and computer-based correlation. The basis and program steps of the correlation method are discussed. Several storms are studied using both methods. It is found that the storms studied contain no feature that might have been missed by a 5-minute scan cycle provided that data from all the three-moment fields (reflectivity, radial velocity, and Doppler spectrum width) at several elevations are utilized in the detection of hazardous phenomena.

17. Key Words	18. Distribution Statement
Lifetime of storm features Aviation weather surveillance Doppler weather radar NEXRAD Radar scan strategy	Document is available to the U.S. public through the National Technical Information Service, Springfield, Virginia 22151.

19. Security Classif. (of this report)	20. Security Classif. (of this page)	21. No. of Pages	22. Price
Unclassified	Unclassified	93	

Form DOT F 1700.7 (8-72) Reproduction of completed page authorized

METRIC CONVERSION FACTORS

Approximate Conversions to Metric Measures

Symbol	When You Know	Multiply by	To Find	Symbol
		LENGTH		
in	inches	*2.5	centimeters	cm
ft	feet	30	centimeters	cm
yd	yards	0.9	meters	m
mi	miles	1.6	kilometers	km
		AREA		
in^2	square inches	6.5	square centimeters	cm^2
ft^2	square feet	0.09	square meters	m^2
yd^2	square yards	0.8	square meters	m^2
mi^2	square miles	2.6	square kilometers	km^2
	acres	0.4	hectares	ha
		MASS (weight)		
oz	ounces	28	grams	g
lb	pounds	0.45	kilograms	kg
	short tons (2000 lb)	0.9	tonnes	t
		VOLUME		
tsp	teaspoons	5	milliliters	ml
Tbsp	tablespoons	15	milliliters	ml
fl oz	fluid ounces	30	milliliters	ml
c	cups	0.24	liters	l
pt	pints	0.47	liters	l
qt	quarts	0.96	liters	l
gal	gallons	3.8	liters	l
ft^3	cubic feet	0.03	cubic meters	m^3
yd^3	cubic yards	0.76	cubic meters	m^3
		TEMPERATURE (exact)		
°F	Fahrenheit temperature	5/9 (after subtracting 32)	Celsius temperature	°C

*1 in = 2.54 (exactly). For other exact conversions and more detailed tables, see NBS Misc. Publ. 286, Units of Weights and Measures, Price $2.25, SD Catalog No. C13.10:286.

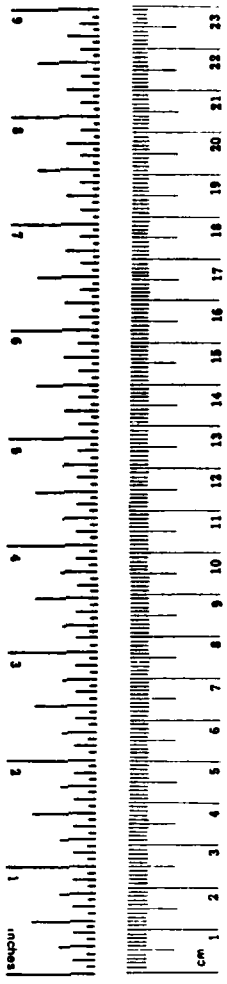

Approximate Conversions from Metric Measures

Symbol	When You Know	Multiply by	To Find	Symbol
		LENGTH		
mm	millimeters	0.04	inches	in
cm	centimeters	0.4	inches	in
m	meters	3.3	feet	ft
m	meters	1.1	yards	yd
km	kilometers	0.6	miles	mi
		AREA		
cm^2	square centimeters	0.16	square inches	in^2
m^2	square meters	1.2	square yards	yd^2
km^2	square kilometers	0.4	square miles	mi^2
ha	hectares (10,000 m^2)	2.5	acres	
		MASS (weight)		
g	grams	0.035	ounces	oz
kg	kilograms	2.2	pounds	lb
t	tonnes (1000 kg)	1.1	short tons	
		VOLUME		
ml	milliliters	0.03	fluid ounces	fl oz
l	liters	2.1	pints	pt
l	liters	1.06	quarts	qt
l	liters	0.26	gallons	gal
m^3	cubic meters	35	cubic feet	ft^3
m^3	cubic meters	1.3	cubic yards	yd^3
		TEMPERATURE (exact)		
°C	Celsius temperature	9/5 (then add 32)	Fahrenheit temperature	°F

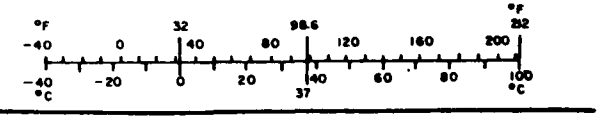

TABLE OF CONTENTS

List of Illustrations

LIST OF SYMBOLS

e_{max}	=	maximum elevation angle of the radar antenna during scan cycle
H_{max}	=	maximum height of radar observations
k	=	scalar constant
M	=	number of samples in each of the two sets being correlated
n	=	number of elevation steps in the scan cycle
r_b	=	largest radius of the blind zone
S	=	total scan time in seconds
ΔS	=	sum total of braking and reversal times at the end of each sector scan and transition times between scan levels
t	=	time
X	=	set of random numbers $\{x_i , i=1,....M\}$
Y	=	set of random numbers $\{y_i , i=1,....M\}$
$\bar{x}$	=	mean value of the set X
$\bar{y}$	=	mean value of the set Y
β	=	time-constant of the decay of the correlation coefficient with time
ρ_{xy}	=	correlation coefficient between two sets of random numbers x & y
$\rho_{xy}(o)$	=	value of correlation coefficient at t=o
$\rho_{xy}(o+)$	=	value of correlation coefficient just after the instant t=o
$\rho_{xy}(\infty)$	=	long-term or steady-state value of correlation coefficient
ψ	=	width of the scan sector in degrees
σ_x	=	standard deviation of the set of rendom numbers X
σ_y	=	standard deviation of the set of random numbers Y
ω	=	antenna rotation rate in degrees/sec

SCANNING STRATEGIES FOR NEXT GENERATION AIR WEATHER RADARS

A Study Based on Lifetimes of Convective Atmospheric Phenomena Hazardous to Aviation

Pravas R. Mahapatra and Dusan S. Zrnic'

1. Introduction

1.1 Weather Hazards to Aviation

There is a serious concern within the aviation community regarding the role of weather phenomena in the safety, accuracy, and economy of air navigation. In particular, the identification of atmospheric convection as a causal factor in aircraft accidents, though comparatively recent, is already receiving rapidly increasing attention, as evidenced by the large number of reports within the last decade which establish such a link [1]-[7]. Because of a higher level of understanding of weather phenomena, better monitoring instrumentation and an increased awareness of the hazard potential of atmospheric convection, many accidents, which in earlier times would have been attributed to pilot error, are now being recognized as weather-related events.

Although an average aircraft in flight spends a larger part of the time at cruise altitude than in takeoff or landing, it is only during the latter two phases that it is more vulnerable to the hazards of weather. This is because at cruise, aircraft have a wide margin above the stall speed and sufficient height to absorb any normal loss of altitude caused by sudden gusts or flight instabilities. Thus in dealing with weather hazards to flight, attention is focused essentially on areas in the vicinity of airport terminals. This does not, however, mean that en route areas should be left unobserved, since, although turbulence during cruise flight is seldom fatal, it can cause considerable discomfort.

Several classes of atmospheric phenomena are potentially hazardous to aviation. On the top of this list are thunderstorms which are usually accompanied by precipitation and turbulence. Heavy precipitation in the form of rain has the dual effect of reducing visibility and affecting the thrust of aircraft jet engines by interfering with combustion. When the precipitation is in the form of hail, its impact may physically damage the aircraft structure. Turbulence induces forces in the aircraft which are randomly time-varying in both magnitude and direction. It causes flights to be "rough" and may induce instabilities

leading to accidents. Of particular concern is the component of induced force occurring at or close to the aircrafts' fugoid frequency (i.e., the frequency at which a solid body moving in a fluid oscillates about its equilibrium path).

Another class of potentially hazardous convective phenomena consists of downdrafts and gust fronts. This class is characterized by the presence of wind shear which may be quite strong. Precipitation may or may not be present: the latter case deserves closer attention since the hazard potential may not be apparent on visual observation. Strong shears endanger aircraft flight by inducing rapid changes in the lift force. Low-level shear is very important in this context since rapid changes in lift are more hazardous when occurring closer to ground than at higher levels.

1.2 Radar Detection of Hazardous Weather

Detection and recognition of atmospheric processes that are potentially hazardous to flight is the starting point of a successful drive to minimize weather-related aircraft accidents, delays, and other inconveniences. In-situ measurements such as those using anemometers and rain gages are not advantageous for this task because 1) such measurement does not provide any prediction capability, i.e., a phenomenon cannot be detected until it reaches the site of the instruments, 2) only the part of the phenomenon at or near the ground level can be monitored. Higher level winds and turbulence cannot be measured.

Remote sensing the atmosphere using a weather radar minimizes both the above limitations. A conventional weather radar provides a volume coverage of precipitation out to a range of a few hundred kilometers. If the radar has coherent measurement or "Doppler" capability [8], then the radial components of windspeed and turbulence and/or shear can be observed in addition to reflectivity (which corresponds to intensity of precipitation) over the observation volume.

For several well-known reasons a weather radar must operate in a pencil-beam mode. Beamwidths usually employed are of the order of a degree. For wider coverage, the beam must scan the volume of space which is to be observed. The usual scanning scheme, and one that will most likely be adopted for NEXRAD, consists of rotating the antenna continuously in azimuth over the desired sector (or full circle) and discretely incrementing the elevation between the successive azimuth scans. The parameters defining such a scan cycle are the azimuth limits of the scan sector, angular speed of the antenna in azimuth, elevation increments and the highest elevation angle to be covered. The considerations for deciding these parameters are discussed in the following section.

1.3 Constraints on the Scan Cycle

Several considerations, practical as well as theoretical, impose constraints on the scan cycle of a weather radar. A proper understanding of these factors is necessary for deciding a scan strategy for NEXRAD radars in their role as detectors of convective phenomena hazardous to aviation.

The limits of the azimuth sector to be scanned by a weather radar are decided by the requirement that the sector must cover the area or phenomenon of interest. For general weather monitoring, such as that conducted by the National Weather Service, the azimuth scan usually covers a full circle. To observe specific areas, such as an air terminal area, or specific features, such as a mesoc[illegible]e, from a distant point, a sector scan may be sufficient. The NEXRAD system, [illegible]ch is being designed with a broad weather application in mind, is expected [illegible] have a full circular scan at most installations. Thus, although in specif[illegible]uations a sector scan may be advantageous, a circular scan is assumed for the p[illegible]pose of the present study.

The elevation increments are constrained by the spatial sampling requirements at maximum range. This, in turn, is governed by the vertical structure of the phenomena of interest. In the present context, the spatial sampling should be fine enough so as not to miss hazardous phenomena through undersampling. The incremental elevation need not be constant over the entire elevation interval, but may be varied to suit the vertical scale of features at different altitudes and the fact that a feature of a given size subtends a larger angle at closer ranges. Such variations may also be introduced to keep the scan cycle time within reasonable limits.

The highest elevation to be covered by a weather radar depends on the maximum height to which hazardous phenomena must be observed and the minimum range at which such observation must be made. The former can be determined by studying various types of convective phenomena and determining the maximum height up to which hazardous levels of air currents, turbulence or precipitation may occur. The minimum range at which storms should be "topped" is a matter of choice and compromise. It would be ideal to be able to observe the tops of storms down to near-zero range, but the resulting hemispherical scan volume would require a long scanning time. It is customary to limit the highest elevation angle to a value much less than 90 degrees and accept a certain "blind zone" as a consequence. The largest radius of the blind zone, r_b, is given as (Fig. 1)

$$r_b = H_{max} \operatorname{ctn} e_{max} \qquad (1)$$

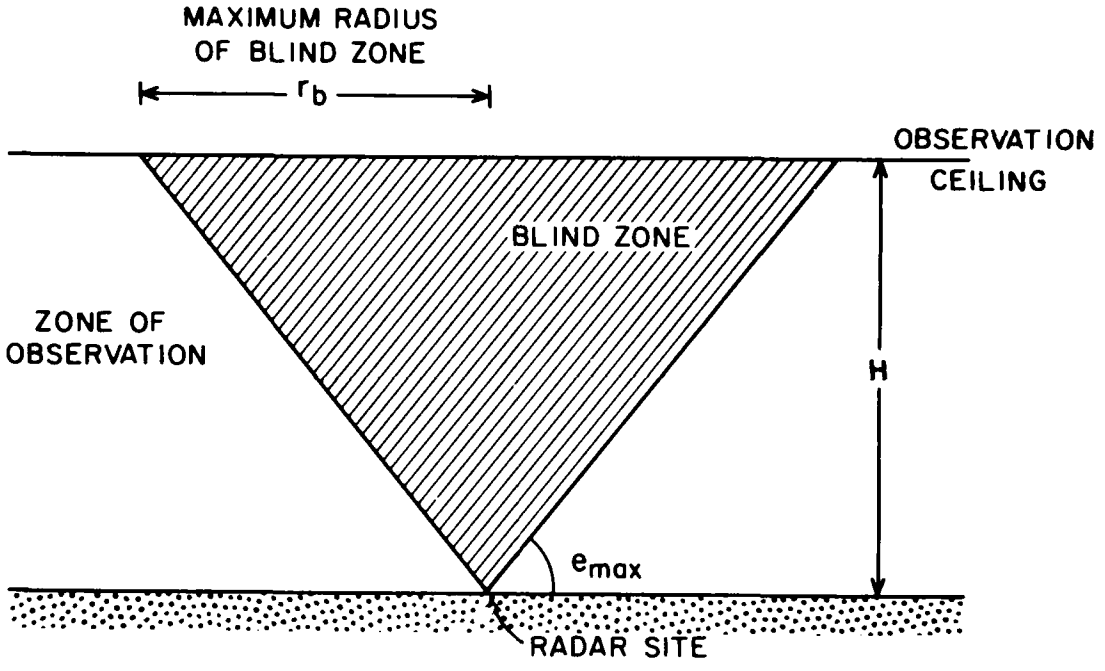

Figure 1 Geometry of radar blind zone.

where H_{max} = maximum height to be observed

e_{max} = highest elevation angle of radar antenna.

More discussion about scanning time follows in a later paragraph.

The angular speed of the antenna in azimuth is a more complex parameter to determine than the previous three. The rotational speed is based on several considerations:

1. Mechanical: The motor drive and control gear tend to be more expensive for a given antenna size as the rotational speed increases. Also, there is a higher energy requirement and reduced bearing life at higher speeds. Thus from a purely mechanical viewpoint, a slower antenna speed is preferable.
2. Signal Processing: Coherent signal processing requires the returns from more than one transmitted pulse for estimating mean velocity and spectral width. The estimation accuracy of spectral moments increases monotonically with the number of samples processed [9]. Typically 64, 128, or 256 samples are used for moment estimation, the higher numbers being necessary under very poor signal-to-noise situations, especially if ground clutter interference is severe, requiring extensive filtering. Antenna rotation during the period of sample collection causes an effective broadening of the beam pattern [10], resulting in "blurring" or loss of resolution. For a given speed of rotation, the lower the number of samples, the less would be the blurring. Alternatively, given a certain degradation in resolution, the more the number of samples to be processed, the slower must be the antenna rotation. Thus, weaker weather targets, such as clear air phenomena, would favor a slower scanning speed. Also, slow scan would be required at very low elevation angles where ground clutter causes strong interference.

   An important signal processing aspect favoring slow scan is the broadening of ground clutter spectrum due to antenna rotation. Nearly all efficient frequency domain filtering techniques to remove ground clutter [11], [12] are based on the premise that the clutter spectrum is confined to a very narrow band centered on the zero-frequency line, whereas weather echoes are centered at mean Doppler frequencies which are typically removed from zero. In such a case, the clutter filter is of a band-rejection type with a deep notch coinciding with the d.c. line. If the above premise is not true, i.e., if clutter has appreciable

bandwidth, then the filter notch, which would have to be much wider than the clutter spectrum to minimize the leakage of the "skirts" of the spectrum (Fig. 2), would block significant amounts of information from the weather spectrum.

If the ground clutter is quasi-stationary and the radar has a non-rotating antenna and a stable transmitter, then the clutter spectrum in the baseband should ideally be a spike located on the d.c. line. All other factors remaining unchanged, if the antenna now starts rotating, then the clutter return from each scatterer would be modulated by the beam pattern. As the antenna rotates faster, the temporal width of the modulation would decrease, resulting in larger frequency spread, and a corresponding increase in clutter leakage through the filter. Thus the consideration of clutter spectral spread also favors a slow rate of antenna scan.

3. Data Update Rate: During the time taken by the radar antenna to complete a cycle of scan, spectral moments of each resolution cell is obtained once. This assumes that signal processing is done in real time. The longer the scan period of a radar, the larger is the interval at which the meteorological status of the scan volume is sampled, i.e., the slower is the data update rate. However, sampling the weather data should not be so slow that atmospheric features may grow to potentially hazardous levels and/or decay out of existence in the period between scans.

The total scan time depends on the width of the sector being scanned, the scan rate and the number of elevation steps in the scan cycle:

$$S = \frac{\psi n}{\omega} + \Delta S \qquad (2)$$

where S = total scan time in seconds

ψ = scan sector width in degrees

ω = antenna rotation rate in degrees/second

n = number of elevation steps in the scan cycle

ΔS = sum total of braking and reversal times at the end of each sector scan and transition times between scan levels.

If the azimuth scan is over a full circle, as is usually the case with weather surveillance, ψ equals 360 and then the scan time depends only on the angular scan rate and the number of scan levels:

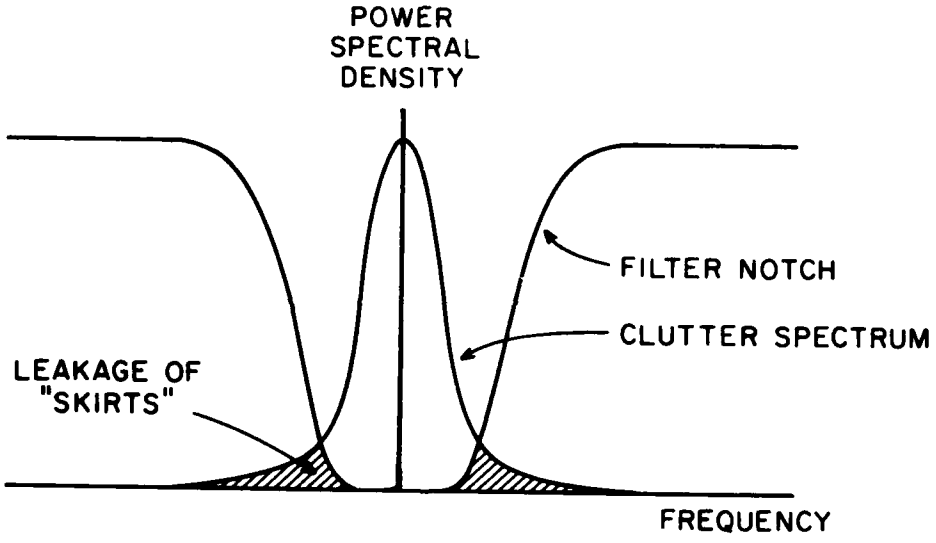

Figure 2 Schematic showing clutter leakage through notch filter.

$$S = \frac{360n}{\omega} + \Delta S \qquad (3)$$

If the scan time is decided from external considerations such as the properties of the weather field, a slow scan rate would force the number of scan levels to be reduced, which makes the spatial sampling coarse. To achieve a finer spatial sampling, a higher scan rate must be employed.

The various influences on scan rate and cycle time may be summarized as follows: There are overwhelming system considerations in a weather radar to favor a slow scanning rate. The major factors forcing a speeding up of the scanning process come from the characteristics of the phenomena that must be monitored. In view of the advantages of slow scanning, the data update rate in an air weather surveillance radar need be no faster than that dictated by the temporal and spatial parameters of hazardous atmospheric features.

The last statement establishes a need for a thorough study of the lifetimes of hazardous atmospheric phenomena. Lifetime may be defined as the time scale associated with the growth and decay of, or major changes in, an atmospheric feature of interest. This report evolves the methodology and studies the lifetimes of typical storm phenomena based on Doppler radar data collected at National Severe Storms Laboratory (NSSL), Norman, Oklahoma.

A discussion on the current thinking regarding the NEXRAD scan cycle is in order here. The NEXRAD project proposal [20] specifies a maximum scan rate of 30°/sec (corresponding to 5 RPM), but leaves the question of scan pattern open to later programming on an automatic or manual basis. As a specific scanning scheme, a full-volume scan every 5 minutes is a consensus in the NEXRAD community. However, FAA is proposing a faster data update rate - once every 2.5 minutes - to guard against the possibility that there may be convective phenomena that appear so suddenly or grow so fast that they may reach hazardous proportions during the interscan period and thus have a chance of going undetected until they cause damage to aircraft. On this point, FAA requirements are somewhat in conflict with those of the other sponsors of the NEXRAD program. This problem can be resolved only through a systematic study of small-scale convective phenomena with the aim to discover if indeed there are potentially hazardous weather features that have a significant probability of escaping detection if a 5-minute scan cycle is employed. This specific question receives continual attention in this report.

1.4 Previous Studies on Lifetime

Attempts have been made in the past, e.g., [13], to study lifetimes of weather features by using radar observations, but they have usually relied only on reflectivity data for this purpose. This is because operational weather radars and most research weather radars have little capability beyond the measurement of intensity of echo return from particular resolution cells. NSSL has built up and implemented a unique coherent signal processing scheme by which the signals collected by a 10-cm Doppler radar are processed in real time to yield reflectivity (precipitation), velocity (wind speeds, large scale shear) and spectral width (small scale shear and turbulence) data over the entire area of observation, which can be recorded and/or displayed simultaneously in color-coded contour displays. It is thus possible to analyze more aspects of a weather feature than earlier studies.

A natural quantitative way to determine the lifetime of an atmospheric feature would be to subject the data on a suitable parameter of the feature to a spatial correlation with varying time lags. This technique has been applied in the past typically for studying internal motions within storm fields [14], [15], and for determining statistical properties of weather echoes [16]. At NSSL this method has been developed through the MS dissertation of GLenn Smythe [17] and has been applied to the study of clear air turbulence to show that the time decay of the correlation function follows the 2/3 power law in accordance with Chandrasekhar's theory of turbulence.

Limited results of the correlation method, applied to lifetime studies, are already available [15, 17] at NSSL and are summarized in Figs. 3 and 4. These results indicate the feasibility of using the correlation method for lifetime estimation. Recently the correlation algorithm has been refined and adapted to include multimoment data, and variable feature size and number.

Earlier results available at NSSL also include data on persistence of gust fronts. These data seem to indicate that gust fronts have a fairly high order of stability (>40 minutes) and hence have little danger of being missed in any practical scan cycle. Attention is therefore focused in this report on the lifetime of thunderstorms which are hazardous phenomena of most frequent occurrence and are capable of containing features with fast growth and decay.

1.5 Organization of the Report

Two methods of lifetime estimation are used for the current study: photo-interpretive and computational. The next chapter outlines the NSSL Doppler facility and the database utilized for both methods of study. The photo-interpretive

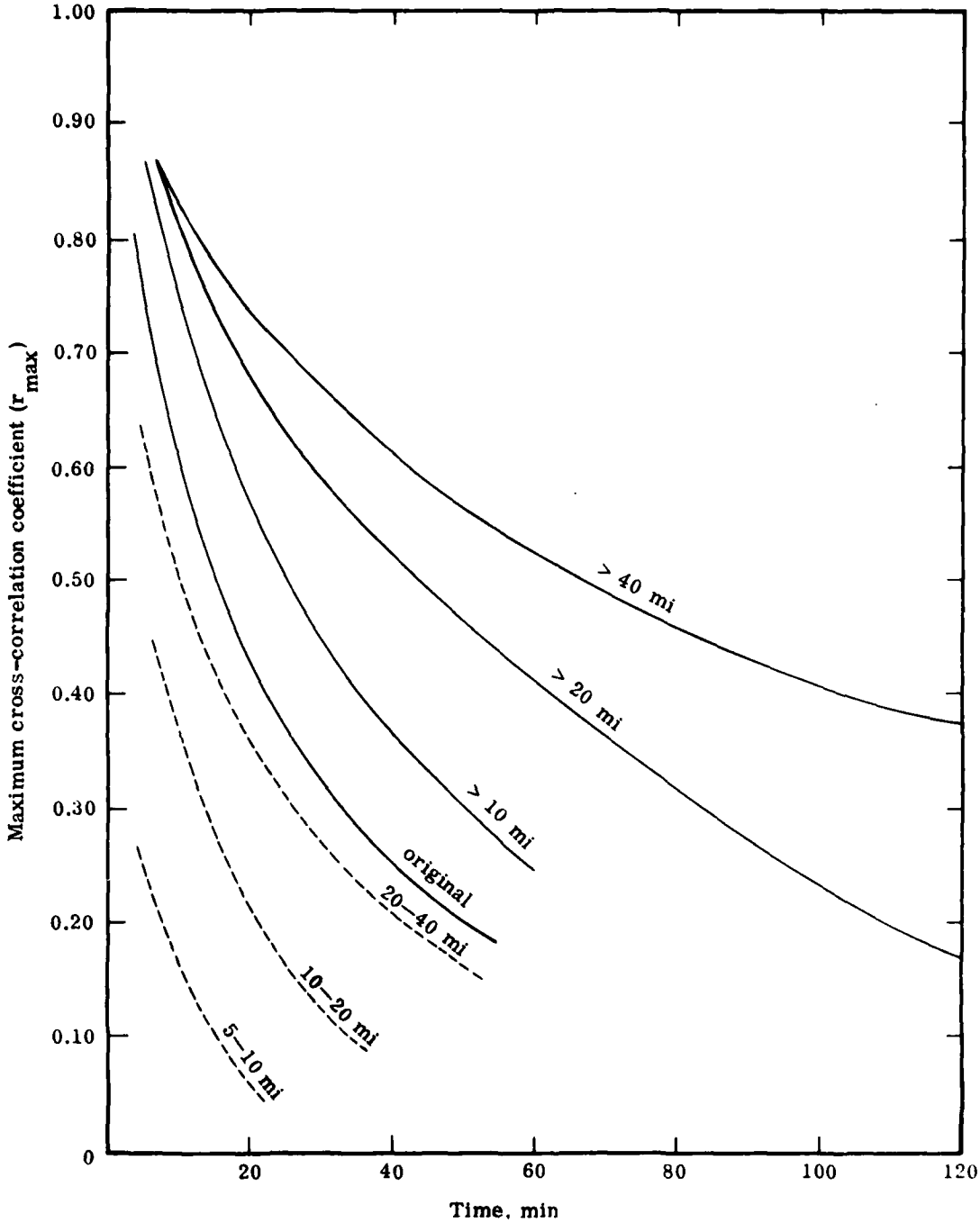

Figure 3 *Stability of features of different scale sizes. The curve marked "original" represents the correlation decay of the original, unfiltered field. For the other solid lines, data were low-pass filtered to eliminate scale sizes smaller than the indicated values. The dashed curves are generated from band-pass filtered data, and the range of numbers indicate scale sizes retained after filtering.*

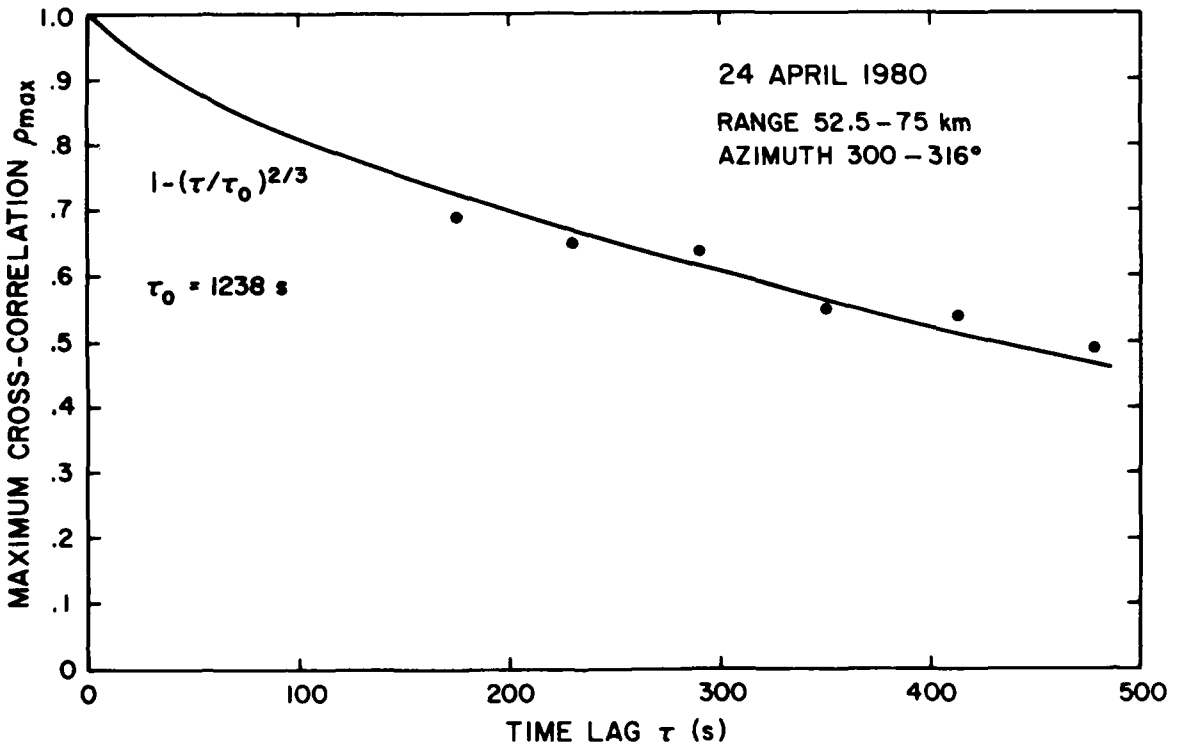

Figure 4 *Stability of a large segment of the velocity field of the storm of April 24, 1980.*

observation of five different storms is reported in Chapter 3 and the basis and results of the correlation procedure are provided in Chapter 4. The last chapter summarizes the major finding of the report, discusses the limitations of the current study and provides suggestions for further work.

Ample photographic and computational data are provided to support the points brought out in this report. The photographs for one storm include all the three spectral moments--reflectivity, radial velocity, and spectrum width--the other storms have been illustrated only by the reflectivity and spectrum width fields.

To understand the nature of the problem and to get a quick idea of the findings of the study, it is enough to see sections 1.3, 3.4, 4.3, and 5.1. The remaining parts of the report contain details that may permit separate conclusions or be used in other studies along allied lines.

2. Database for the Study

2.1 NSSL Doppler Facility

National Severe Storms Laboratory operates two Doppler radars, located at Norman and Cimarron in Oklahoma. For the purpose of this study, data from only the Norman radar are used. The principal parameters of the Norman Doppler radar are given in Table I. Of interest in this study is the pulse-pair mode of operation

TABLE I CHARACTERISTICS OF NORMAN DOPPLER RADAR

Antenna	
Half-Power Beamwidth	0.81 deg
Gain	46.8 dB
First Side Lobe Level	21 dB
Polarization	Vertical
Transmitter	
Wavelength	10.22 cm
Pulse Repetition Time	768/922/1075/1229 μs
Pulse Width	1 μsec (150 m)
Peak Power	750 kW
Receiver	
System Noise Figure	3.3 dB
Transfer Function	Doppler - linear; Intensity - logarithmic
Dynamic Range	70 dB
Bandwidth (3 dB)	1.2 MHz
Min. Detectable Signal (S/N=1)	-108 dBm
Data Acquisition	
Time Series	16 range gates
Pulse Pair (Hardwired)	Reflectivity, radial velocity and Doppler spectrum width based on 32, 64, 128 or 256 samples.

in which three spectral moments, namely reflectivity, mean velocity and spectrum width, are computed for each resolution cell in the scan volume. The block diagram of the radar receiver and signal processor, including the display, are shown in Fig. 5. The pulse-pair spectral moment estimator is hardwired. The control, comparison and decision functions, including the display control, are presently being performed by a Ling computer, but are scheduled to be transferred to a much more powerful Interdata real-time computer with array processing facility which will substantially increase the capacity for complex on-line signal processing and data handling.

The data used for the present study is stored on 7-track magnetic tapes in BCD format. The tapes contain the three spectral moments, in addition to time and other housekeeping information. The data processing for lifetime estimation discussed later in this report is done off-line based on raw data from these tapes.

2.2 Method of Data Collection

Bulk of the data collection at NSSL is carried out during the spring season when the central American plains, and in particular the area surrounding the NSSL radars, is meteorologically very active. The spring program extends about three months during which the data collection team remains on special alert to monitor atmospheric phenomena during any part of the day. However, since it is expensive as well as strenuous on the part of the crew to keep the radar and data system operating all the time during the program, the system operation is based on the most accurate weather forecast available to the team. Since phenomena of scale sizes of interest to aircraft safety are usually too small for accurate prediction over any significant length of time, the radar usually starts observing them only after they begin to appear on the scene. In this process the period of growth of the phenomena is quite often missed. This is a limitation of the data collection process.

The present study on lifetime determination was started at NSSL fairly recently and data specifically tailored for lifetime estimation have been collected during the spring programs of 1980 and 1981. During 1980, the scan pattern shown in Fig. 6(a) was used for lifetime data collection. However, certain data processing difficulties were experienced because of the odd number (three in this case) of scan levels, and the scan pattern was modified to that shown in Fig. 6(b) during the spring program of 1981. This provides data for lifetime determination at four levels whose heights above the ground depend on the distance of the storm feature from the radar.

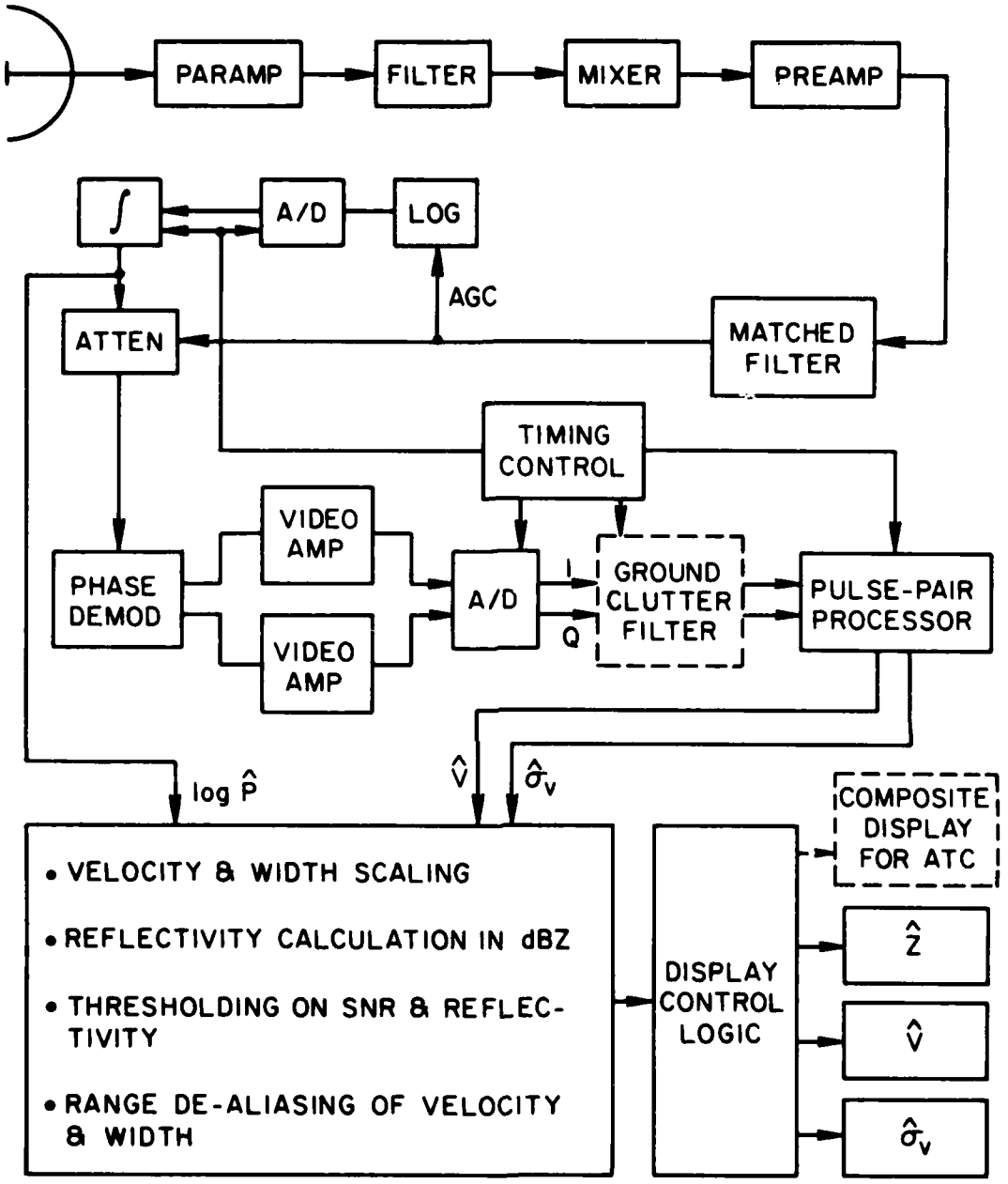

Figure 5 *Schematic of NSSL Doppler radar receiver/processor. The dashed blocks are not present in the current configuration but are desirable for air weather surveillance.*

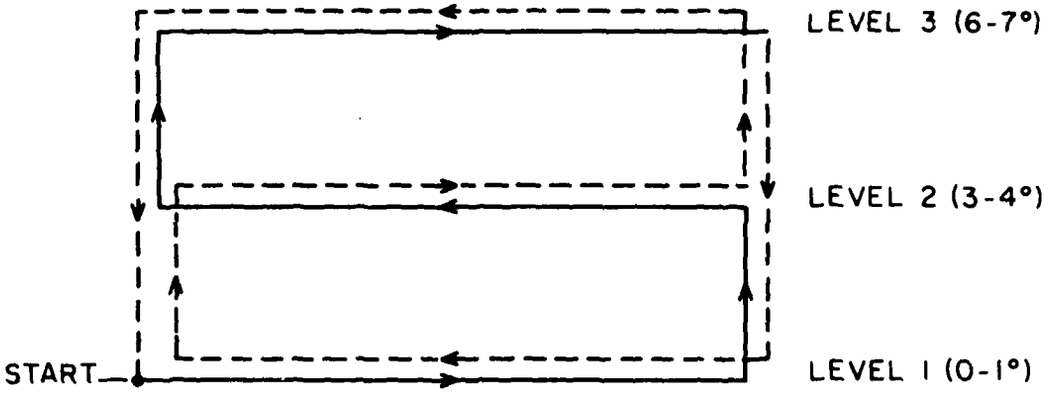

(a)

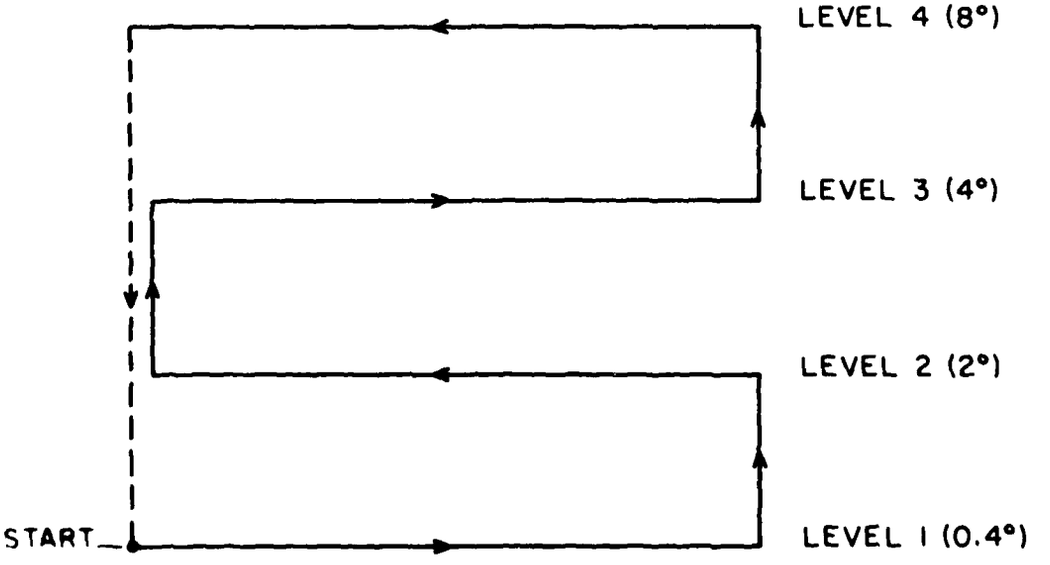

(b)

... lifetime data collection during (a) 1980 Spring ... Spring Program. The sector widths are variable. ... scan levels were also occasionally varied.

Since the current pedestal of the Norman radar antenna is capable of driving it at speeds only up to 10 degrees per second (less than 2 rpm), rapid scan data over the entire storm volume for lifetime study are not available.

The spring program data collection at NSSL involves not only radar observation, but also readings from surface and tower-based instrumentation, rawinsondes and instrumented aircraft flights. In the present study, only radar data are used since this is the only instrument that provides a complete picture of convective phenomena. The other measurements involve a coarse spatial sampling, from which only the large scale phenomena can be reconstructed with any accuracy.

The number of storms during a typical spring season which are suitable for good data collection is finite. Since data must be collected for a large number of diverse studies at NSSL during each spring program, the data specifically tailored for any one study is limited. This applies to the lifetime studies as well.

3. Lifetime Determination by Photo-Interpretation

3.1 Need for Photo-Interpretation

Two approaches for lifetime determination were started simultaneously at NSSL at the beginning of 1981, one based on photo-interpretation and the other on computer-assisted correlation. Although the second is the more quantitative method, it was realized that its implementation would require considerable time for the development and proving of software. Photo-interpretation, on the other hand, could yield quick results for tentative conclusions. The versatile and high-quality color display for spectral moments, developed and operating at NSSL, makes the photo-interpretive approach straightforward.

Besides the short-term consideration, there exists a case for retaining photo-interpretation on a long-term basis, even when an automatic method has been developed. This is because, although lifetime computation based on correlation is relatively straightforward, its preceding operation, namely the identification and delineation of phenomena that may be potentially hazardous to aviation, cannot, as yet, be performed nearly as reliably by automatic means as by trained human observers. Thus occasional visual identification of hazardous features, and tracking their evolution with time, would provide a necessary cross-check on the performance of automatic methods. This is especially true when the weather field observed by the radar is complicated, with multiple features of diverse types and possibly with range folding, causing overlay.

3.2 Photographic Data for the Study

Data for the photo-interpretive study of feature lifetimes are obtained from the color displays of spectral moments of weather fields. The moments displayed are reflectivity, velocity and spectrum width. The first is obtained from the return power received by the radar from individual range cells and the other two are obtained by using the pulse-pair algorithm. The major processing steps before display are shown in the block diagram of Fig. 5. Each moment is quantized and displayed separately on a color cathode ray tube. Sixteen levels of quantization are used, each corresponding to a different shade of color. The resulting display for each moment is a pseudo-color field giving a pictorial presentation of the various phenomena and features within the field.

The display control software at NSSL is quite powerful, providing a number of flexibilities to the display. The shades of color can be adjusted for best visual clarity, or the display may be converted to black-and-white with the quantized levels represented by shades of gray. The center of the PPI display can be moved relative to the center of the CRT--it may even be made to lie outside the CRT area. This capability, combined with a variable magnification along the radial direction and the ability for sectoral presentation, makes it possible to optimally display selected parts of the field. Housekeeping data pertaining to the field under view are displayed on the right hand margin of the CRT. The coordinates of any point on the display may be read by moving in a cursor point whose coordinates are also included in the data on the right margin.

The data utilized for photo-interpretation were obtained during the 1980 and 1981 spring programs using the Norman radar. The next section contains detailed observations on several storms for which data were collected in a format suitable for lifetime study. In studying the persistence of storm features in reflectivity, radial velocity and spectrum width fields, although comments are made regarding any major change in the storm structure within the time scale of interest, particular attention is focused on those features which pose a potential threat to aviation. For the purpose of this study, significant features are defined as those with one or more of the following attributes:

1. Reflectivies exceeding 40 dBZ
2. Velocities exceeding 20 m/s (approx. 40 knots)
3. Spectrum width exceeding 4 m/s.

3.3 Observations

3.3.1 The Storm of April 24, 1980

For the storm of April 24, 1980, data suitable for lifetime studies are available over a period of about 12 minutes starting at 1728 hrs. Three elevation levels are covered at approximately 0.4°, 3.6°, and 7°. At each of these levels, the evolution of the significant features in all the three moment fields is followed using photographs of the fields taken at intervals of about a minute.

The photographs were originally taken in full color off the NSSL moment displays. Color copies of the photo-mosaic were submitted to FAA as a part of an interim report [19]. In this report, black-and-white copies of the color mosaic are provided to minimize the cost of reproduction. However, this necessarily involves some loss of information and, less importantly, of appearance and clarity.

The significant part of the storm has an elongated shape, centered 80 km west of Norman and oriented roughly East-West, the length and width being about 50 and 10 km, respectively. It is observed that the overall dimensions, orientation and location of the storm remains fairly stable over the 12-minute observation period.

Reflectivity Field: The principal features of the reflectivity field at 0.4° elevation are identified in Fig. 7. Features 1, 2, and 3 are high-reflectivity areas ($\geq$ 50 dBZ) signifying heavy precipitation rates. Over the 12-minute period considered, these relatively large features tend to persist, although discernible changes in their internal structure may take place (see Fig. 8(a), left column). These fine structures and changes in them may not, however, be of interest in air traffic control since aircraft would be expected to avoid entire hazardous areas. A very important observation concerning the reflectivity field is that in the high-reflectivity features 1, 2, and 3 the peak reflectivtiy of each feature remains unchanged over 12 minutes of observation, so that a scanning cycle lasting for any period up to 12 minutes is not likely to miss the information on the maximum precipitation rate in a given area.

Feature 4 (identified in Fig. 7) may be called a "reflectivity hole", indicating a no-precipitation region in a high-precipitation continuum. This feature, which is quite well-defined at the beginning of the observation period, diffuses and opens out towards the end, indicating significant change. The change, however, is much less pronounced over any 5-minute

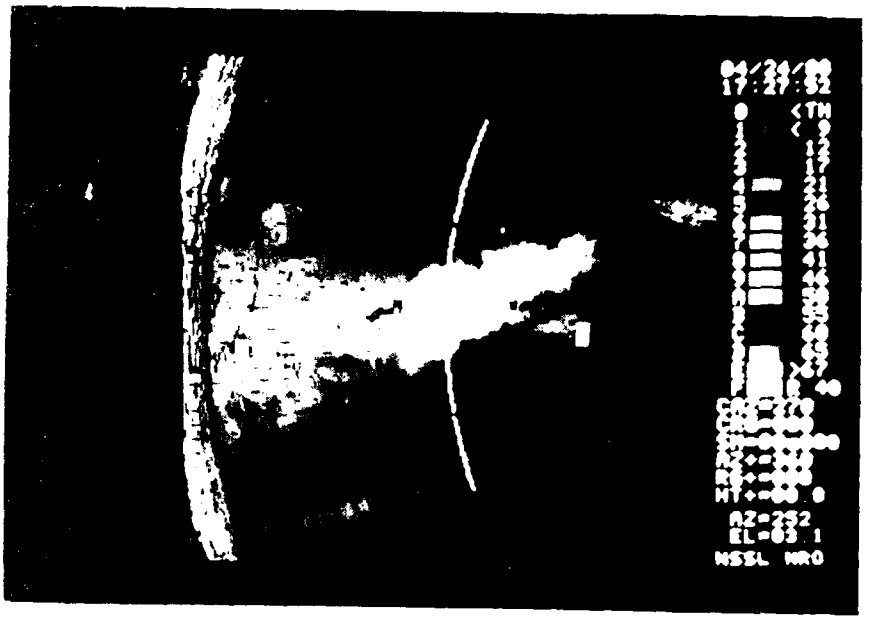
AZ=232
EL=03.1
NSSL MRO

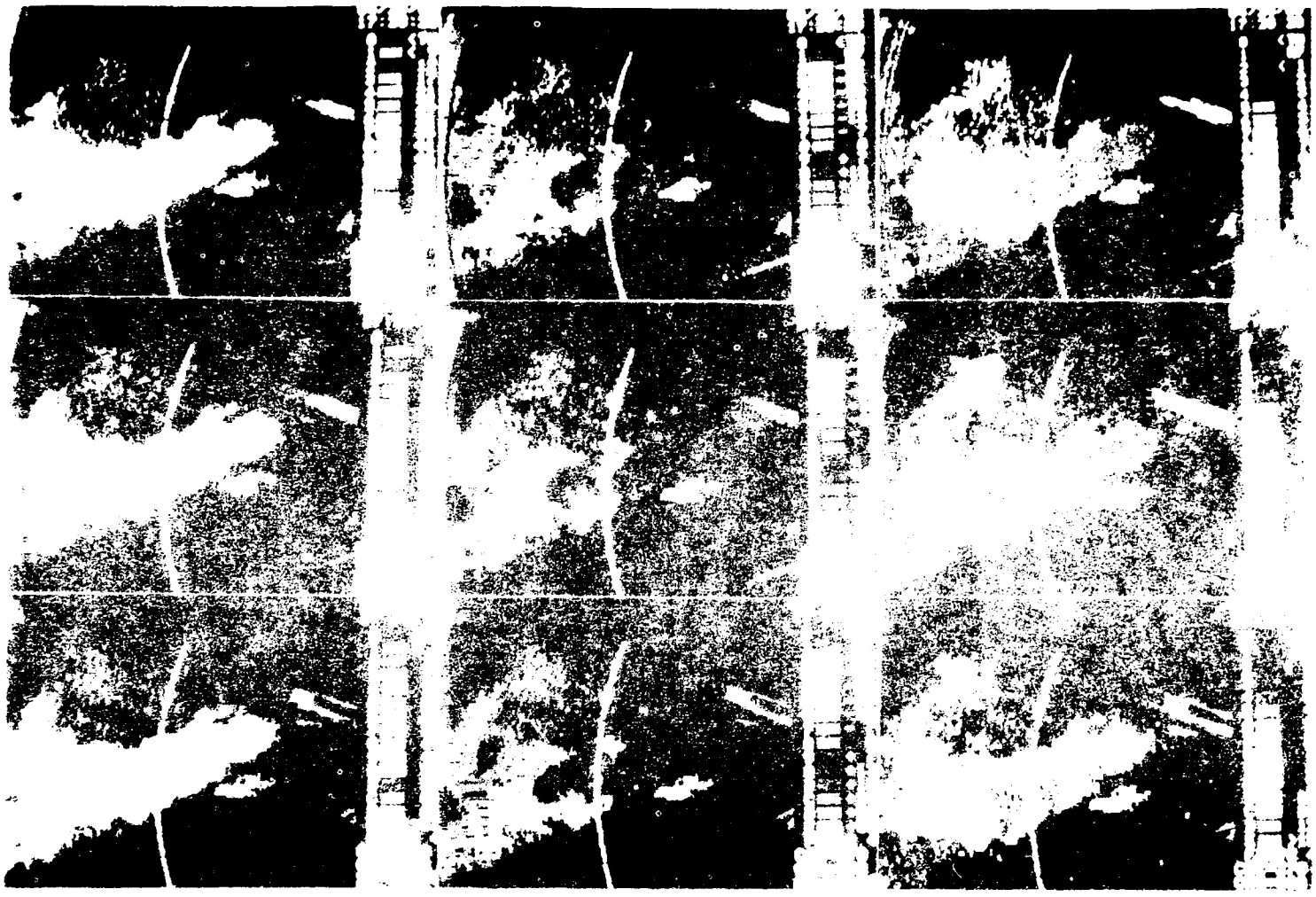

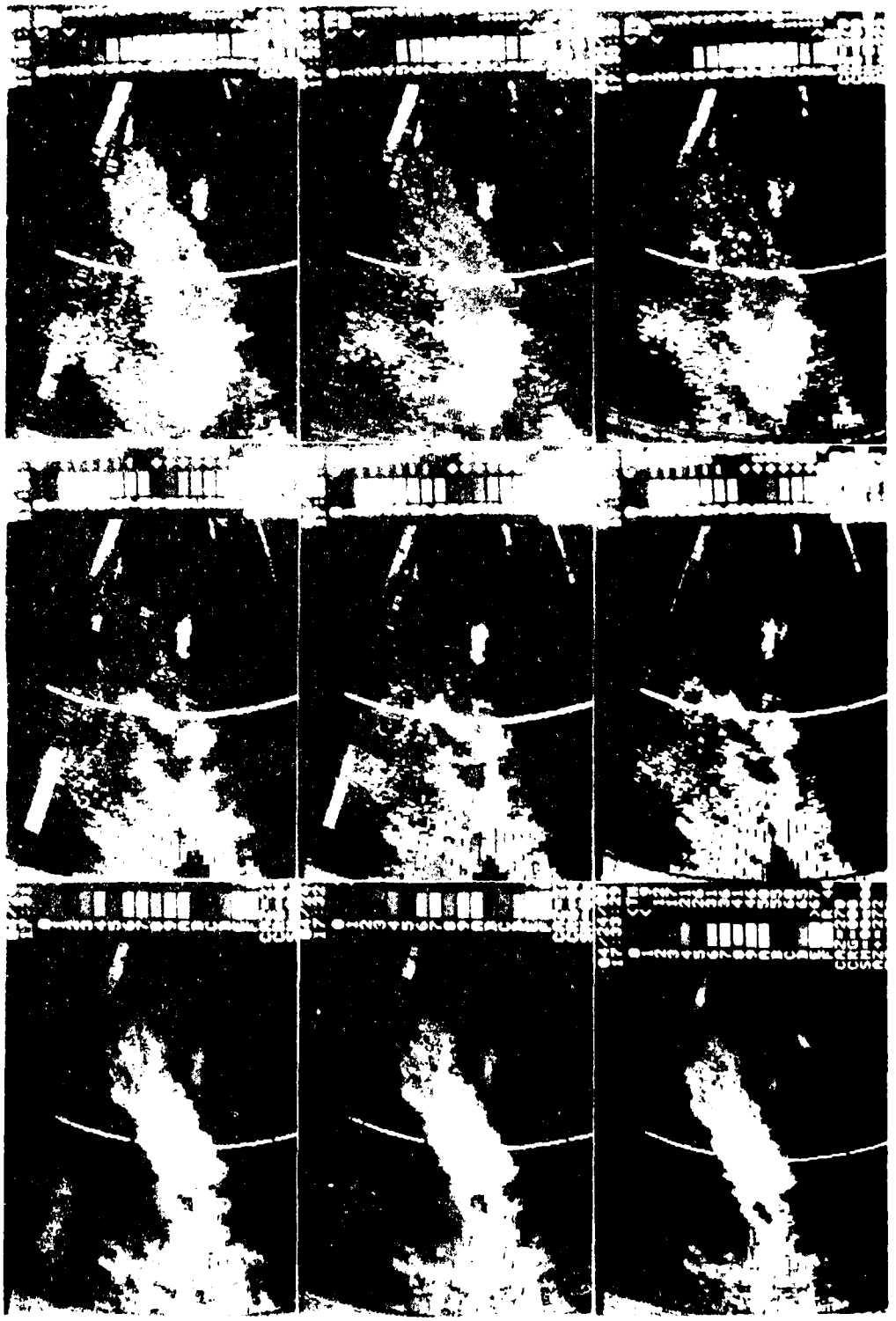

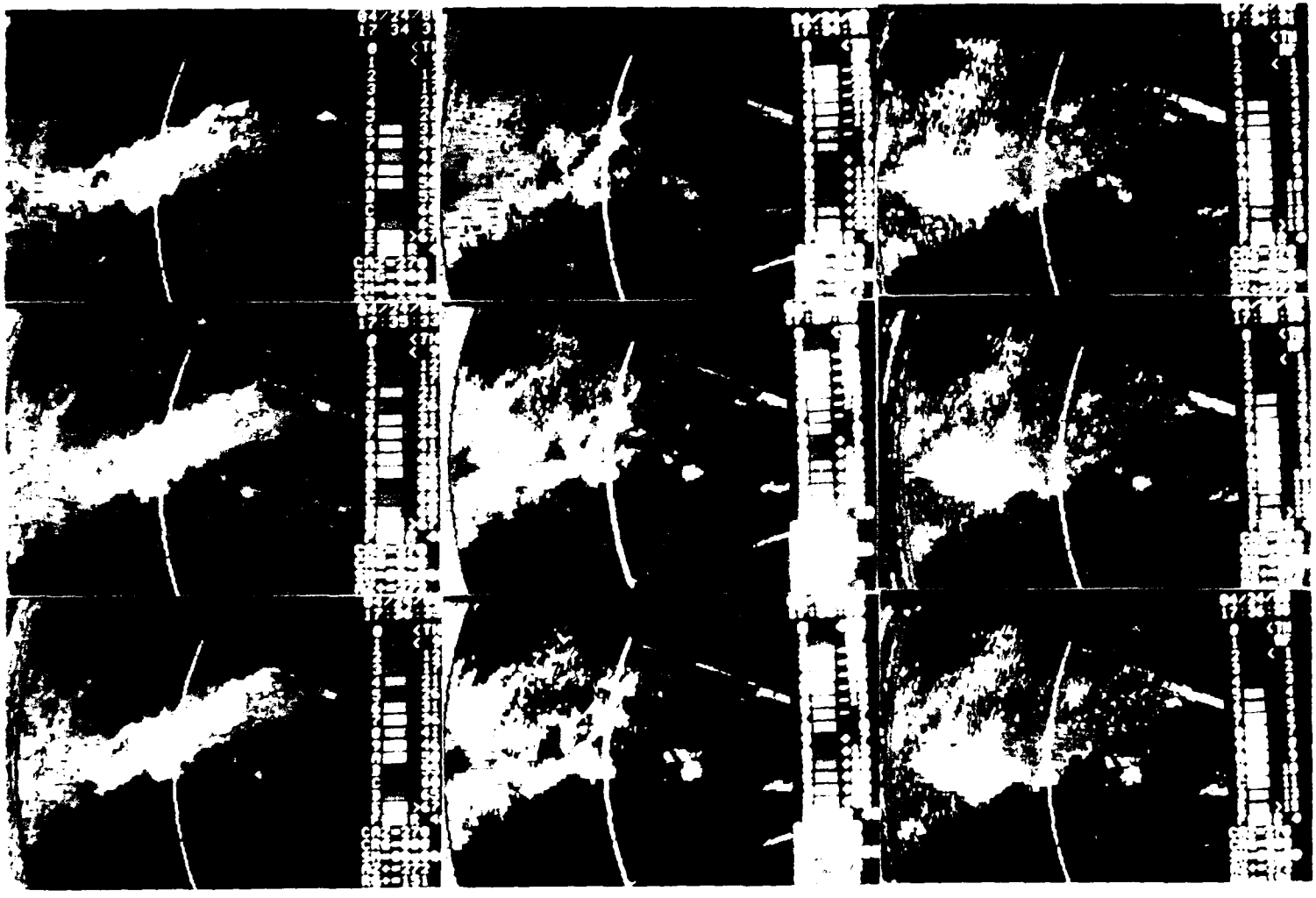
REFLECTIVITY
RADIAL VELOCITY
SPECTRUM WIDTH

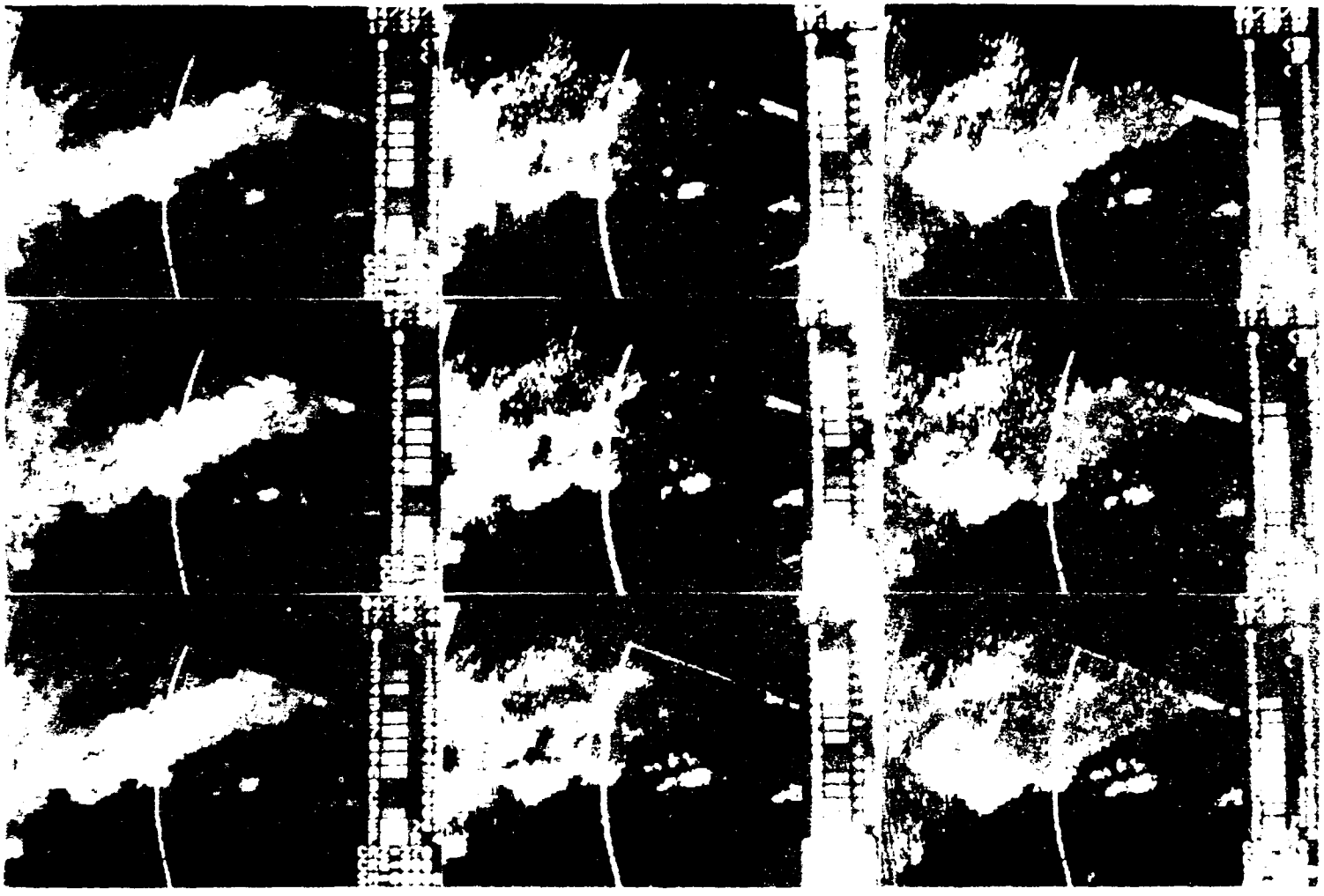

REFLECTIVITY RADIAL VELOCITY SPECTRUM WIDTH

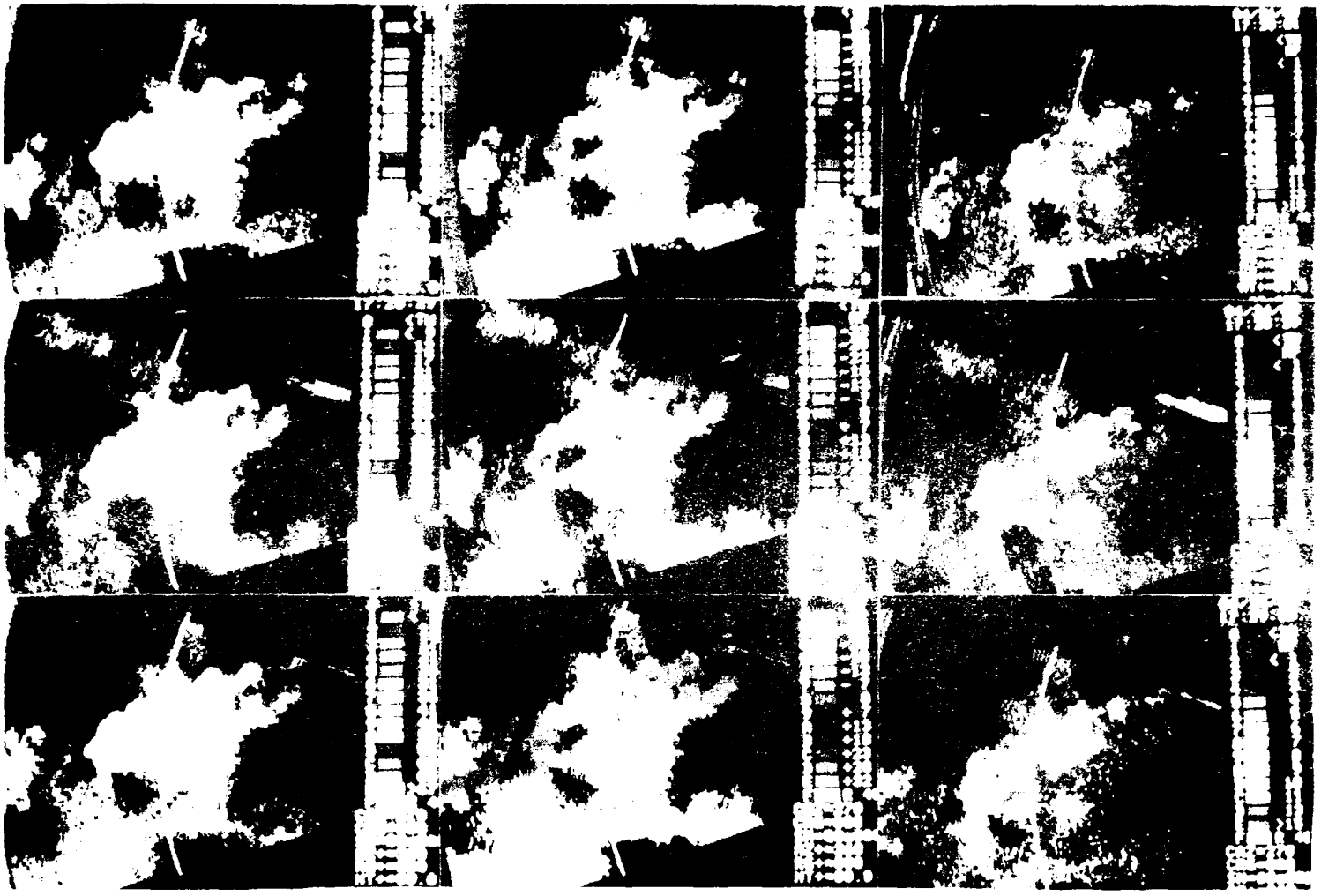

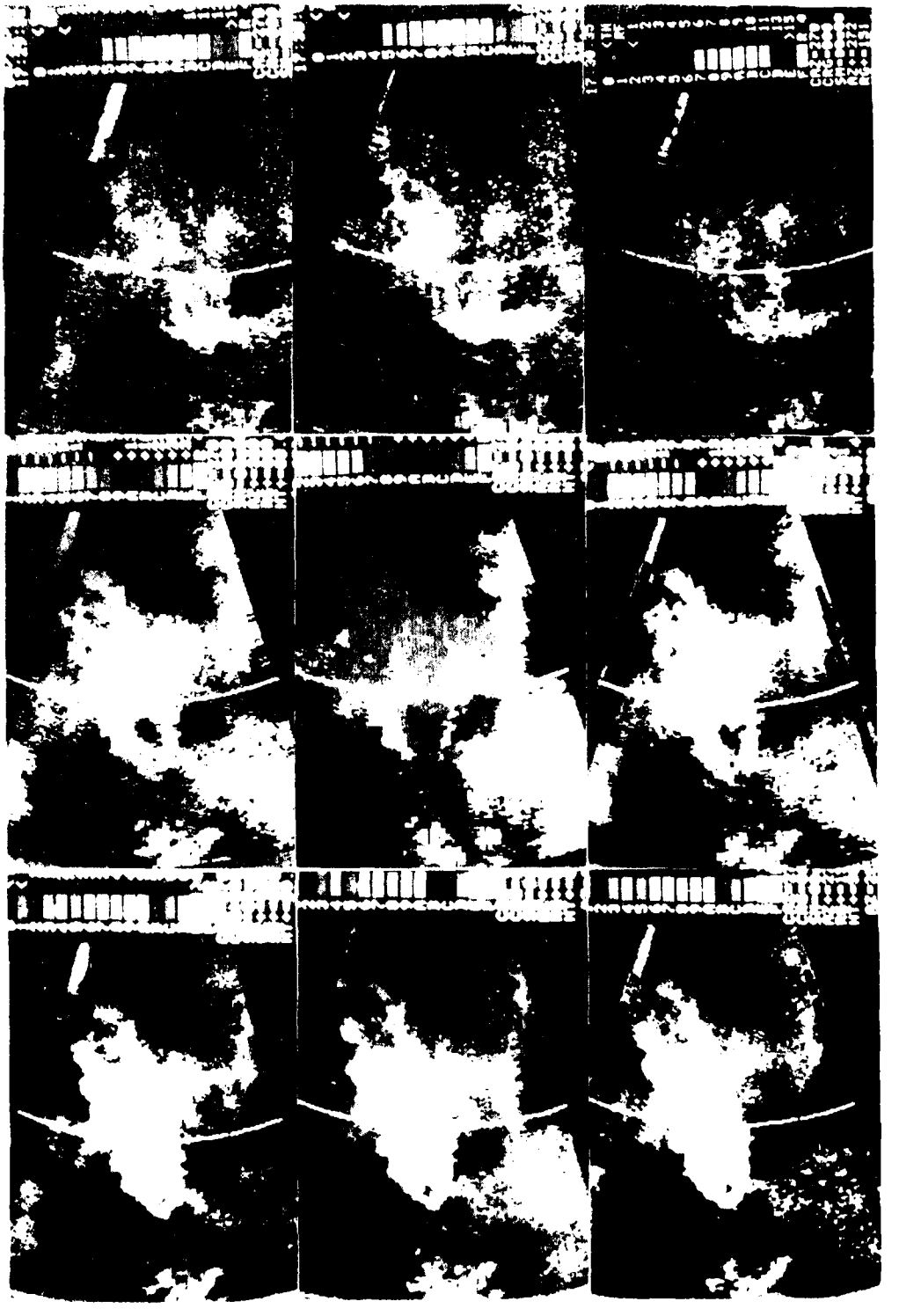

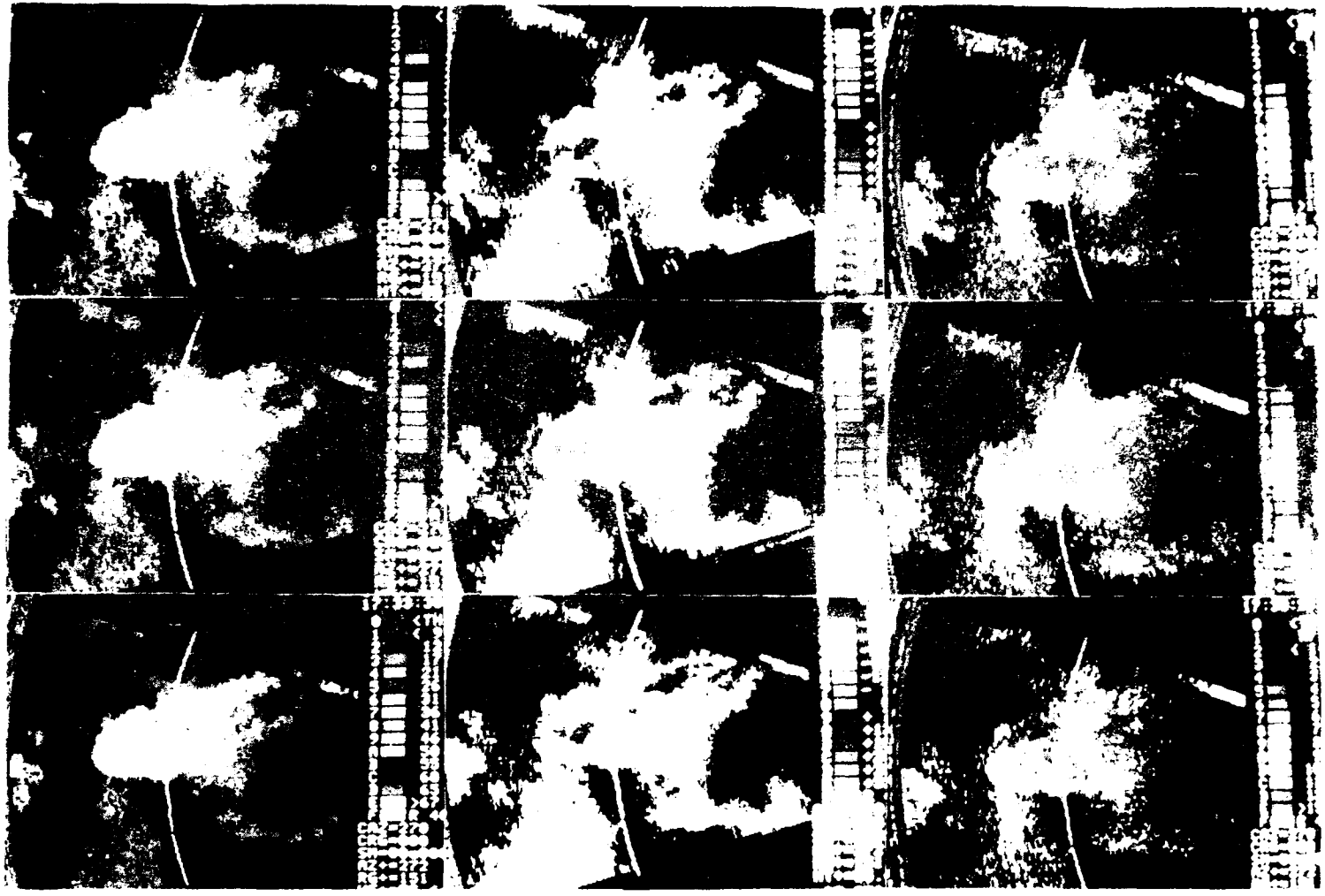
RADIAL VELOCITY

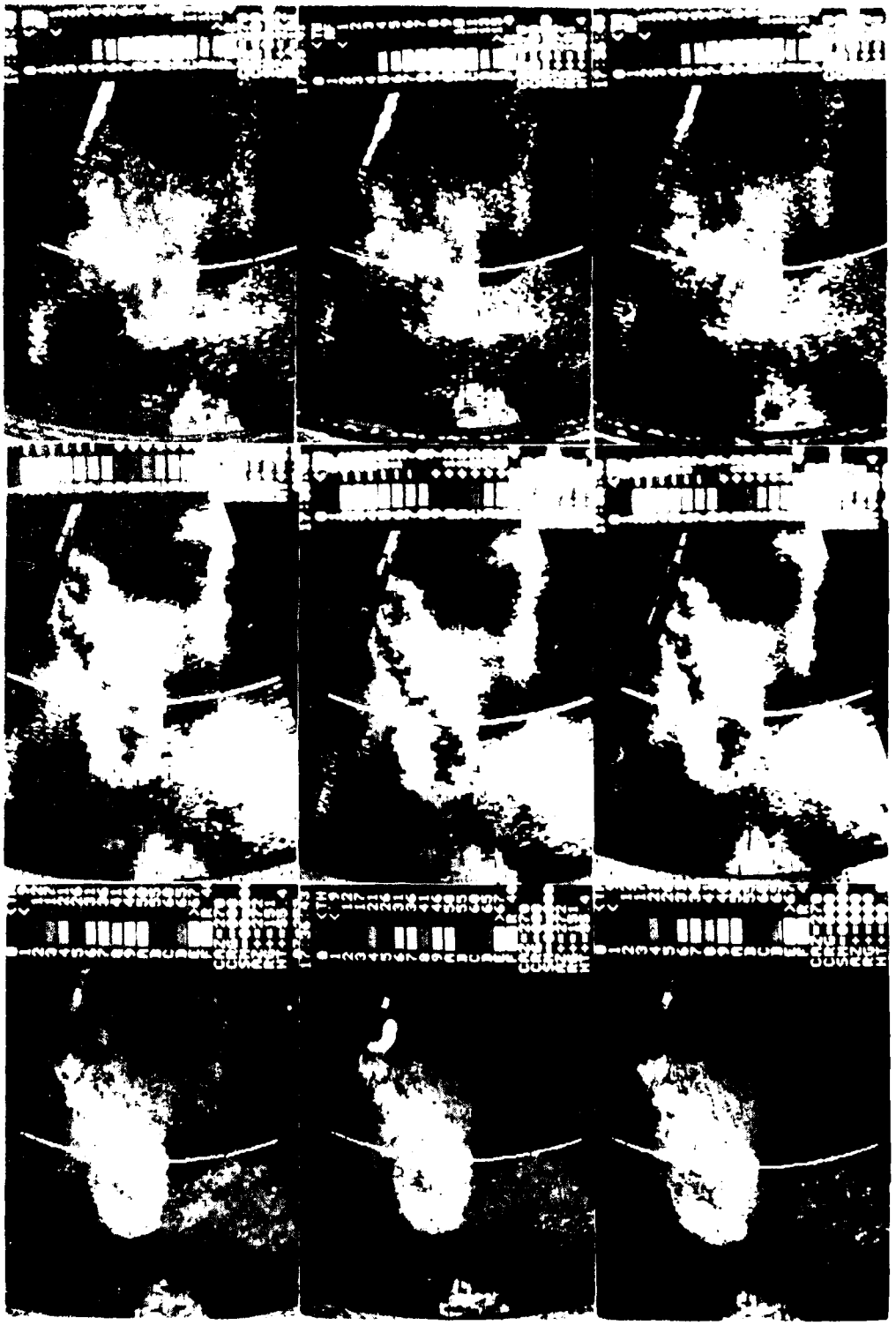

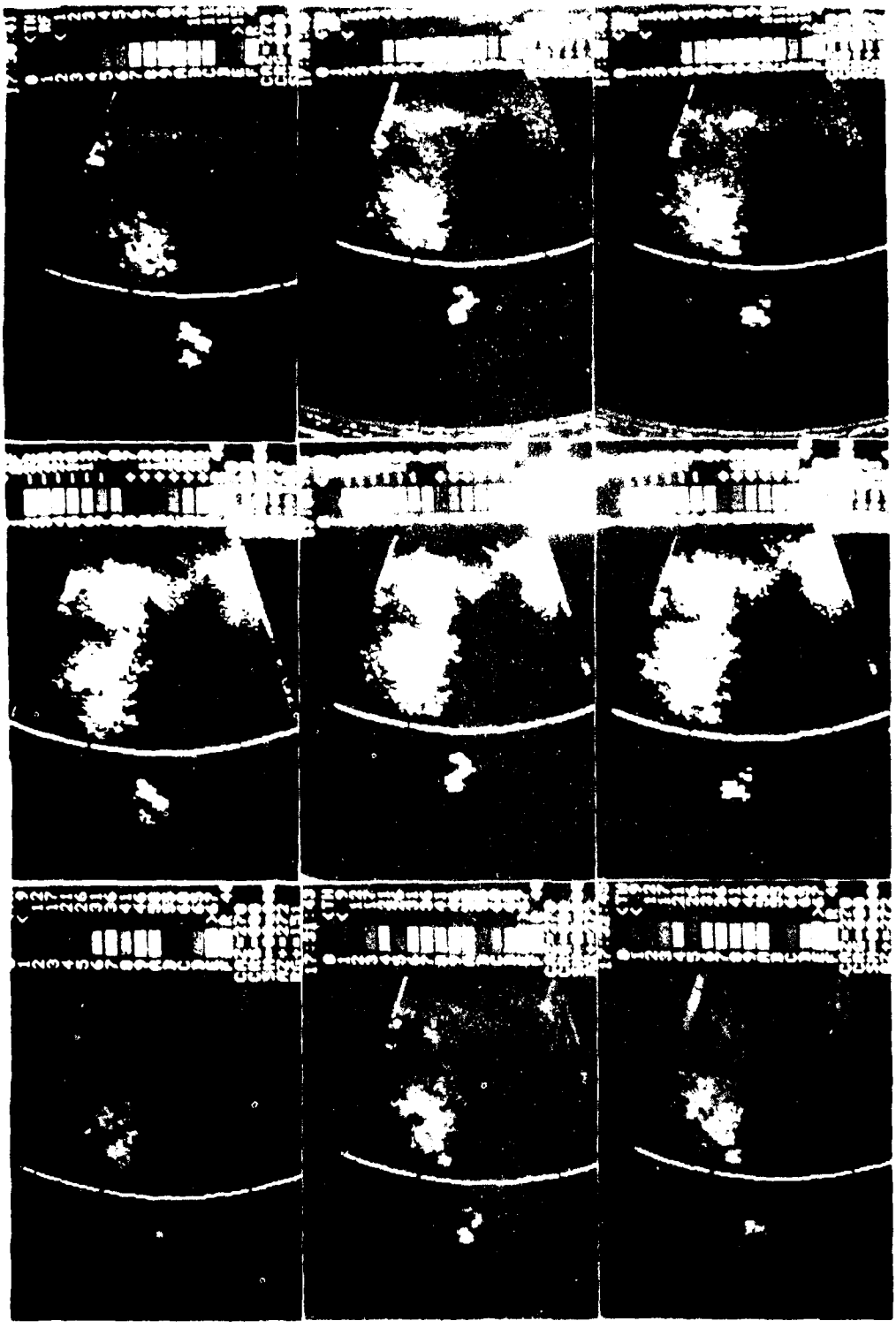

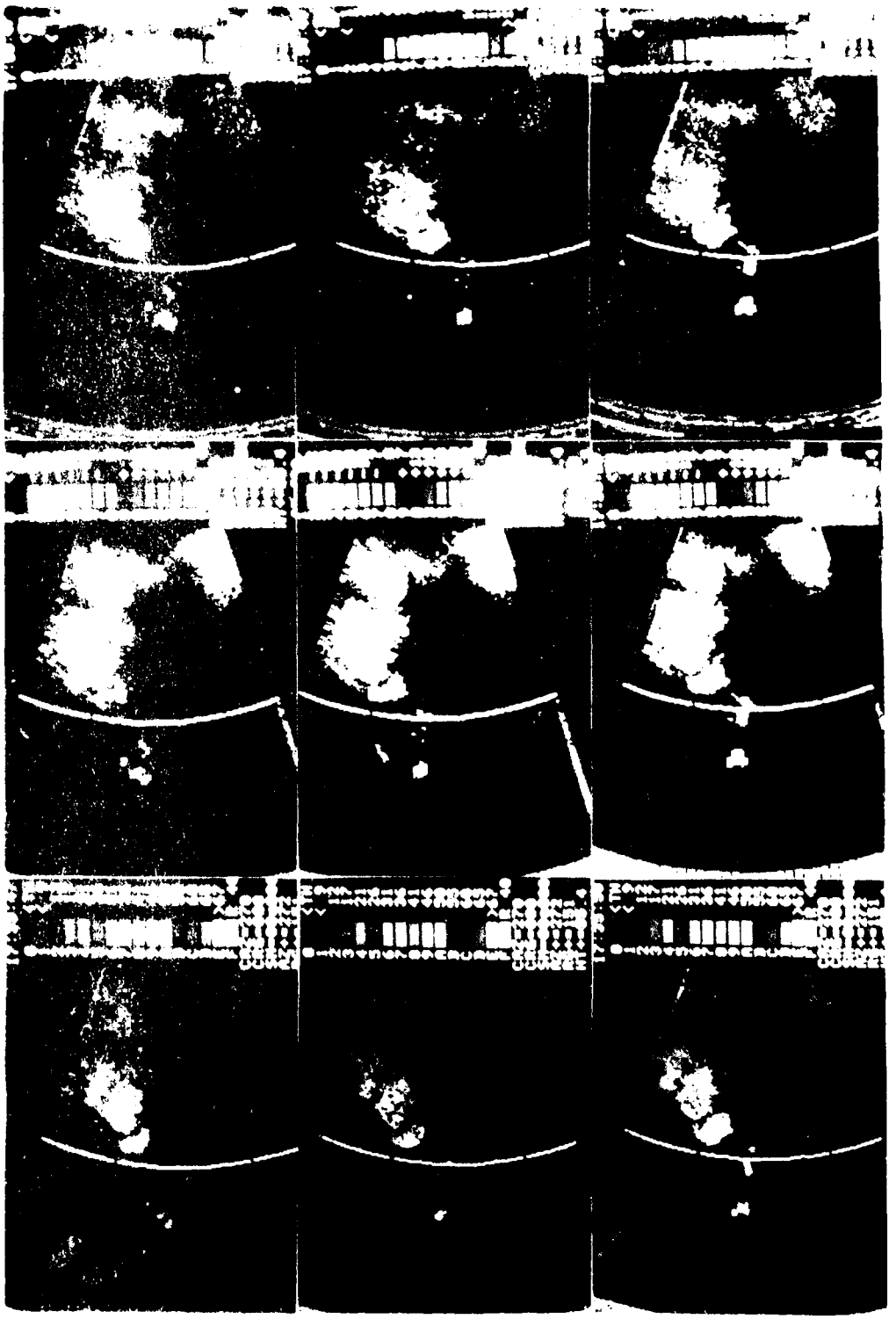

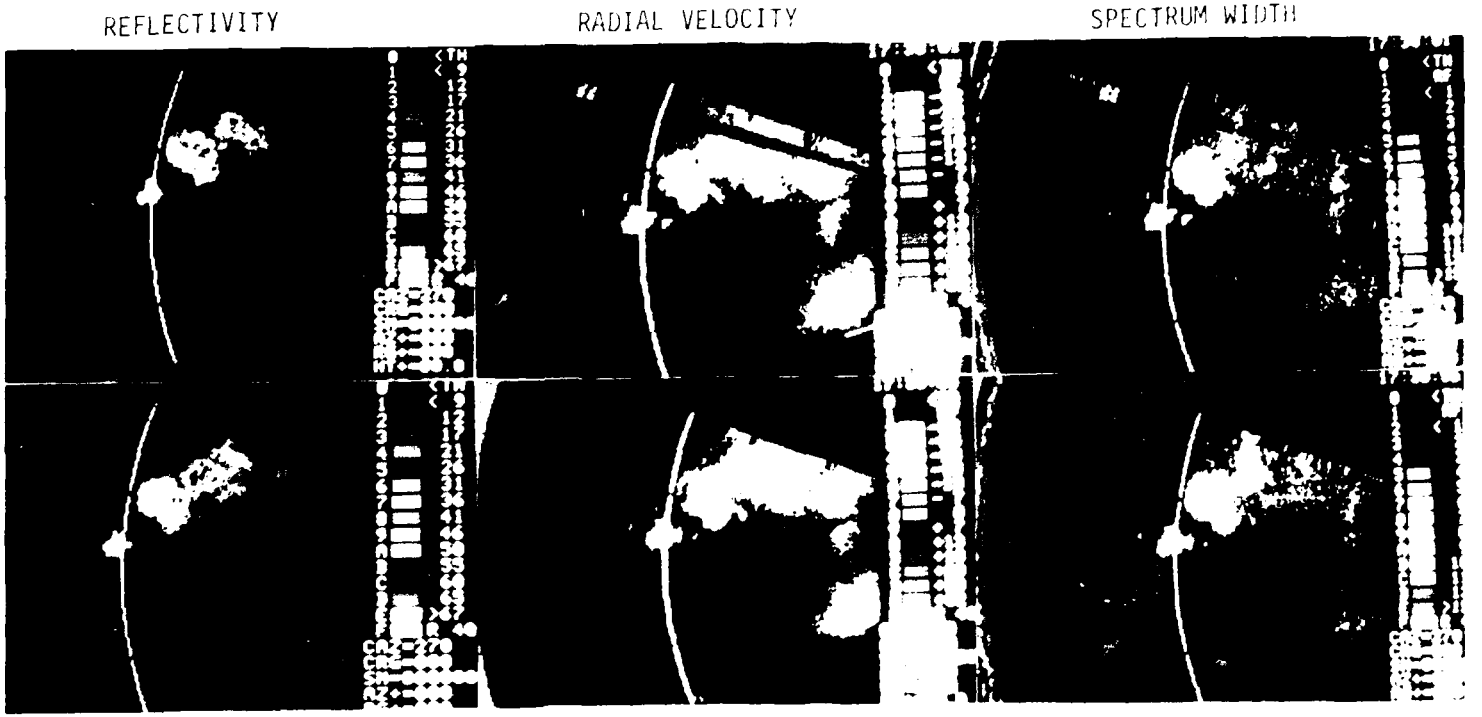
REFLECTIVITY
RADIAL VELOCITY
SPECTRUM WIDTH

period, except at 17:31 hrs, when a relatively rapid decrease in precipitation has occurred at the southeastern rim of the "hole". The reflectivity levels involved, before and after the change, are, however, not too large ($\leq$ 30 dBZ), so that this situation may not be considered hazardous to air traffic.

A very significant observation is the persistence of Feature 5. It is a weak feature ($\leq$ 20 dBZ) isolated from the main body of the storm, and is relatively small (5 x 3 km). During the observation period, it shows just enough changes to indicate that it is not a patch of ground clutter, but its stability over the 12-minute period indicates that even a small, weak and isolated feature would not remain undiscovered at fairly slow scan rates.

Velocity Field: The velocity field (Fig. 8(a), center column) of the April 24 storm at 0.4° elevation contains only one major high velocity feature (reaching 28 m/s) in addition to a large low-velocity mass. The high velocity feature undergoes significant changes over relatively short periods. For example, between the two frames at time instants 17:29:53 and 17:31:28, the high-velocity zone has diffused considerably, the rate of diffusion being much slower in the subsequent frames. However, during any 5-minute stretch of time, the velocity feature has not lost its identity, implying that with a relatively slow scan rate, although a high velocity feature may undergo changes, it is not likely to go undetected. The large, low-velocity patch remains fairly stable during the observation period.

Spectrum Width Field: The spectrum width field, in general, should not be relied upon as the sole means of feature identification because of its higher susceptibility to noise and sidelobe interference. However, since turbulence fields (especially those which induce in the aircraft frequencies comparable to its fugoid frequency) are of great importance to aircraft safety, the spectrum width display forms a valuable addition to the other displays. In the April 24th storm, the spectrum width field and the major features in it appear to be about as stable as those in the intensity field (see Fig. 8(a), right column).

There is reason to suspect that the bright feature on the botton edge of the width field (in the later pictures of the series shown) may not be a real feature, but a spurious one caused by the strong feature 1 of Fig. 7 appearing through the antenna sidelobe. This reinforces the caution that the width field data must be edited using data from the other two

fields before warnings are issued to aircraft.

Vertical Scales of Features: Although the present study is concerned primarily with lifetimes of storm features, the vertical continuity of hazardous atmospheric phenomena is a pertinent aspect of study here since it affects scan strategy directly. A feature which has a small vertical extent can be missed by falling between two successive cones of scan (at two elevation angles) just as it can by being temporally too transient. The scan pattern employed, as shown in Fig. 6(a) permits some conclusions to be drawn regarding vertical continuity of storm features.

Comparing the reflectivity fields of low-elevation and mid-elevation scans (Figs. 8(a) and 8(b), respectively), it is found that the features 1 and 3 (peak reflectivities 55 and 50 dBZ, respectively) extend to the mid-level scan (~5 km height), preserving their peak reflectivity values. Feature 2 of Fig. 7, which is also a strong feature (reaching 50 dBZ) is absent at mid-elevation. Also, the low precipitation area (~20 dBZ) is much more extensive at mid-altitude than at the lower altitude.

Further on a high-elevation (~10 km) (see Fig. 8(c)), most of the features have disappeared except a trace of feature 3.

The velocity fields at mid-altitude (Fig. 8(b) show winds which are both strong (30 m/s) and extensive (covering an area larger than 50 x 50 km). This feature, which may be of particular concern for aircraft safety, would have been missed if scans were made only at the lower and upper elevation angles, leaving the middle level unobserved. The higher level (Fig. 8(c)) also displays strong wind fields over significant areas, but these areas do not overlap those at the middle level, so that the phenomenon at the higher level cannot be considered as the vertical extension of the process occurring at the middle level.

The turbulence field at middle level is quite significant and may be considered as a vertical extension of the field at the lower level. The field at the higher level, which is still quite strong, however, represents only a small part of the fields down below.

It is thus seen that the scanning interval in elevation shown in Fig. 6(a) is too coarse for feature detection in the sense that the change in features, between these widely separated levels, can be abrupt. Hence, it is desirable to scan at vertical separations closer than what is employed in this study. From RHI plots of other storms taken at NSSL, it appears that vertical separations of about 1.5 km would be adequate to detect

most atmospheric phenomena of interest to aircraft safety. The angular elevations corresponding to these heights would depend on the distance of the radar relative to the feature location.

Higher Level Features: The temporal stability of the features in all the three fields at both the middle and the high elevations (Figs. 8(b) and 8(c) follow the same pattern as discussed in the case of low level scan. Since all features at all levels remain quite stable over the 12-minute period and are nearly unchanged over any 5-minute period, the 5-minute scan cycle is not expected to cause loss of features at any elevation.

3.3.2 The Storm of June 16, 1980

The photographs of the PPI display of this, as well as the subsequent storms reported in this section, were taken in black-and-white for the sake of economy. For the same reason, velocity fields are not included in this photo series, but only reflectivity and spectrum width fields are presented, since heavy precipitation and turbulence are of greater concern to aircraft safety than steady windspeeds. Further, to minimize the number of pictures shot, many frames from the reflectivity field sequence are omitted where either the reflectivity level was too low or the evolution was too slow. However, pictures of the spectrum width field are shown at approximately 2.5-minute intervals, since the primary question is to decide whether a 2.5-minute scan would reveal any significant features or changes that may not be detected by a 5-minute scan. To shoot the black-and-white pictures, the color displays for the three spectral moments were converted to black-and-white. Such a conversion facility is available at a software level at NSSL's Norman Doppler radar installation. While 16 levels can be very easily distinguished in a color display because of color contrast, only a few shades of gray can be distinguished in a black and white picture. The pictures presented here contain only one or two gray shades in addition to black and white areas.

The reflectivity and spectrum width fields of the June 16, 1980, storm at 0.4 and 3 degrees elevation are shown in Figs. 9(a) and 9(b), respectively. At the lower elevation, reflectivity remains less than 41 dBZ and hence is not considered hazardous. The visible area has one large patch (~40 km), a smaller patch and a few small fragments. Over a 10-minute period each one of these features, including the very small ones, remain virtually unchanged in intensity, area and location; the only change is a slight reshaping of the boundaries. The bright areas in the spectrum width field represent values in excess of 4 m/sec. Such values are usually considered undesirable from the point of view of flight

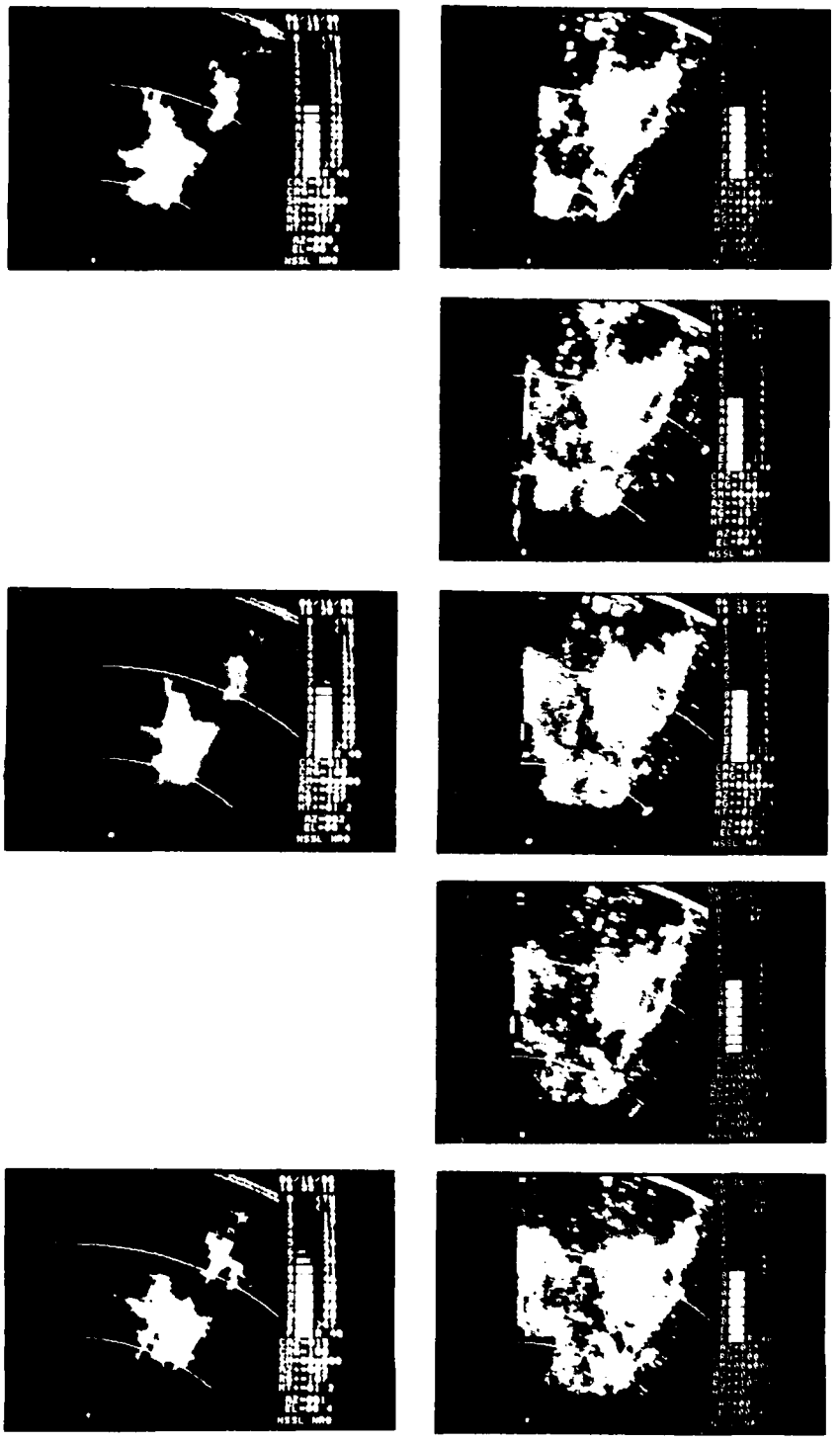

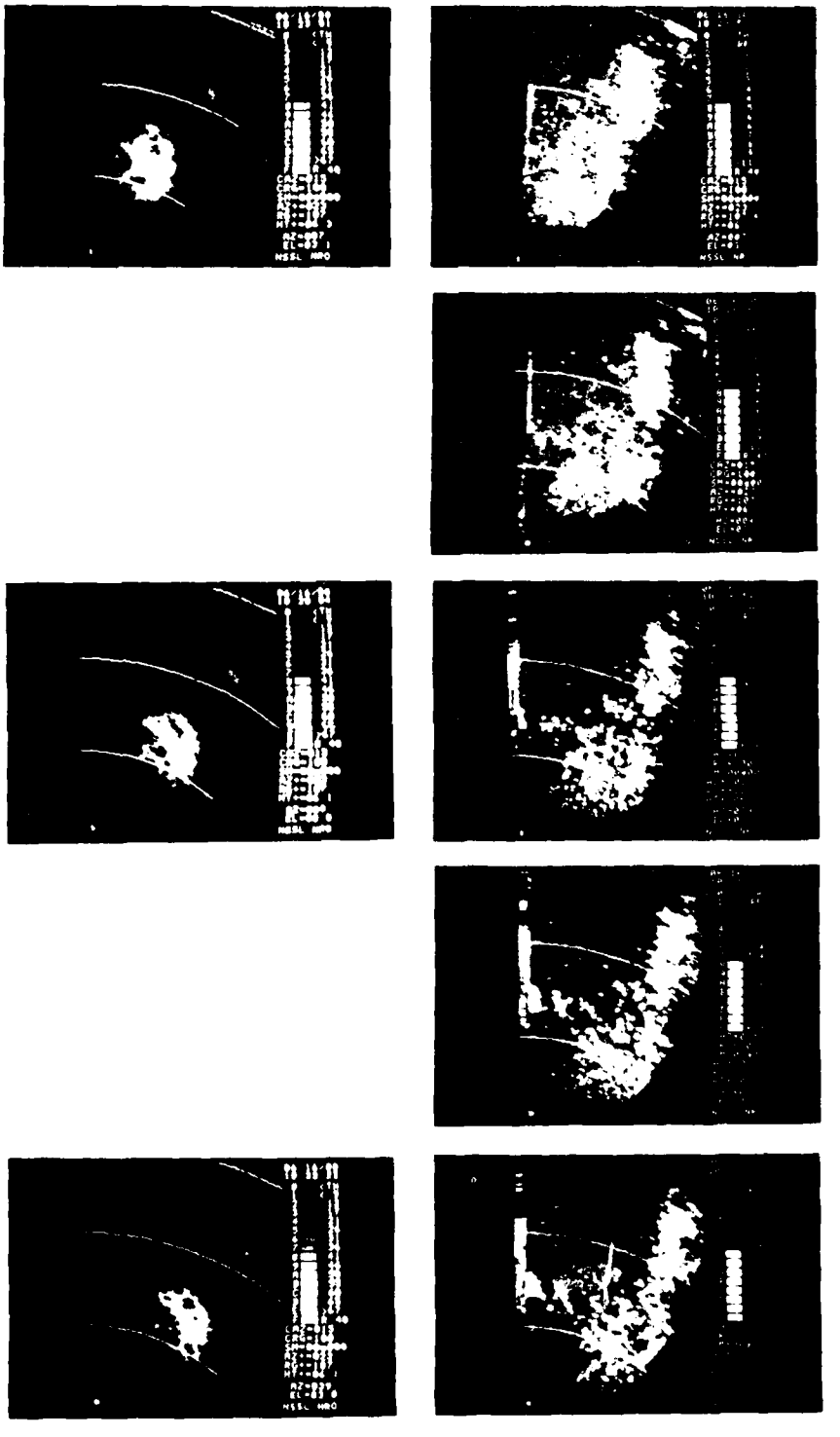

safety and passenger comfort. Over the 5-frame sequence in Fig. 9(a), there is a slight thinning out of the bright area, but its general extent and distribution remains remarkably invariant. The same behavior is exhibited at 3° elevation angle (Fig. 9(b), where the reflectivity field contains two features, one large (~25 km) and one very small (~6 km), both of which show high persistence. The spectrum width field, which shows extensive, though porous, bright areas, is equally stable.

3.3.3 The Storm of June 17, 1980

This storm was scanned using the 3-level scan scheme of Fig. 6(a), but with scan levels fixed at 0.5, 7.5, and 15.0 degrees. Photographs of the PPI displays are shown in Figs. 10(a) 10(b), and 10(c), respectively. Because of low levels of precipitation (<41 dBZ) and very slow evolution of the storm only one representative snapshot of the reflectivity field is given in each of Figs. 10(a) and 10(b). At both of these elevations, the spectrum width field is nearly frozen, with a slow drift toward the east. The only significant change is the gradual disappearance of the vertical tongue coinciding with the cursor circle in the top two frames of the 0.5° elevation sequence of Fig. 10(a) (the cursor is more clearly visible in the second frame, time 09:13:42). The tongue, however, is surrounded by a large area of high turbulence and hence is not the deciding factor in choosing the flight path of aircraft. At 15° elevation (Fig. 10(c)), the storm is "topped" at a relatively close range--about 50 km. The PPI display of the spectrum width field shows almost no change between two frames taken at over 4 minutes interval. Because of light precipitation, the reflectivity field contained almost no feature and hence has not been included in Fig. 10(c).

3.3.4 The Storm of April 3, 1981

The storm of April 3, 1981, was a well developed storm with widespread areas of high precipitation. The photomosaic for this storm, shown in Fig. 11, is completely filled, i.e., both reflectivity and spectrum width fields are shown for each time instant and at each elevation angle they were collected.

The storm had an elongated shape oriented roughly in SSW-NNE direction and located south of the Norman radar. At the lowest elevation of 0.4°, Fig. 11(a), the significant part of the storm has an approximate length of 70 km and width of 15 km. The highest reflectivity exceeds 50 dBZ, and there are significant parts of the storm above this threshold. Over the 10-minute period shown in Fig. 11(a), there is a gradual shrinkage of the area of precipitation, but the rate of such shrinkage is too slow to have any significant influence on scan strategy. The reflectivity still exceeds 50 dBZ over sizeable areas at the end

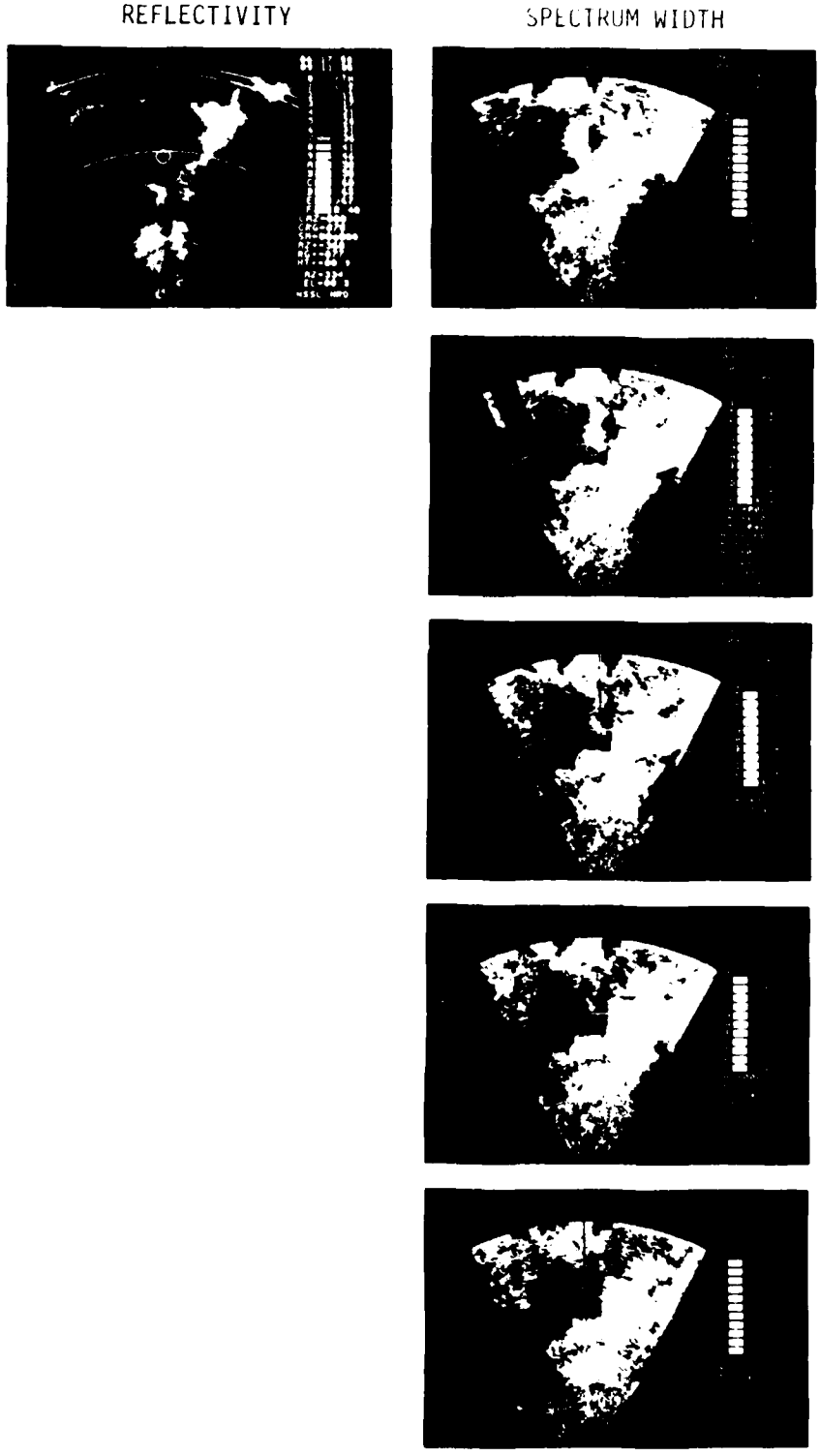

Figure 10(a) *Spectral moment displays of June 11, 1981 storm at 0.4° elevation. Reflectivity field was weak and nearly static. Hence only one representative frame is shown for reflectivity.*

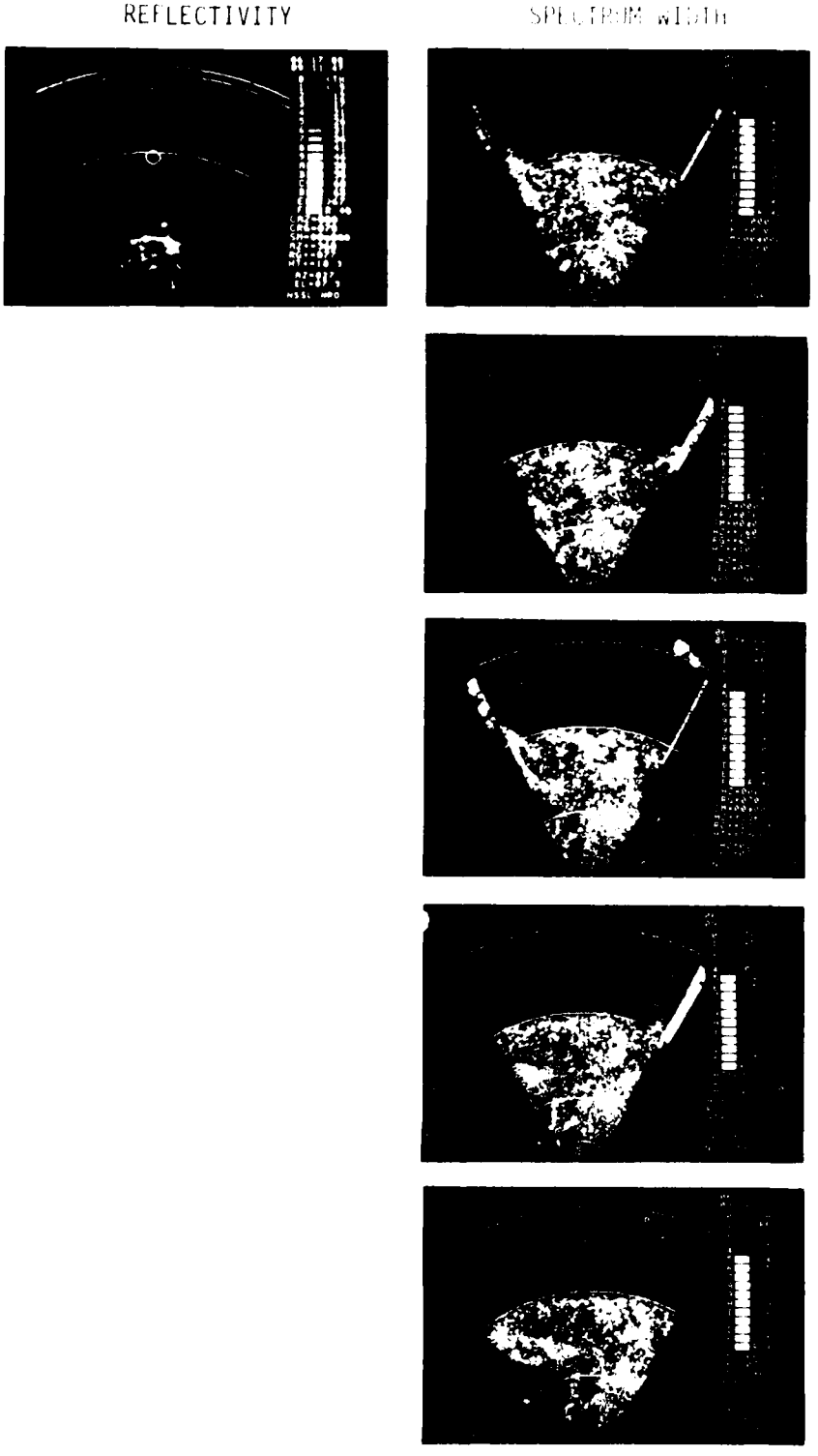

Figure 19(a) Spectral moment fields for a [illegible] elevation. Only one frame of the multi-[illegible] for the same region as in Figure 18(a).

SPECTRUM WIDTH

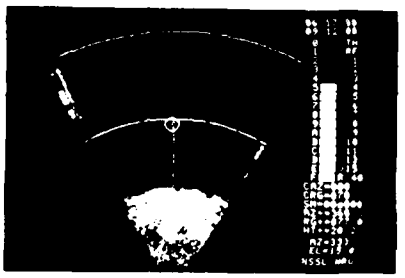

of the period. The spectrum width field shows the same order of stability as the reflectivity field. The spotty white areas, with spectrum width equal to or exceeding 4 m/sec, have a very slow growth at first, reaching a maximum in the penultimate frame (time 14:38:36) before showing a tendency to thin out. However, neither the reflectivity nor the spectrum width field show any sudden changes involving appearance or disappearance of a significant feature, during any 5-minute period, i.e., between alternate frames of the photo sequence in Fig. 11(a).

At a scan elevation of 2°, the storm initially has the same approximate extent and intensity, Fig. 11(b), as at 0.4°. But subsequently it widens significantly, with an appreciable increase in the area of heavy precipitation (>50 dBZ). The change, however, is again gradual, without any significant features appearing or disappearing. The spectrum width field at 2° elevation behaves in a manner very similar to that at the lower elevation, slowly intensifying over the first four frames and then showing signs of weakening.

At the highest elevation angle of the scan (8°), the cross section of the significant portions of the storm (reflectivity >31 dBZ) have shrunk to a very small area, Fig. 11(c). In this sequence of pictures, which are taken at approximately 5-minute intervals, the evolution of the storm is more rapid than the lower two elevations. Starting from a very small (~3 km) and weak (<41 dBZ) patch at 14:32:32, the feature is found to grow to moderate size (~8 km) and high intensity (>50 dBZ) at 14:41:40. When the high-elevation scan is viewed in isolation, this may look like a somewhat fast growth rate. However, such a behavior is typical of thunderstorms during growth phase, since precipitation in a thunderstorm cell usually starts at mid-altitudes and propagates both upward and downward, often quite rapidly. At isolated scan elevations, the rate of increase of reflectivity may reach values as high as 10 dBZ/min. sustained over a period of 2 or 3 minutes [21].

Precisely for this behavior of thunderstorms, flight advisories should not be based on observations at any one scan level; rather, radar pictures at several levels must be combined if elements of surprise are to be minimized. In the case of April 3, 1981, storm, if the pictures corresponding to 0.4°, 2°, and 8° are viewed together, the chances of guiding aircraft into the storm area are reduced to a negligible level. In the context of NEXRAD operation, where a larger number of scan levels are envisaged (one study [22] suggests 14 scan levels), the possibility of misjudgment because of rapid variations at one or a few levels is further reduced.

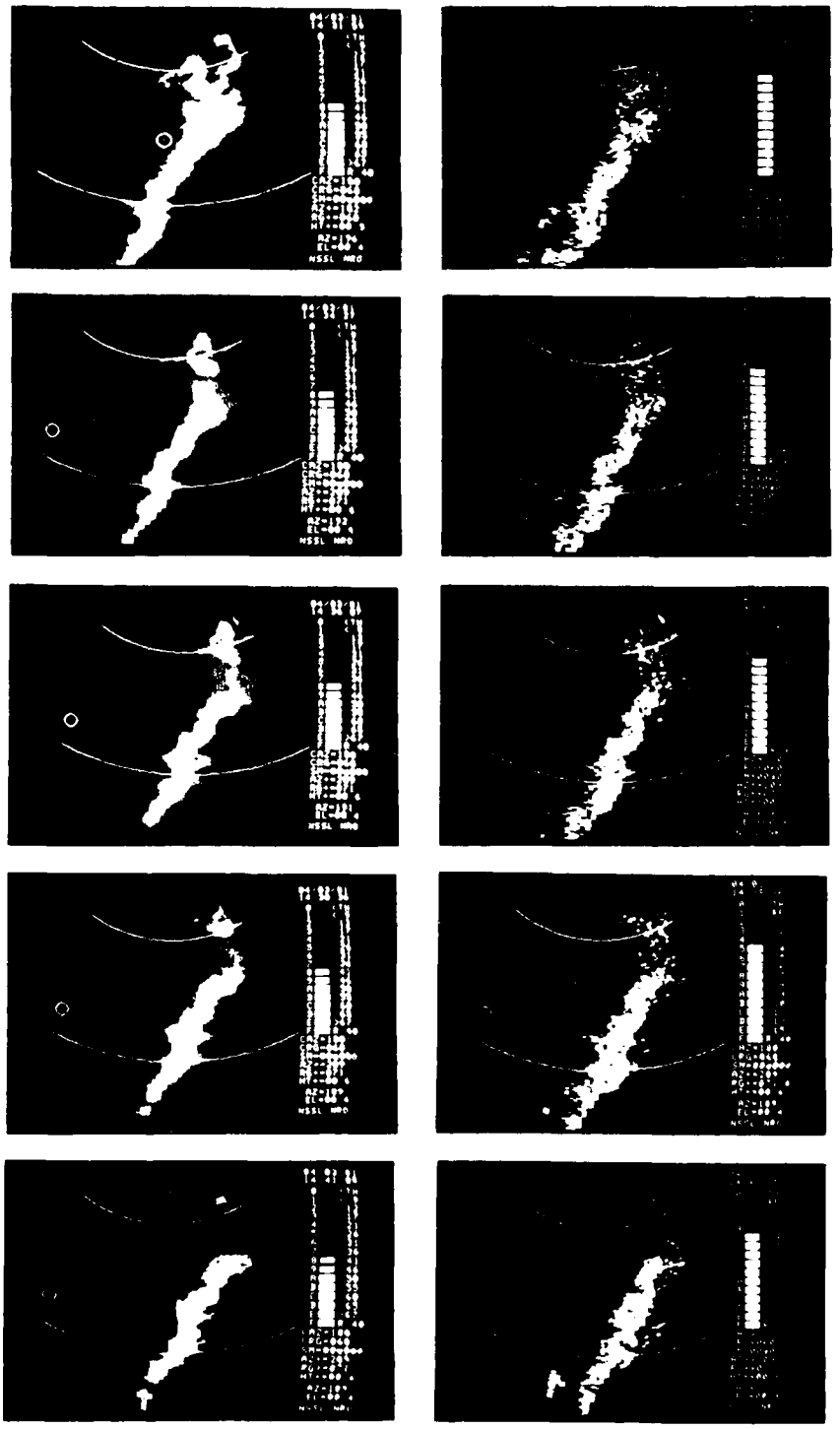

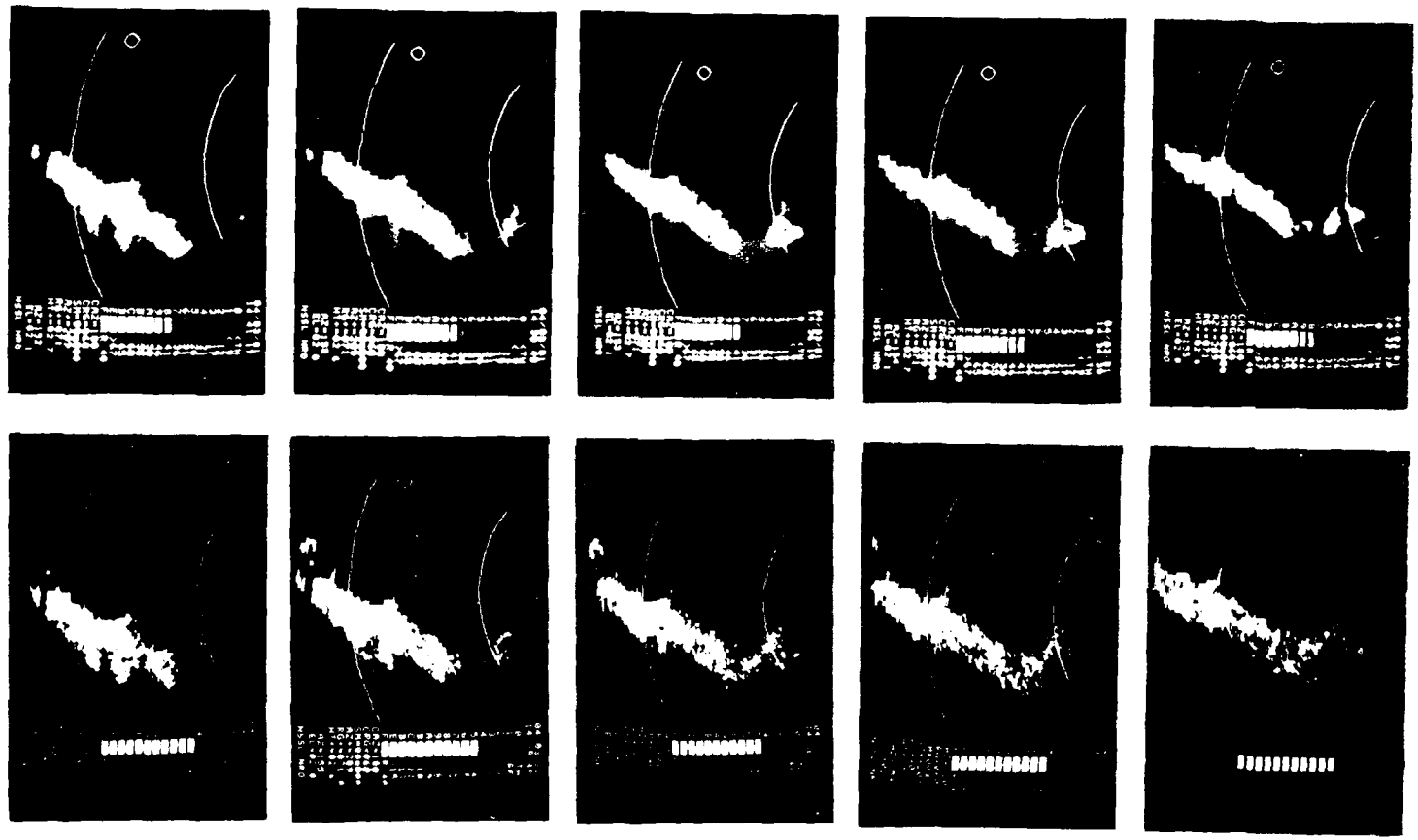

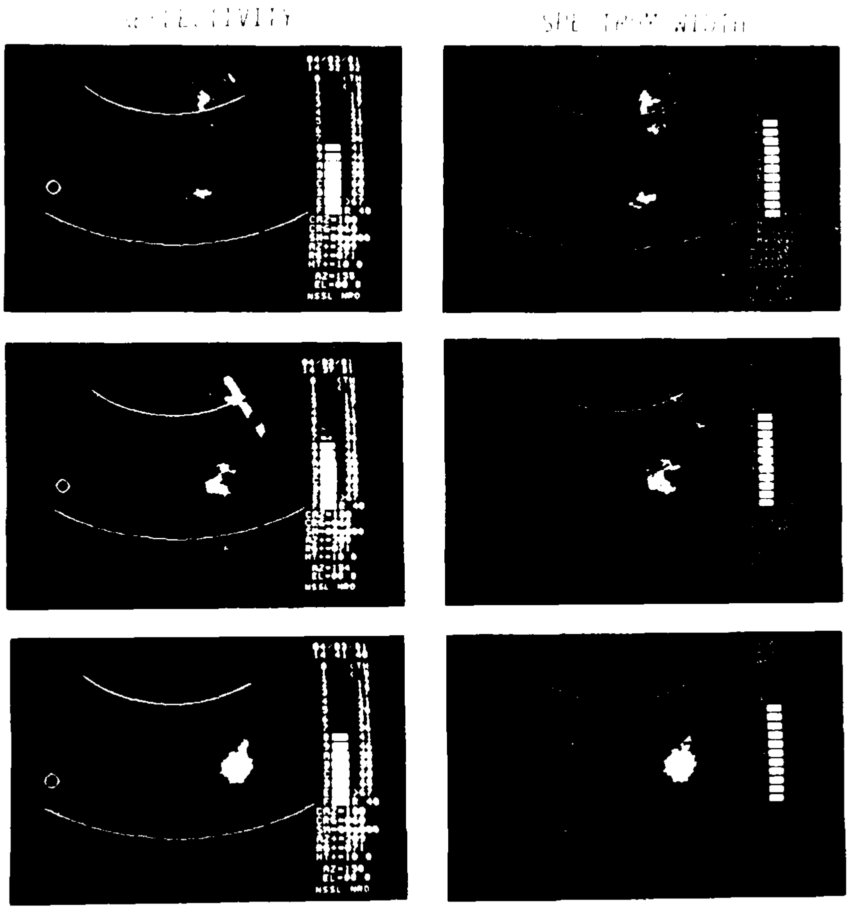
NSSL NPO

In Fig. 11(c), the spectrum width photo sequence gives the mistaken impression that the high-turbulence area also grows along with the high-precipitation area. In the display system from which the photographs in this series are taken, threshold is applied only on the signal strength (reflectivity) and the points that pass the threshold test are displayed in all the three moment fields. Thus when the outermost boundary of a storm on the spectrum width display grows or shrinks, it does not mean that the area of high turbulence does so; the storm boundaries on the spectrum width display merely follow those on the reflectivity display. In this particular case, since the storm contained highly reflective areas, a threshold level of 30 dBZ was used to minimize the effect of sidelobe interference in the display.

3.3.5 The Storm of April 19, 1981

In the storm that occurred northeast of the Norman radar in the evening of April 19, 1981, the areas of significant reflectivity are scattered (Fig. 12). At 0.4° elevation, Fig. 12(a), the patches that exceed 31 dBZ of reflectivity are small in area and sparsely distributed. The pattern is nearly identical after 5 minutes without any loss or gain of even the smallest features. The spectrum width field has large areas in excess of 4 m/sec. The distribution of these areas is invariant over a 5-frame (9-minute) photo sequence. At 2° elevation, Fig. 12(b), the precipitation distribution is sparser, and the turbulence more intense and widespread, but the temporal evolution of either field remains very slow.

3.4 Summary and Conclusion

Time-lapse photographs of the PPI displays of the reflectivity and spectrum width fields of five storms that occurred in central Oklahoma during the spring seasons of 1980 and 1981 have been presented in this chapter. For one of these storms, the velocity fields are also shown. The purpose has been to locate features that may appear or intensify fast enough to justify an update interval of 2.5 minutes in preference to 5 minutes.

A thorough examination of the picture sequence has shown that none of the significant or potentially hazardous features contained in any of the five storms showed growth (or even decay) that is so rapid that a 5-minute scan would have missed it. At isolated scan levels, moderate to fast growth rates may be observed, but when viewed as possible extensions of processes occurring at other levels (and hence suitably combined with observations from those scans), the element of surprise is nearly eliminated.

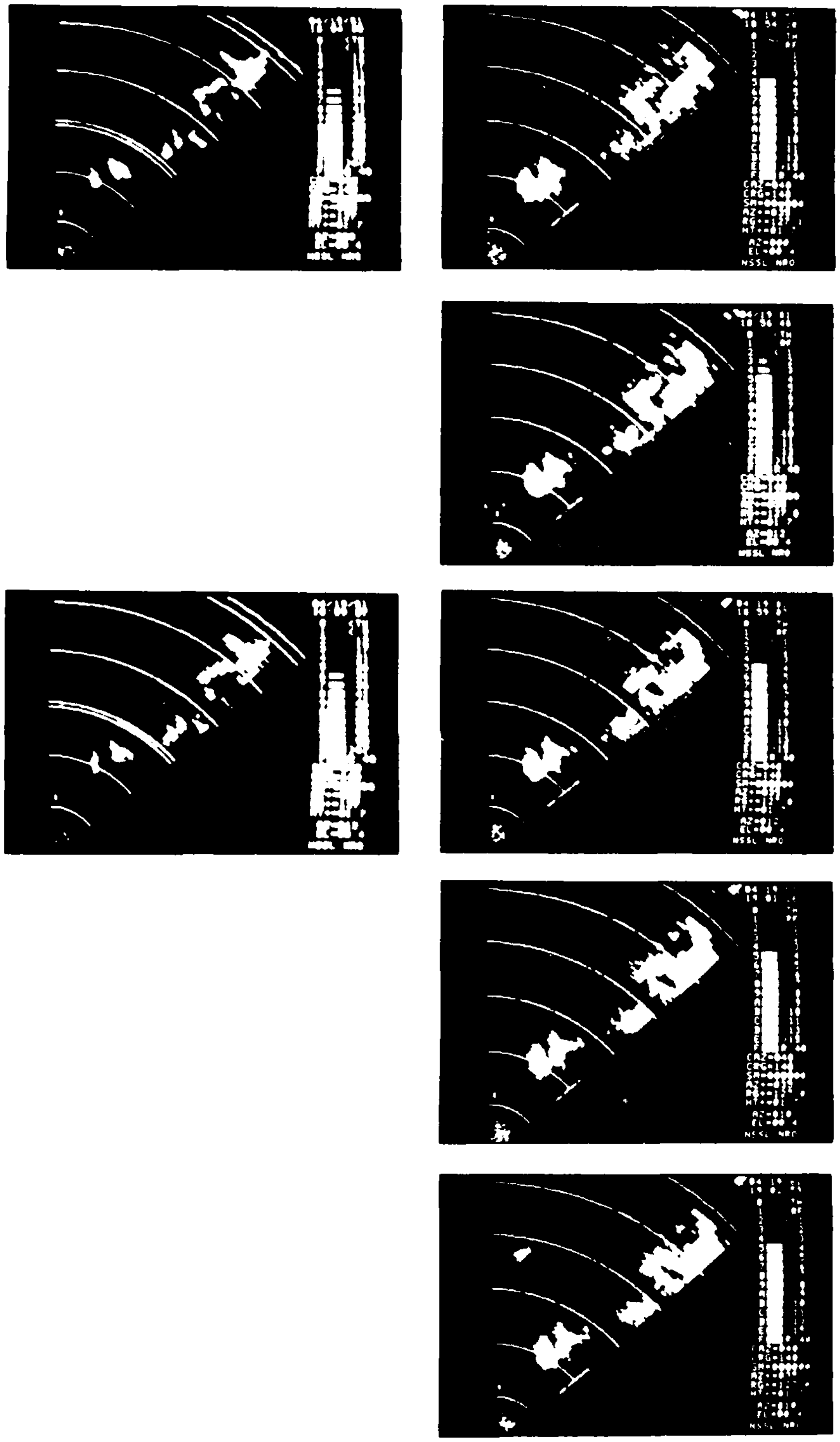

REFLECTIVITY

4. Lifetime Determination by Computer Correlation

4.1 Basis of the Correlation Method

Correlation is an established way of finding the "amount" of similarity between two fields of statistical data. When the two fields consist of dissimilar parameters and/or have no a priori commonality of origin, the process of correlation is called cross correlation and is utilized to find the causal relationship between the two fields. Autocorrelation, in contrast, is performed between two fields having an evolutionary relationship, i.e., one of the fields evolves from the other in time, space or both. A major difference between auto- and cross correlations is that the autocorrelation coefficient always reaches a maximum value of unity (corresponding to the beginning of evolution, when the two fields are identical) whereas the cross correlation coefficient does not necessarily approach that value.

The correlation coefficient ρ_{xy} between two fields of random numbers $X\{x_i, i=1,\ldots, M\}$ and $Y\{y_i, i=1,\ldots, M\}$ is defined as

$$\rho_{xy} = \frac{\frac{1}{M}\sum_{i=1}^{M}(x_i-\bar{x})(y_i-\bar{y})}{\sigma_x \sigma_y} \tag{4}$$

where $\bar{x}$, $\bar{y}$ are the mean values of the sets X and Y

σ_x, σ_y are the standard deviations of the sets X and Y

M is the number of samples in each set.

The correlation coefficient equals unity either when the sets X and Y are identically equal or when each member of one set may be obtained by multiplying the corresponding member of the other set by a constant, i.e.,

$$\rho_{xy} = 1 \tag{5}$$

when

$$x_i = ky_i \tag{6}$$

where k is a scalar constant.

The correlation method is a potent tool for studying the evolution (growth and decay) of weather phenomena. This is so because the correlation coefficient, which measures the similarity between fields, may be used to determine how much of the original characteristics are retained by a section of a weather field

with lapse of time. The method works as follows:

1. To study the rate of decay, an instant is chosen before the start of rapid decay and the state of the weather field at that instant is taken as the reference or zero-lag field.
2. The parameter to be correlated is selected to be either reflectivity. velocity or spectrum width.
3. A series of later instants, typically a minute to a few minutes apart, are chosen and the states of the field at these instants are called lag fields.
4. The successive lag fields are correlated, one at a time, with the reference field and the correlation coefficient is plotted as a function of time. The general shape of such a curve is a decreasing exponential, its rate of decay corresponding to that of the phenomenon under investigation. The time taken by the correlation coefficient to fall below a suitable threshold value, e.g., 0.5, is a quantitative measure of the decay rate of the features contained within the field.
5. To study the rate of growth of weather fields, the fully grown field should be used as the reference and correlation with successive fields should be performed with lags taken backward in time. Again, the growth period may be defined as the interval during which the correlation coefficient stays above a suitable threshold.
6. The total lifetime of a feature is the sum of the growth period, the stable period and the decay period.

4.2 Description of the Correlation Procedure

Starting from the raw data stored on tapes, three programming stages are involved in determining feature lifetime by computer correlation:

1. Raw data editing
2. Data interpolation
3. Correlation

An initial process of editing is necessary to "clean up" the raw data from Doppler radar which may be contaminated from several sources, chief among which are noise and range folding. The editing program identifies those points (resolution cells) in the data field where the signal-to-noise ratio is too poor for the data to be reliable. The data at such points are deleted and a marker is set up to identify these points during later processing. The editing program also performs range unfolding wherever possible and discards the points at which range ambiguity cannot be resolved.

Raw Doppler data are collected and stored at discrete azimuthal increments of the order of a beamwidth. These increments vary considerably. Also, azimuth sampling is not synchronized from scan to scan, so that the data grid corresponding to scans at different times are not coincident. This feature is retained even after editing, since editing is performed on a radial-by-radial basis. To minimize errors that may arise from the use of a nonuniform and noncoincident data grid, an interpolation process is performed to reduce the data from all scans to a standard grid.

The significant operations in the correlation program are shown in the flow chart in Fig. 13. The program has the following features:

1. The parameter to be correlated can be selected to be reflectivity, radial velocity, or Doppler spectral width. If reflectivity is selected, it can be specified either in dBZ or absolute value (i.e., 10 raised to the power of dBZ/10).
2. A mapping facility is provided to aid in selecting the features for lifetime study. If the MAP option is selected, the program prints out the values of the parameter to be correlated (as appearing on the zero-lag field) in a matrix form, azimuth varying horizontally and range vertically. For maximum visual impact, the information at all azimuth angles at a given range is confined to one horizontal line. To achieve this an integer format is used and one or, at the most, two digits are used to express the parameter value at each data point. This involves a scaling procedure such that the most significant part of the information is contained in one or two digits. Signs are dropped. If the scan sector width is too large and it is not possible to accommodate all the azimuth positions on one line of computer printout, then the program trims the edges and provides a map of the center portion of the sector.
3. Features of interest may be located on the map and their coordinates and sizes as well as the number of features are fed as data to the program. The routine can handle multiple features in a single run.
4. The range and azimuth interval over which each feature is to be moved for searching the maximum correlation is entered into the program. Care must be exercised in choosing these intervals: too little freedom may result in missing the correlation peak, and too much of it has the danger of introducing spurious correlation peaks into the search area.

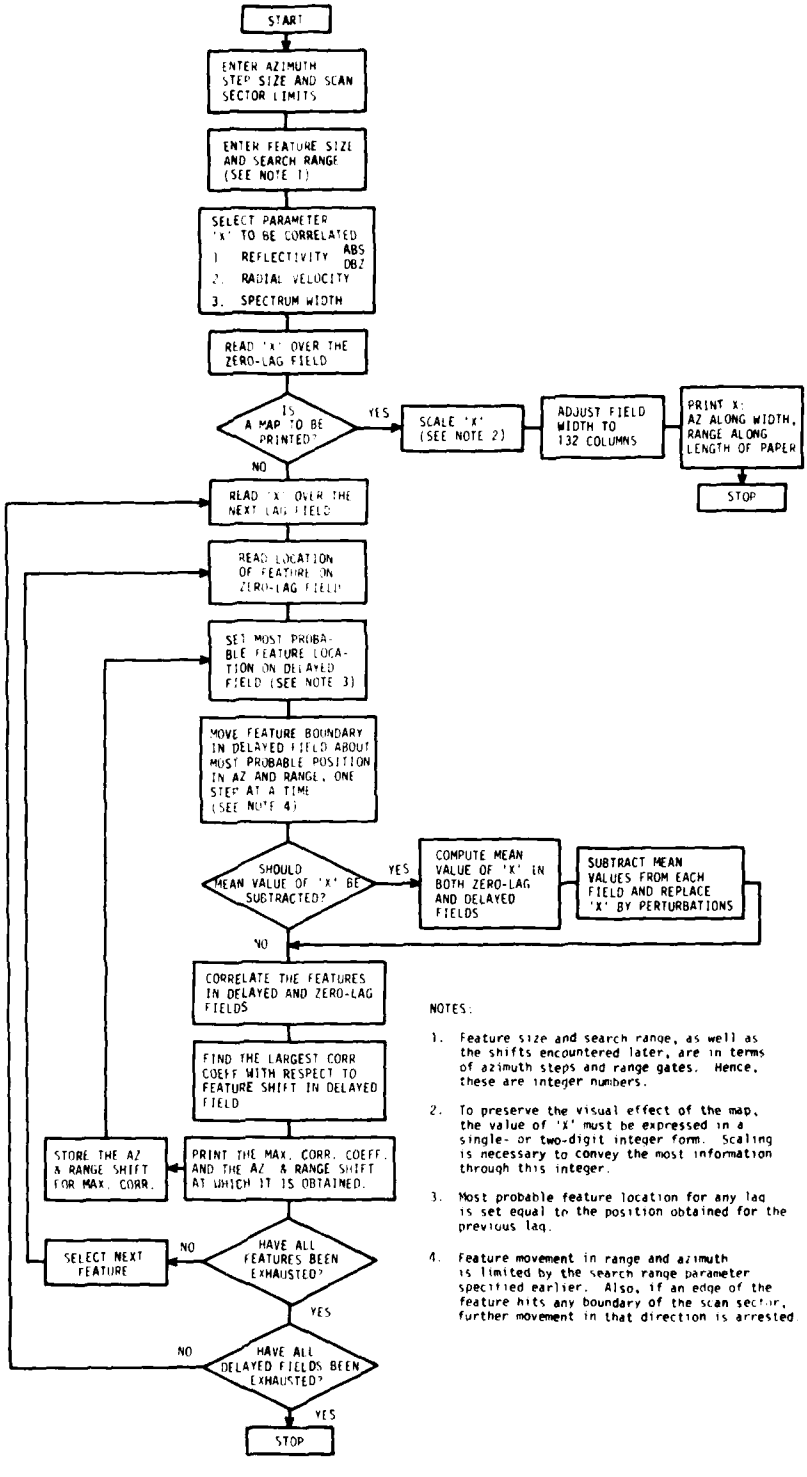

Figure 13 Simplified flowchart of the program for the determination of maximum correlation coefficient of each of several features at each of several time lags.

5. A feature in the first lag field is moved to each possible position within the designated area (as specified in #4 above) and correlated with its precursor in the zero lag field. The position that gives the highest correlation is assumed to be the position of the feature in the first lag field. The value and position of maximum correlation are recorded. The geometry of the correlation process is shown in Fig. 14.

6. The process is repeated for all the features specified in step #3 above for all the lag fields. For each lag field, the search area is centered at the maximum correlation position of the previous lag field, but the actual correlation is performed with the original feature in the reference field.

The correlation program, in its present stage of development, has the following limitations:

1. No automatic feature identification capability is built into the program; features in the original or reference field must be visually identified. Automatic feature identification is an involved problem by itself, and efforts are well under way elsewhere, such as those by R. Crane, to evolve algorithms for this purpose. There is also the basic question of the need for automatic feature recognition at this point in the lifetime study. The lifetime algorithm is not meant for operational implementation for air traffic control purposes, but is intended to generate statistics regarding the persistence of hazardous atmospheric features. Such studies can be carried out in a laboratory, non-real-time environment involving trained personnel. Also, the number of cases for which data suitable for lifetime studies can be collected during a year is limited, so that visual scanning of data fields is a practical proposition.

2. In developing the current lifetime algorithm, it is assumed that features merely translate in a polar coordinate, in addition to undergoing internal changes. Other possible motions such as rotation, shear, stretching, etc., are ignored. This is done to keep the problem tractable. The essential result of this assumption is that the search for highest correlation is done only by moving the feature parallel to itself along range and azimuth directions. The departure of the maximum correlation coefficient from unity is ascribed to white noise and internal readjustments within the feature. The drawback of such a procedure is that a part of correlation degradation, which might have been recovered by considering other types of motion, in general goes to make feature decay appear faster. The extent of such apparent decay enhancement is not known. However, it poses no serious problem

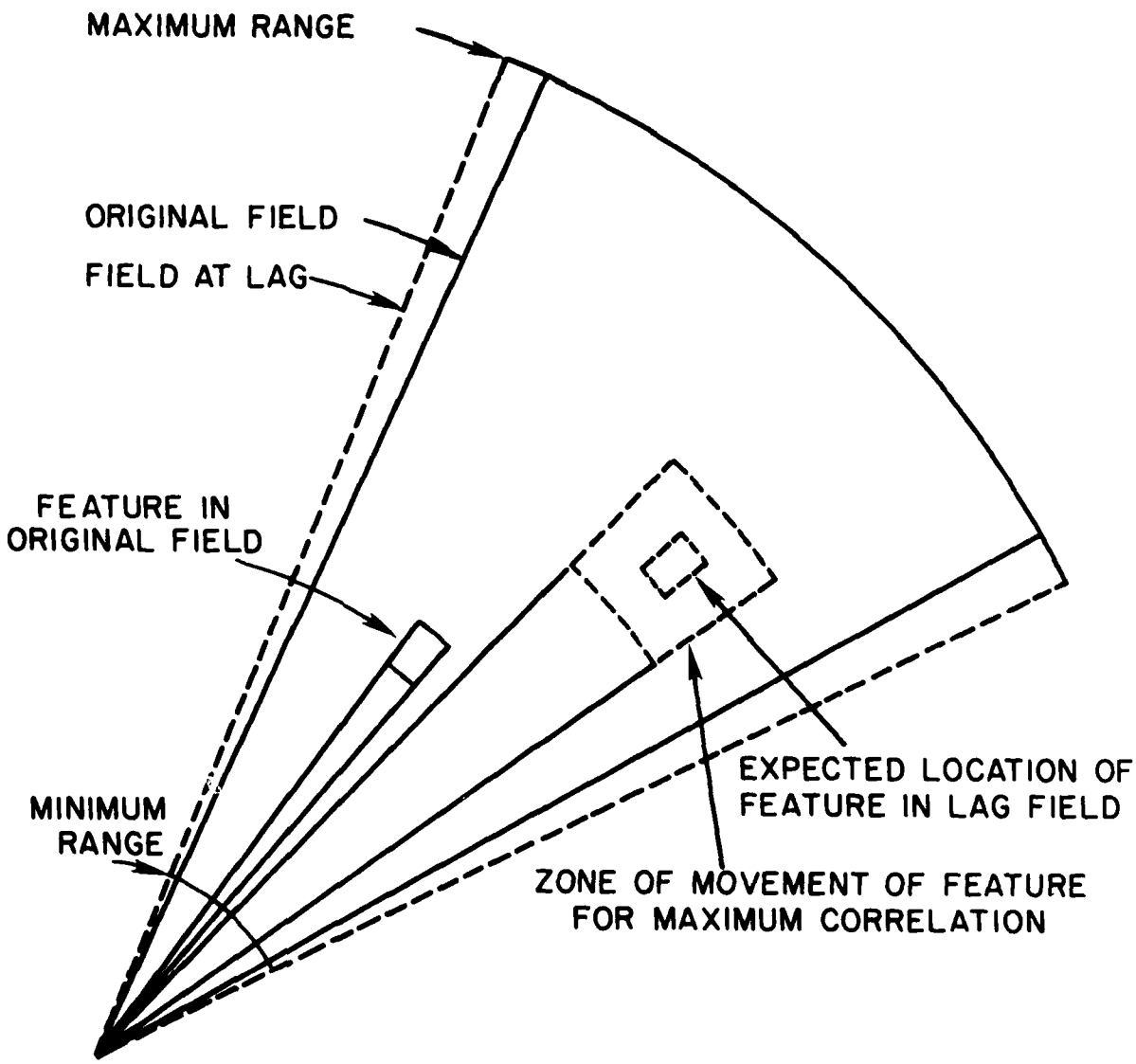

Figure 14 Geometry of the feature correlation process.

for this study since the estimate of lifetime tends to be conservative by being on the lower side.

3. At present, the three stages of the lifetime estimation procedure can handle only increasing values of azimuth, i.e., only those data obtained during clockwise scans on the PPI can be processed. This limitation has been retained again for the sake of simplicity, and causes no real problem since data for lifetime study are obtained by sector scan for rapid storm coverage; thus every alternate scan is a clockwise scan. Because the main interest in the current study is to decide between scan cycle times of 2.5 minutes or higher, even alternate scans over a sector provide sufficient temporal resolution for this purpose.

4.3 Results

Doppler radar data for several storms were subjected to correlation processing using the program sequence discussed in the last section. Several graphs are presented in this section corresponding to different features at a few scan levels for each storm. Each graph presents correlation coefficients of either the reflectivity, velocity or the spectrum width field of a particular feature at the initial time with the same field at a series of later time instants. A best-fitting curve in a least-squares sense is also drawn through the points to show the trend and to obtain a numerical value for the decay rate of the correlation coefficient.

Like all natural decay phenomena, the decrease of the correlation coefficient with time is expected to follow an exponential law of the type

$$\rho_{xy}(t) = \rho_{xy}(o^+) \exp(-\beta t) \qquad (7)$$

where $\rho_{xy}(t)$ is the maximum correlation coefficient between the zero-lag field and the field at time lag t.

$\rho_{xy}(o^+)$ is the maximum correlation coefficient between the zero-lag field and the field configuration slightly later.

β is the time-constant of the decay.

Although the correlation coefficient $\rho_{xy}(o)$ of a field with itself is unity by definition, $\rho_{xy}(o^+)$ would, in general, be less than unity because of the presence of white noise.

Equation (7) is based on the assumption that the steady-state value of the correlation coefficient is zero. However, becasue of the presence of phenomena

of different scale sizes, the actual decay law would be a superposition of many exponentials of the type given by Eq.(7). Thus, over a limited period such as the 10 or 12 minutes interval for which lifetime data have been collected and analyzed, the decay curve may appear to settle down to a nonzero steady-state value. Such a tendency was observed in many of the graphs obtained from the computer-aided correlation procedure. To account for such behavior, the following modified form of Eq. (7) was used to obtain the best-fitting curve for the computed correlation coefficients:

$$\rho_{xy}(t) = \rho_{xy}(\infty) + [\rho_{xy}(o^+) - \rho_{xy}(\infty)] \exp(-\beta t) \qquad (8)$$

Here $\rho_{xy}(\infty)$ is the steady-state value of the correlation decay curve. It may be noted that Eq. (8) is a more general form which reduces to Eq. (7) if $\rho_{xy}(\infty)$ is assumed to be zero. Thus if indeed Eq. (7) is the best fit for a particular set of points in preference to Eq.(8), the optimization program which minimizes the rms error would automatically select Eq.(7) by assigning zero to the steady-state value.

Before proceeding to present the results of computation, it is necessary to establish a way of interpreting the correlation history curves to obtain a quantitative measure of lifetimes. This in turn requires an understanding of the significance of the three parameters of curve(s), namely, $\rho_{xy}(o^+)$, β and $\rho_{xy}(\infty)$. The first of these may be interpreted as the true autocorrelation of the feature at zero lag, i.e., white noise effects are isolated. Thus, the more the noise content in the observations, the more will $\rho_{xy}(o^+)$ fall short of unity. To obtain a quantitative estimate of lifetime, it appears logical not to set an absolute threshold, but a threshold that is a certain fraction of $\rho_{xy}(o^+)$. At this point a certain amount of arbitrariness is inevitable. We measure lifetime of a feature as the interval during which the maximum correlation coefficient curve, as a function of time, remains above 0.5 $\rho_{xy}(o^+)$.

The other two parameters, i.e., β and $\rho_{xy}(\infty)$ depend on the relative scales of structures within the feature being correlated. A larger value of β, corresponding to faster decay, usually signifies a strong fine structure within the feature. On the other hand, a large residual or steady-state correlation $\rho_{xy}(\infty)$ indicates the presence of significant large scale structures. Thus, the correlation history curves given below provide more information regarding the evolution of each feature than a single number signifying its lifetime.

A brief discussion is in order here on the choice of features for correlation. It would be ideal to study each individual cell within the storm, but automatic recognition and location of the center and boundary of each cell is a highly involved problem by itself and has not been attempted here. Instead, feature selection is done by looking at a computer printout of the moment field. For simplicity, a "rectangular" feature shape has been used, i.e., the feature is bounded between two radials and two range circles. The features have been generally so chosen as to include a peak (which may be local) in at least one of the moment fields. However, consideration has also been given to their "trackability", i.e., the presence of distinct characteristics such as significant two-dimensional gradients or variations, etc. Not all the features discussed in the following paragraphs are significant in the sense outlined at the end of section 3.2; however, they have been included to increase the statistical base available for this study. The assumption here is that there is no fundamental statistical difference between strong and weak features.

The results of computer correlation of April 24, 1980, storm Doppler data are presented in Fig. 15. The data were collected using the "normal" mode, i.e., a transmitted pulse train with uniform pulse spacing and a range gate of 150 meters. The radial lines are interpolated to a grid at 0.5° interval. A feature is taken to extend over 20 range gates and 20 radials, which translates to 3 km x 10 degrees in spatial coordinates. Figure 15(a) corresponds to a scan elevation of 0.4°. Six features are studied and the correlation history of all the three moments (corresponding to reflectivity, radial velocity and Doppler spectrum width) are shown. Several observations can be made from this set of graphs:

1. Different features within the same storm can have widely differing range of correlation values. For example, in Fig. 15(a)(i), reflectivity correlation coefficients for feature #2 lie between 0.25 and 0.54, whereas those for feature #5 remain consistently above 0.87 during the period of observation.
2. In the reflectivity field, features with large values and gradients generally have higher correlation values than those with small peak reflectivities and weak gradients. As an example, the peak reflectivities of features #1 through 6 in Fig. 15(a) are 23, 26, 35, 58 and 61 dBZ, respectively. Here, although small increments in peak reflectivities do not necessarily result in a corresponding increase in correlation, as between the first and second features, the last three features, which have very

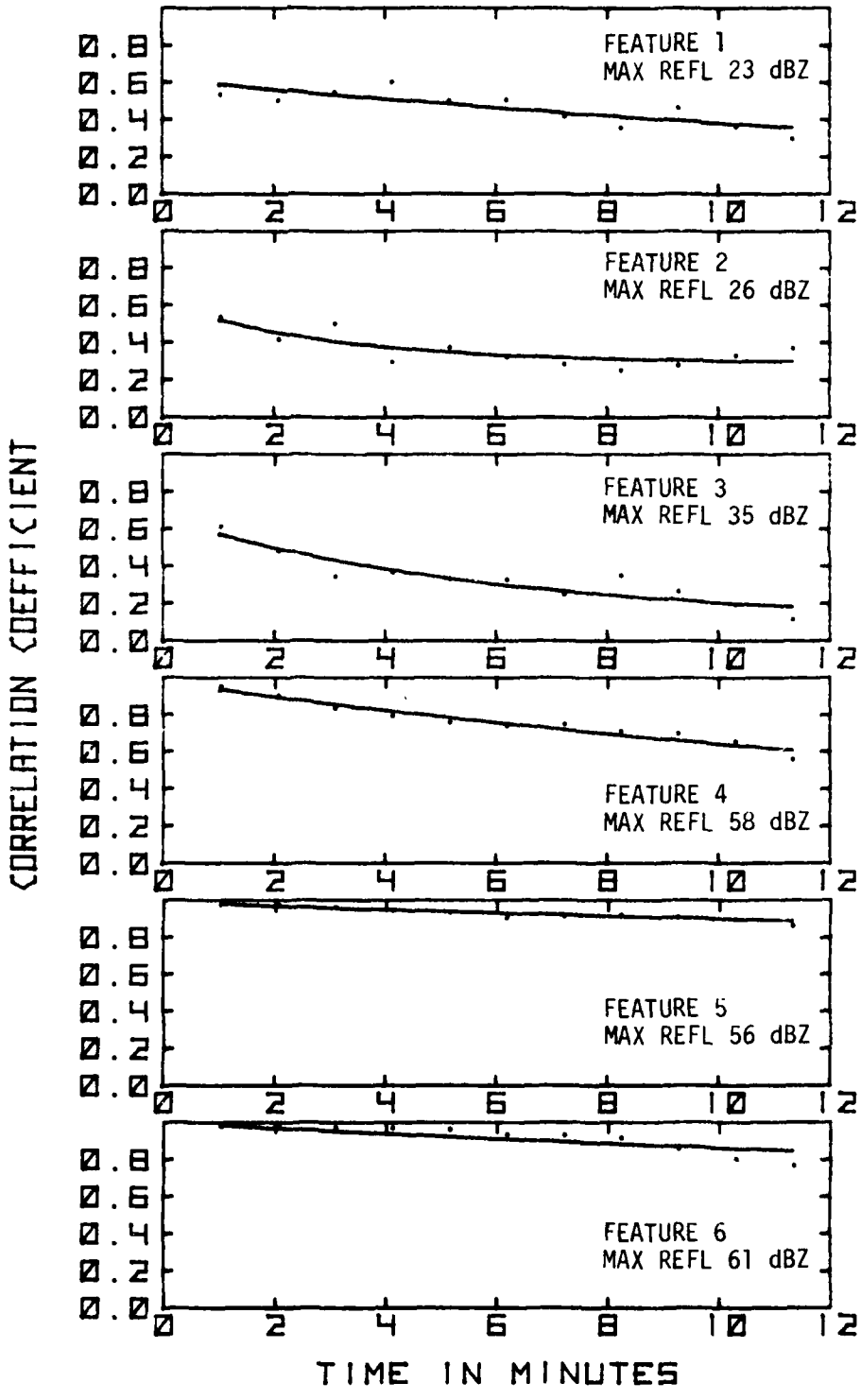

Figure 15(a)(i) Reflectivity correlation evolution of April 24, 1980 storm at 0.4° elevation.

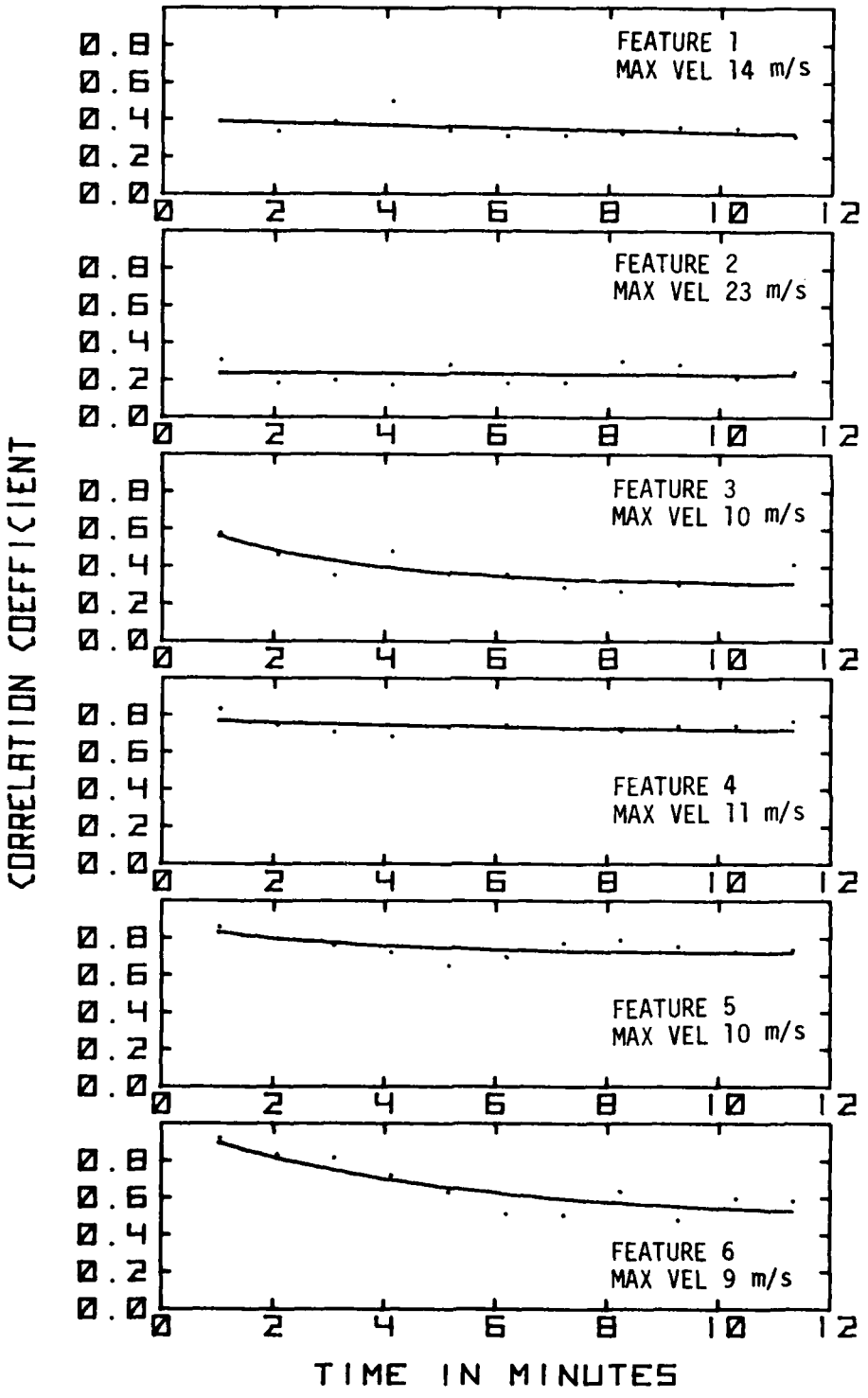

Figure 15(a)(ii) Velocity correlation evolution of April 24, 1980 storm at 0.4° elevation.

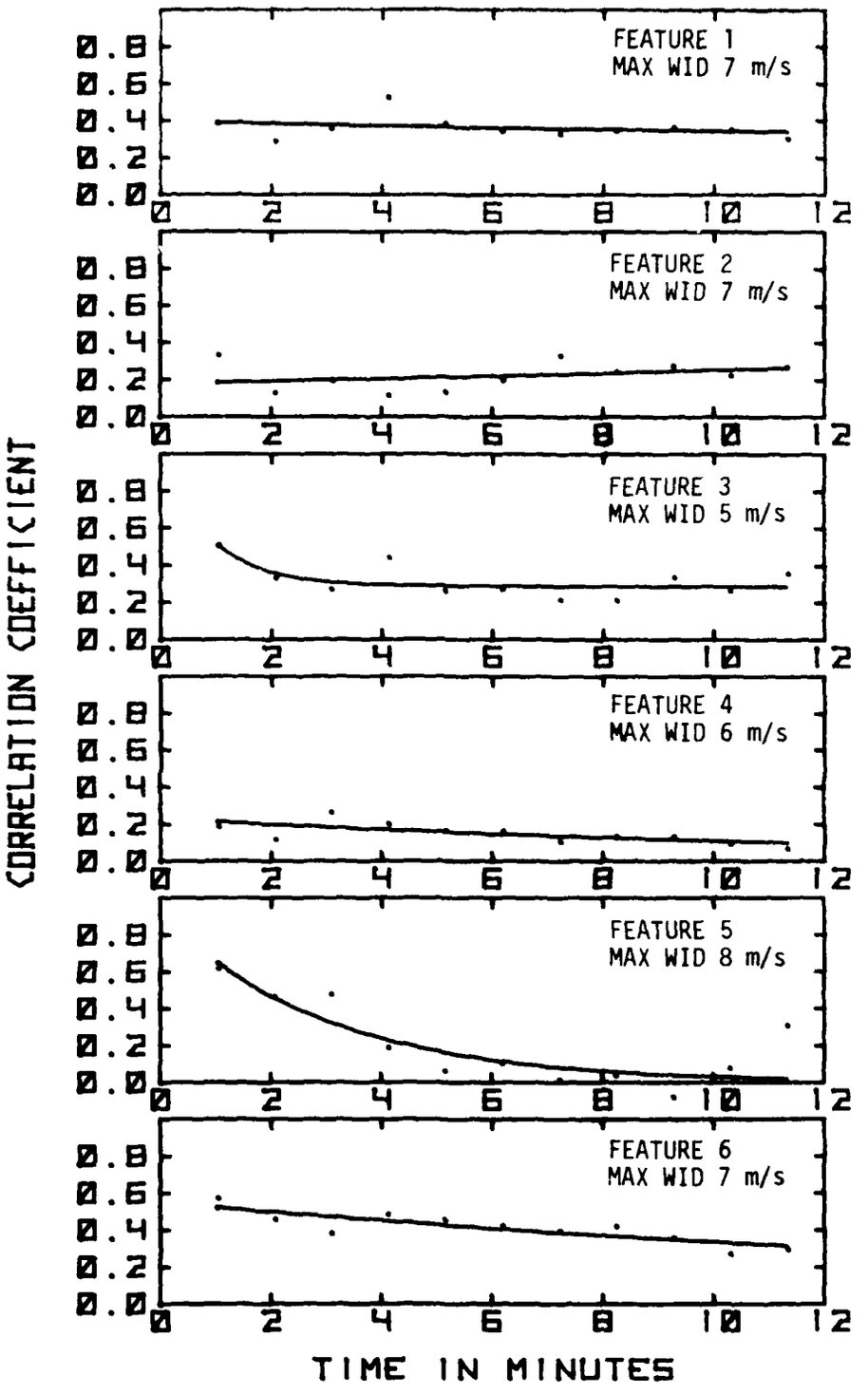

Figure 15(a)(iii) *Spectrum width correlation evolution of April 24, 1980 storm at 0.4° elevation.*

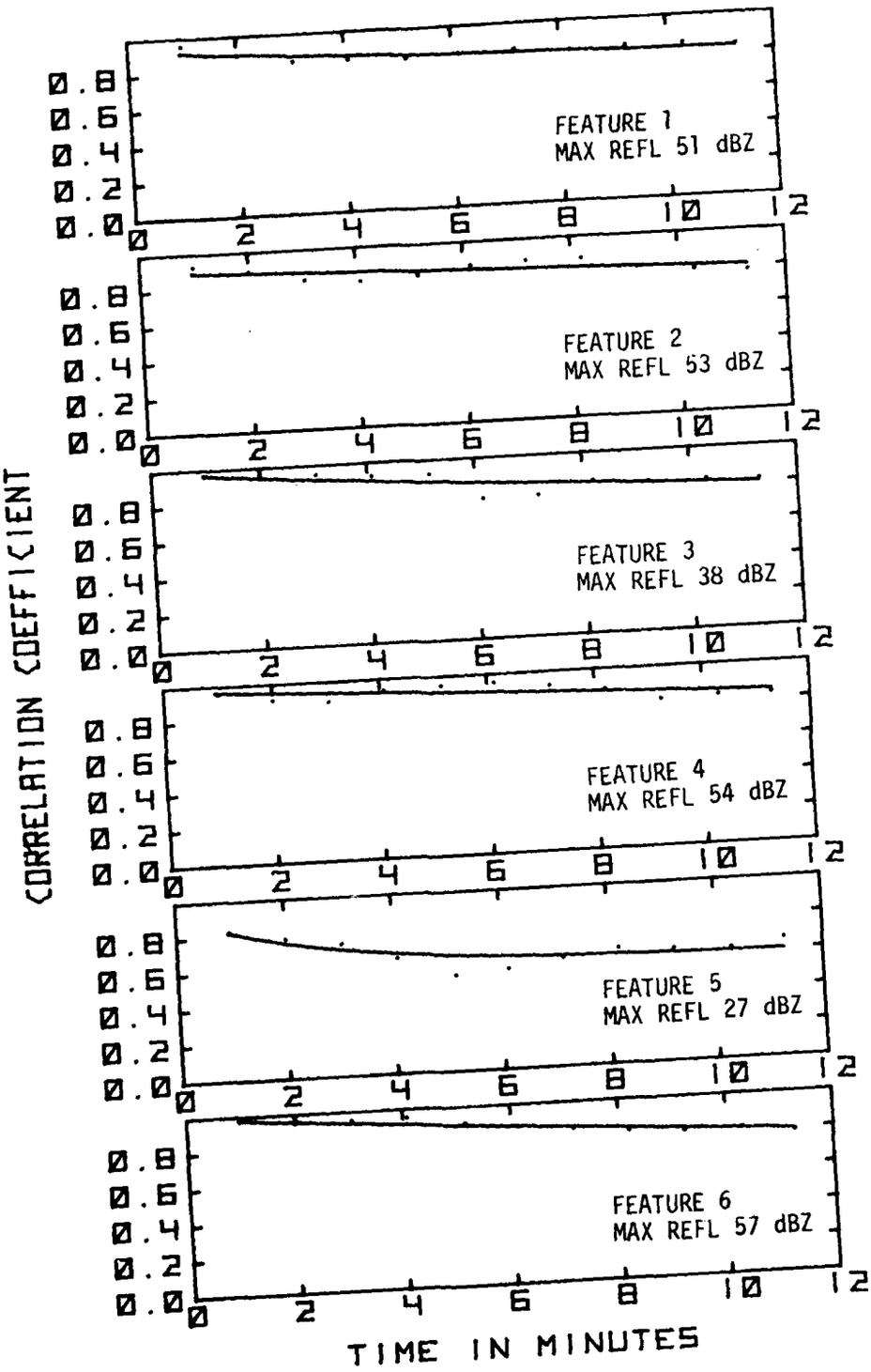

Figure 15(b)(i) Reflectivity correlation evolution of April 24, 1980 storm at 3.5° elevation.

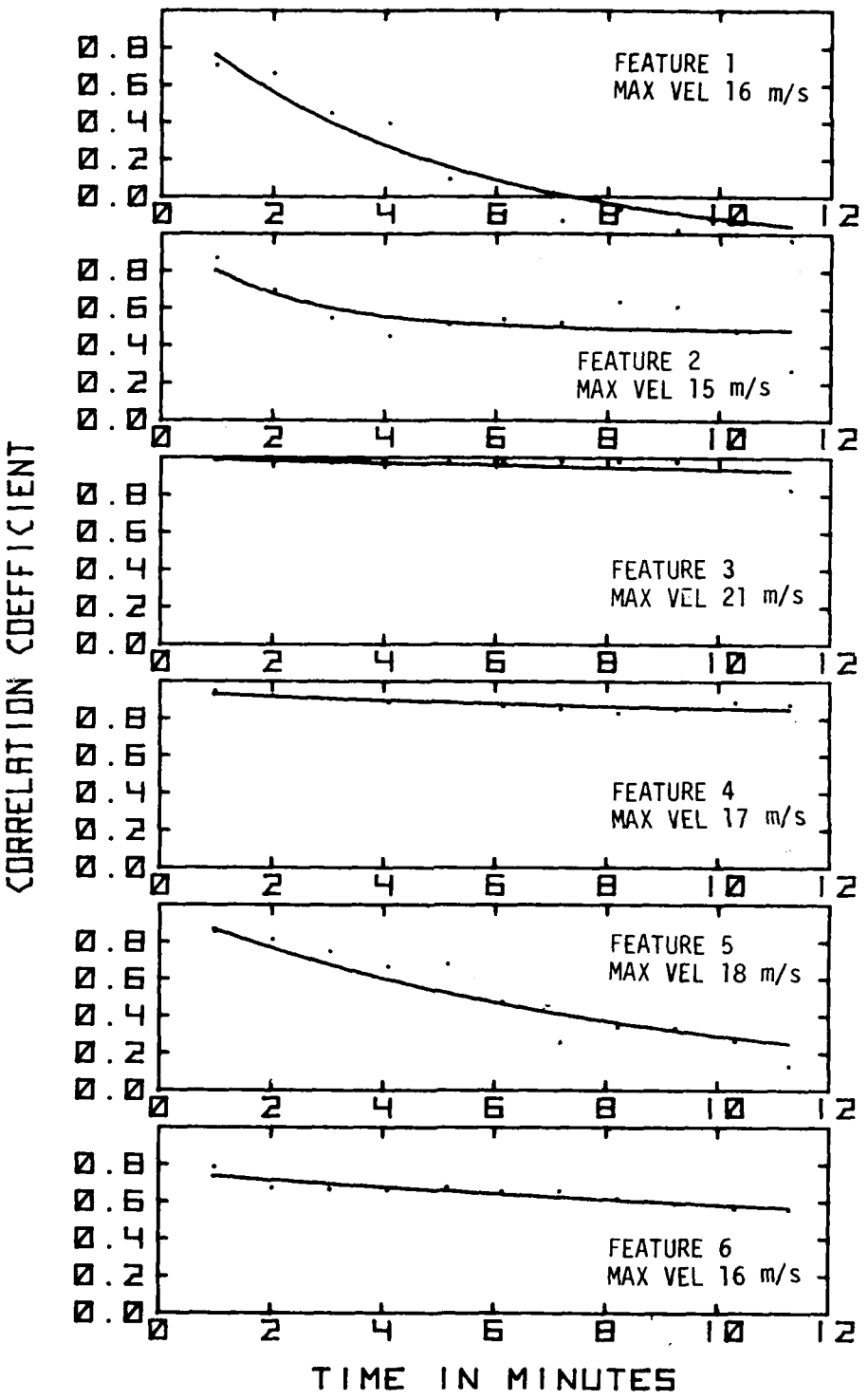

Figure 15(b)(ii) Velocity correlation evolution of April 24, 1980 storm at 3.5° elevation.

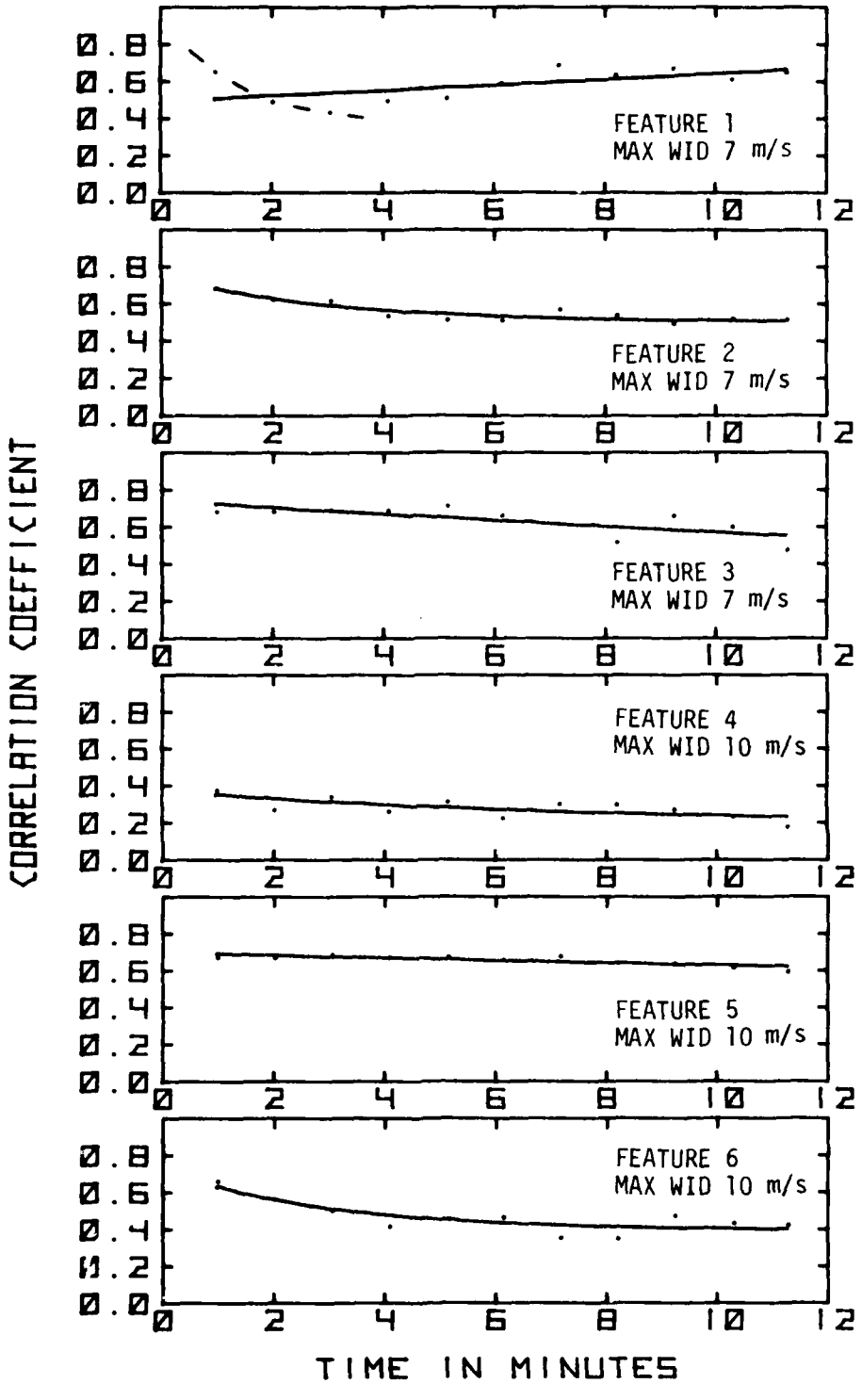

Figure 15(b)(iii) *Spectrum width correlation evolution of April 24, 1980 storm at 3.5 elevation. The initial rapid decay of feature no. 1, emphasized by joining the first three points by a dashed curve, is due to the presence of a strong fine structure in the field. For further discussion, see text.*

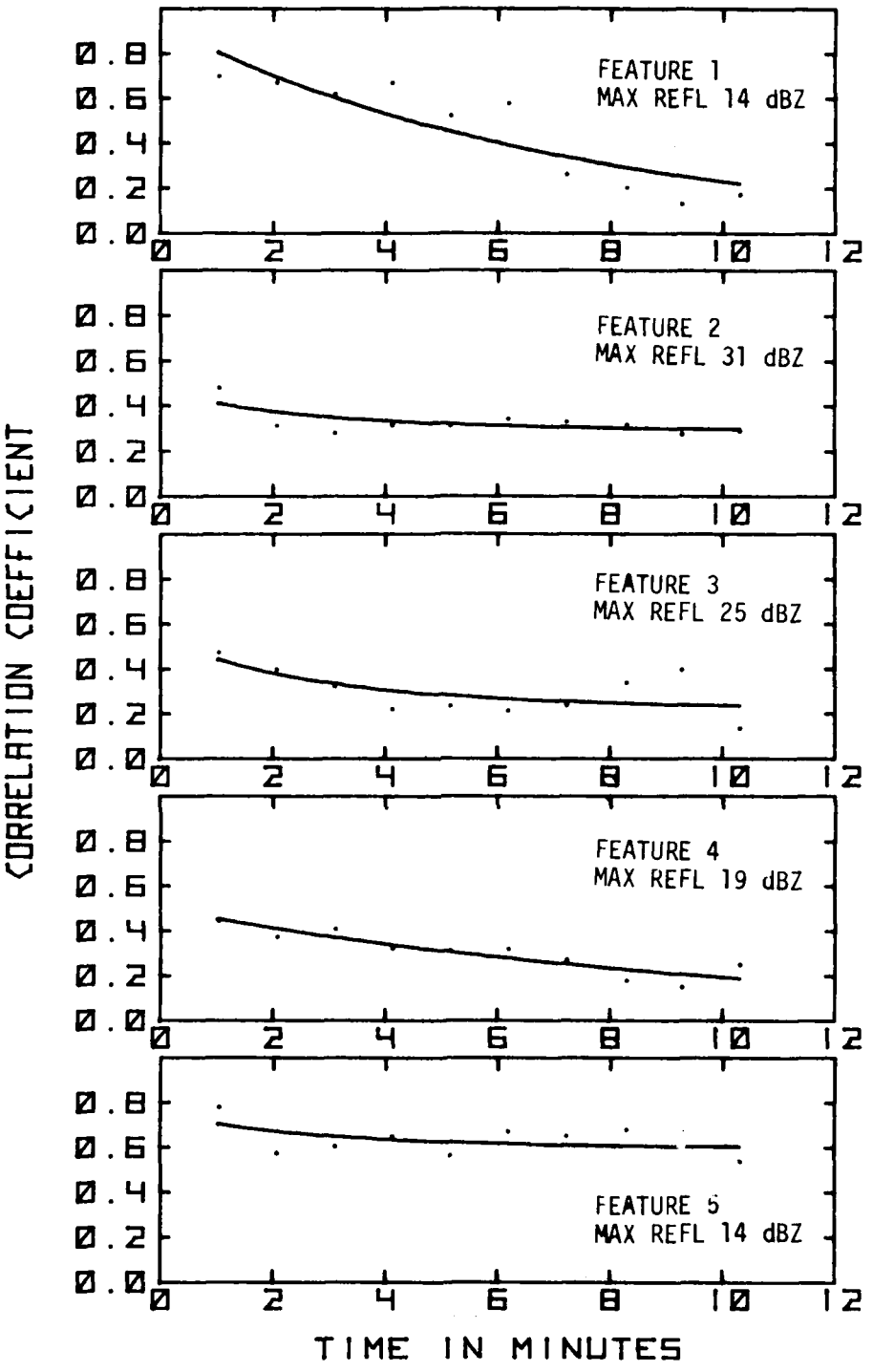

Figure 15(c)(i) Reflectivity correlation evolution of April 24, 1980 storm at 7.0° elevation.

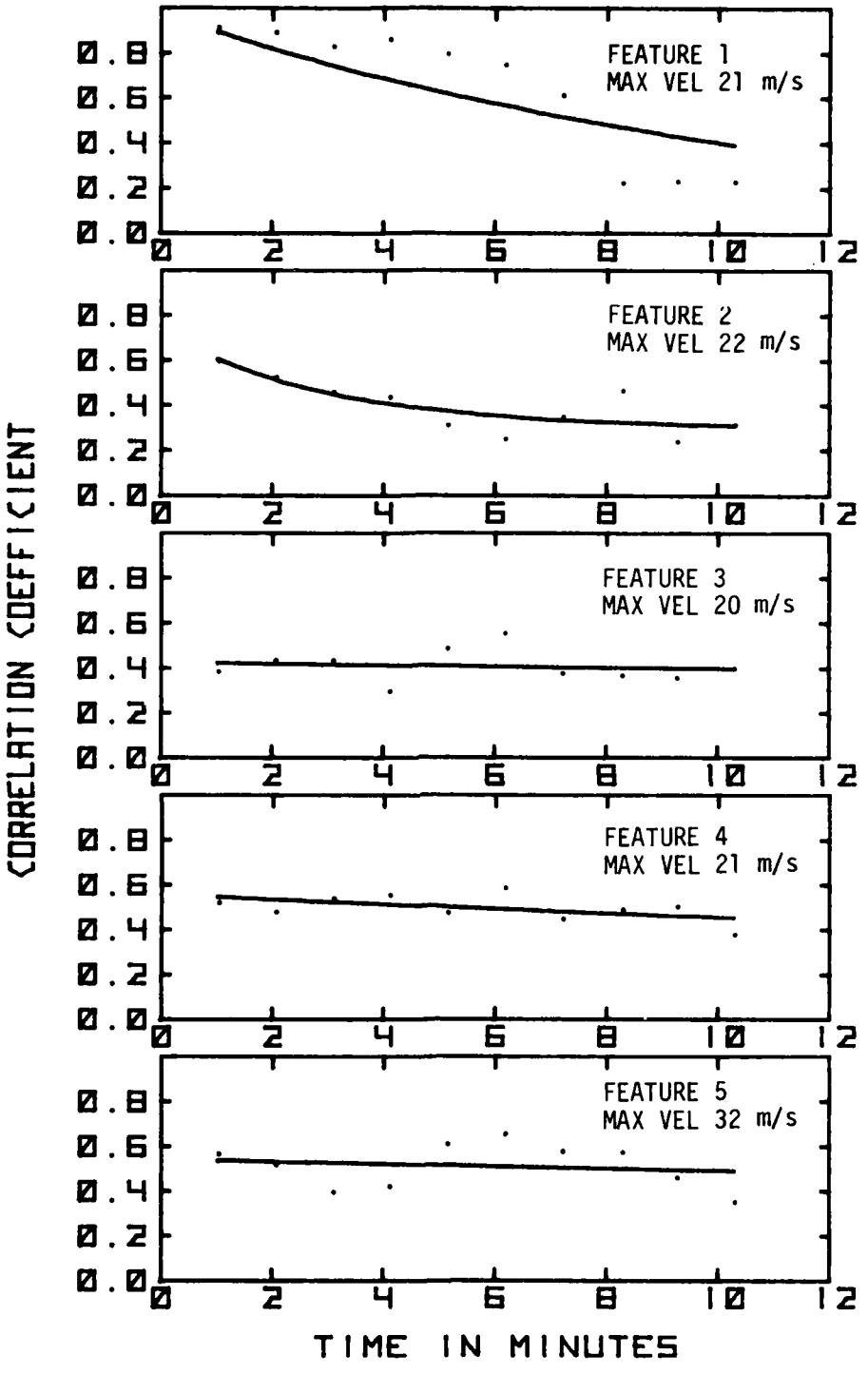

Figure 15(c)(ii) Velocity correlation evolution of April 24, 1980 storm at 7.0° elevation.

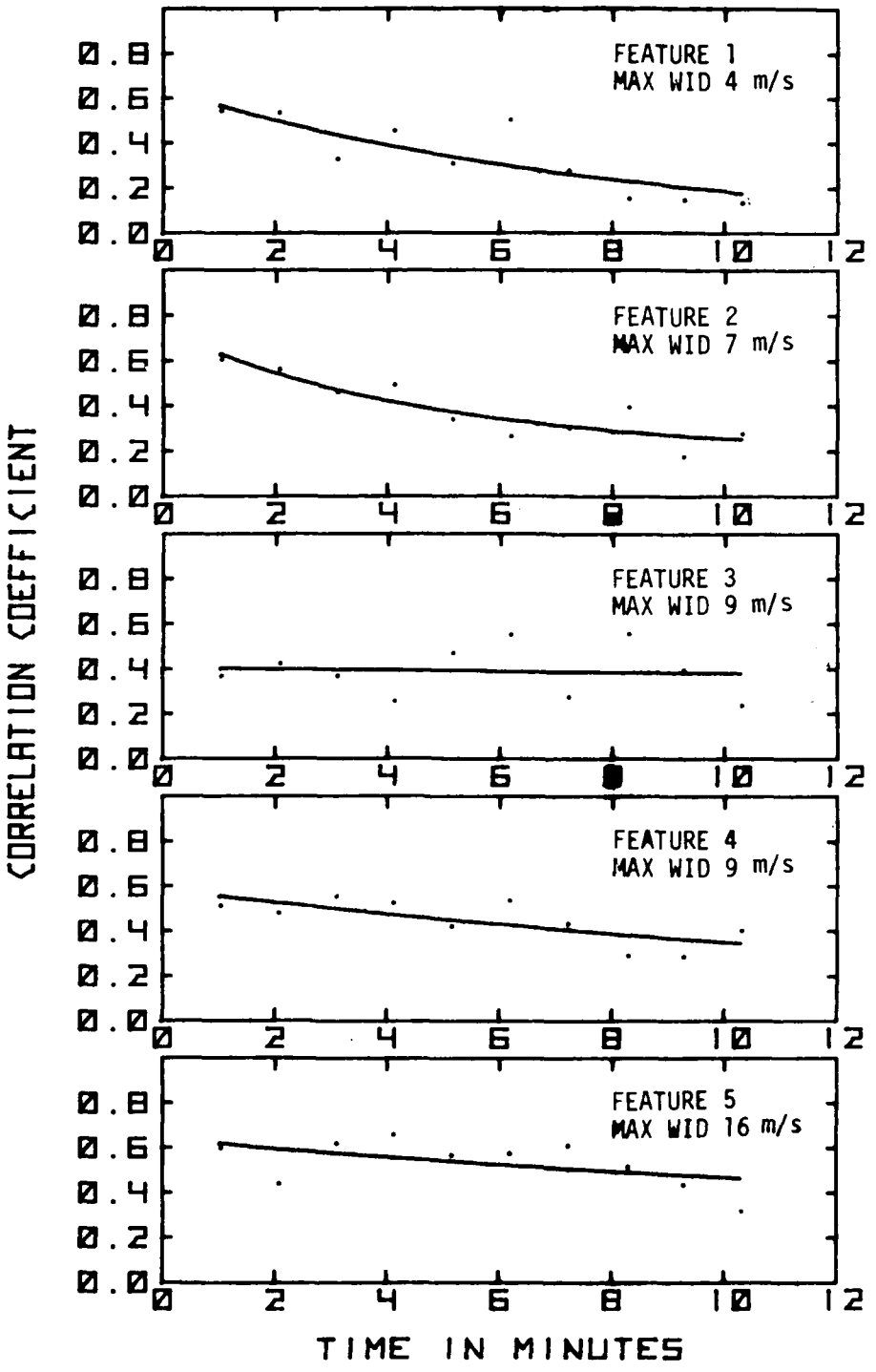

Figure 15(c)(iii) Spectrum width correlation evolution of April 24, 1980 storm at 7.0° elevation.

high peak reflectivities, have a much higher average correlation level than the first three. A high reflectivity level contributes to high correlation by minimizing the noise contribution to the shortfall of the correlation coefficient from unity. A high reflectivity gradient within the field causes larger departure of individual cell reflectivities from the feature mean. Large departures further minimize the effect of noise and, because of longer persistence, increase long-term correlation as well.

3. The correlation values in general decrease from reflectivity field through velocity field to the spectrum width field. This signifies that the noisiness in the field increases with the order of the moment. However, it is not clear how much of this noise is due to the high frequency meteorological variations and how much comes from the estimation uncertainties. But based on the signal-to-noise ratios normally encountered for echoes from storms and the behavior of estimators, we believe that the larger contribution should come from the first source. We note here that in a previous study [17] of clear air phenomena the strongest correlation was associated with the velocity field. Clearly, further research and inter-comparison of the correlation fields are in order.

4. The lifetimes of features can vary substantially depending on which field is used to estimate it. As an extreme example, in Fig. 15(a), judging by the reflectivity and velocity fields, feature #5 has a lifetime well above the 12-minute observation period, but based on spectrum width, its lifetime is of the order of 3 minutes. This observation leads to the caution that weather surveillance should be carried out using all the three spectral moments to improve the chance of detection.

5. All six features have lifetimes greater than 5 minutes, in at least one parameter field.

In Fig. 15(b) are shown correlation results for middle elevation levels, 3.4 to 3.6°. These results support the observations made above. The reflectivity map at this elevation shows heavy precipitation, exceeding 40 dBZ over extensive areas and 50 dBZ in several places and hence the reflectivity correlation of all the features at this elevation shows high values, Fig. 15(b)(i). The velocity field shows a lot of diversity. In Fig. 15(b)(ii) the velocity correlation of the first feature shows rapid decay, with a lifetime of about 3 minutes, finally reaching negative values. However, in the other two fields, i.e., reflectivity and spectrum width, the feature shows high persistence, well in excess of 12 minutes. The same is true of feature #5, though the difference between its

lifetimes in the velocity and the other two fields is less dramatic. From the three sets of graphs in Fig.15(b), the observation is again made that in at least one of the moment fields, each feature has a lifetime exceeding 5 minutes.

A discussion is in order here regarding the anomalous behavior of the spectrum width correlation of feature #1 in Fig.15(b)(iii). Such behavior recurs in a few more cases later. Instead of the expected monotonic decrease, the correlation history curve actually shows an increase with time. Such behavior may be caused by one or a combination of the two factors: (1) statistical uncertainties (2) the internal structure of the feature. If the feature contains a strong fine structure, i.e., rapid small-scale variations, such variations would die out or rearrange themselves relatively quickly, causing the maximum correlation coefficient to drop rapidly initially. This appears to be true if one considers the first three data points in the graph, which have been manually joined by a broken line to show the trend. After the maximum correlation coefficient has fallen sufficiently, spurious correlation peaks begin to compete with it. If a spurious peak exceeds the true peak, the correlation program loses track of the "original" feature and switches over to the location of the spurious peak. However, since the part of the field that caused the spurious peak is uncorrelated to the original feature, once the original feature is lost, the program will jump from one spurious peak to another (always settling for the highest peak in the vicinity of the previous peak), thus presenting an erratic behavior on the correlation evolution graph. Such a random string of points has a finite probability of showing an increasing trend. Loss of track of the original feature may be made less frequent by building in more complexities into the correlation program which recognize and follow more attributes of a feature than just the correlation coefficient. Such finer aspects have not been included in the present work for the sake of obtaining quicker results.

The results for the high level scan at 7° are shown in Fig.15(c) for five different features. Although the precipitation at this elevation was weak (maximum reflectivity 31 dBZ) the results are in general agreement with the observations made earlier. Because of lower reflectivity, the reflectivity correlation coefficients shown in Fig.15(c)(i) are smaller than those corresponding to the lower two elevations. Also, the scatter of points is larger due to relatively higher noise effects. The lifetimes of all the five features in Fig.15(c) are longer than 5 minutes.

The stability of features at two scan levels, 0.8° and 1.8°, of the storm of June 17, 1980, is represented by the sets of graphs in Figs.16(a) and 16(b), respectively. Six features have been considered at each elevation and correlation has been performed for each feature in all the three moment fields. The results show that each feature at each elevation in this storm persists over 5 minutes.

Figure 17 shows correlation results for a storm that occurred in central Oklahoma on April 3, 1981. The data for this storm were collected using the "expanded" mode of radar operation. In this mode, a sampling interval of 1 microsecond is used for Doppler processing and 4 microseconds for reflectivity measurements. Thus, in the radar data, points in the reflectivity field are spaced 600 meters apart in range, whereas those in the other two fields have a range spacing of 150 meters. Hence, a feature extending over 20 range gates and 20 radials in the interpolated grid has a spatial size of 12 km x 10° in the reflectivity field, whereas in the other two fields it has a size of 3 km x 10°. Since features in the three fields do not coincide, the graphs in Figs. 17(a)(i), 17(a)(ii) and 17(a)(iii) should not be viewed as the evolution of the three moments of the same five features; the features in each field have been selected independent of the other two. Again Fig.17(a) shows a lifetime far greater than 5 minutes for each feature in each field.

Since the velocity field of the storm at 0.4° elevation was very extensive, a further set of six features were considered in the velocity field only. The correlation evolution of these features are shown in Fig.17(a)(iv). Although the wind field was quite strong, reaching radial speeds of 18 m/s, the correlation coefficients in Fig.17(a)(iv) are seen to be rather low. This behavior may be traced to the relative uniformity of the wind field. When the value of the parameter being correlated has a small range of variation over the entire feature, irrespective of the actual parameter value, its perturbation over the mean is small, perhaps of the same order as the basic measurement uncertainty. Then the uncertainty acts as white noise, causing the correlation coefficients at all delays but zero to be small. To test this hypothesis, correlation evolution was computed for three large features, each extending over 60 range gates and 50 radials (9 km x 25°). The results are shown in Fig. 17(a)(v). When a larger number of points in a white noise process are correlated, the central spike (or delta-function located at the origin) becomes sharper and the scatter of points is reduced. The graphs in Fig.17(a)(v) show such a behavior, with low,

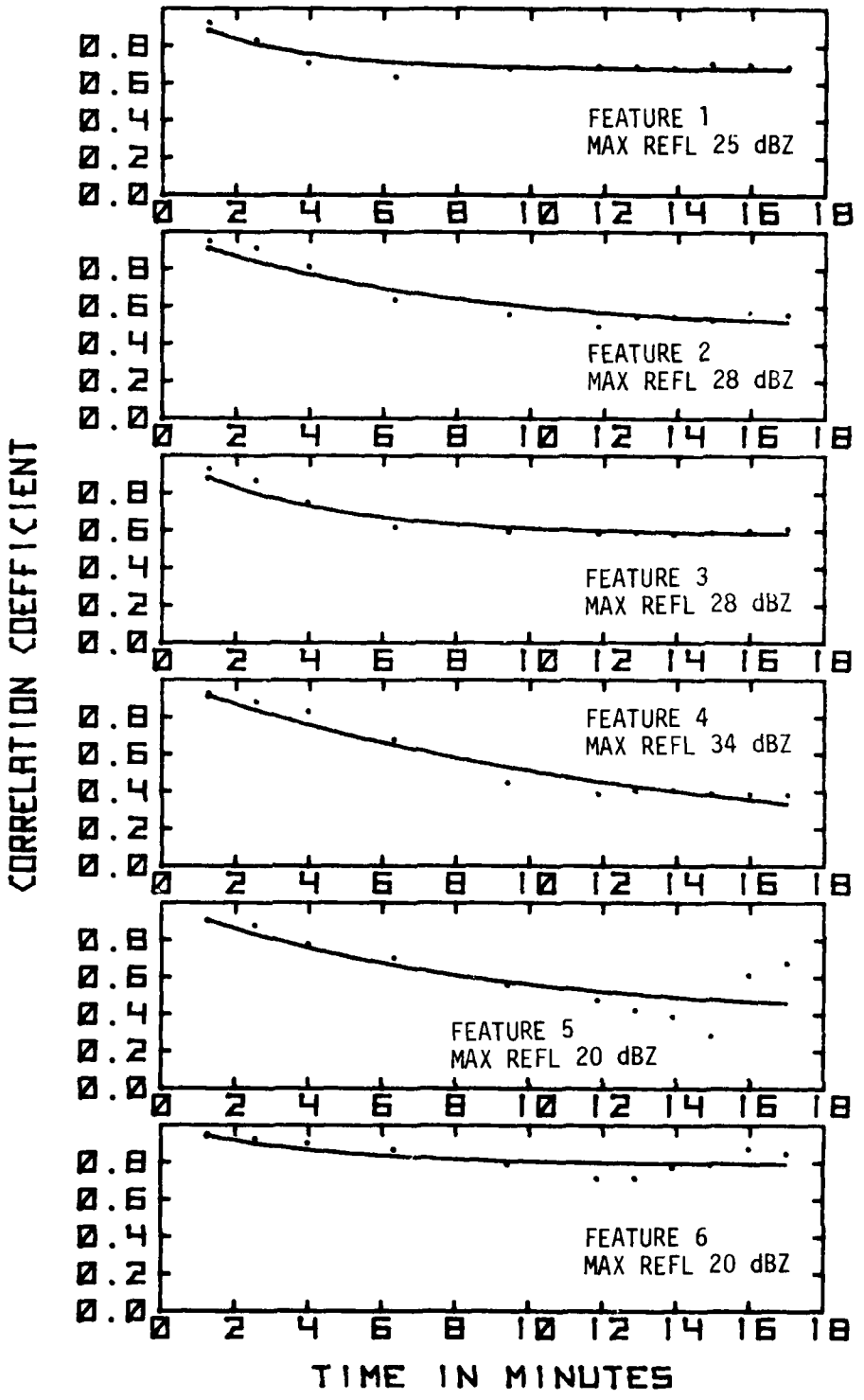

Figure 16(a)(i) Reflectivity correlation evolution of June 17, 1980 storm at 0.8° elevation.

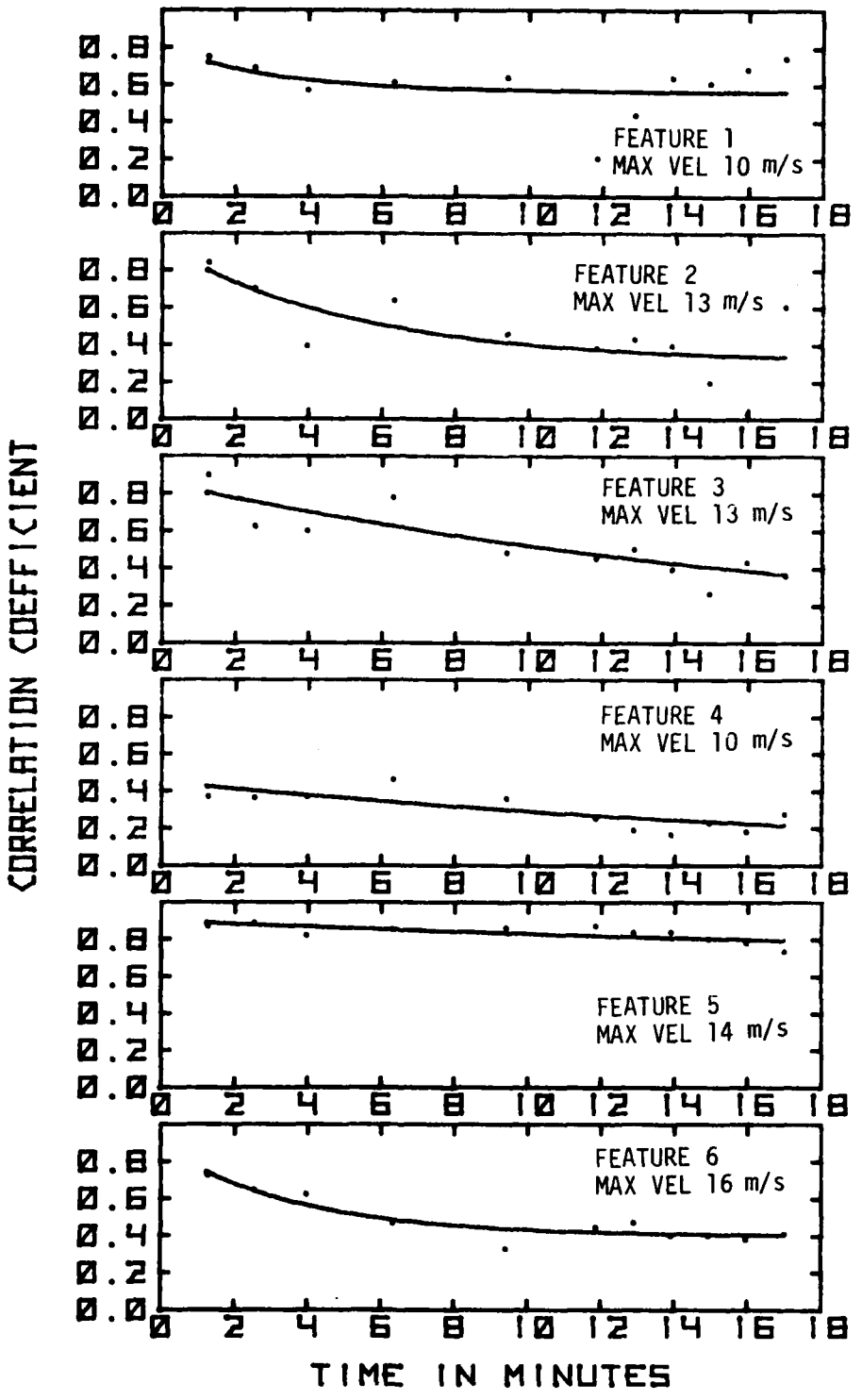

Figure 16(a)(ii) *Velocity correlation evolution of June 17, 1980 storm at 0.8° elevation.*

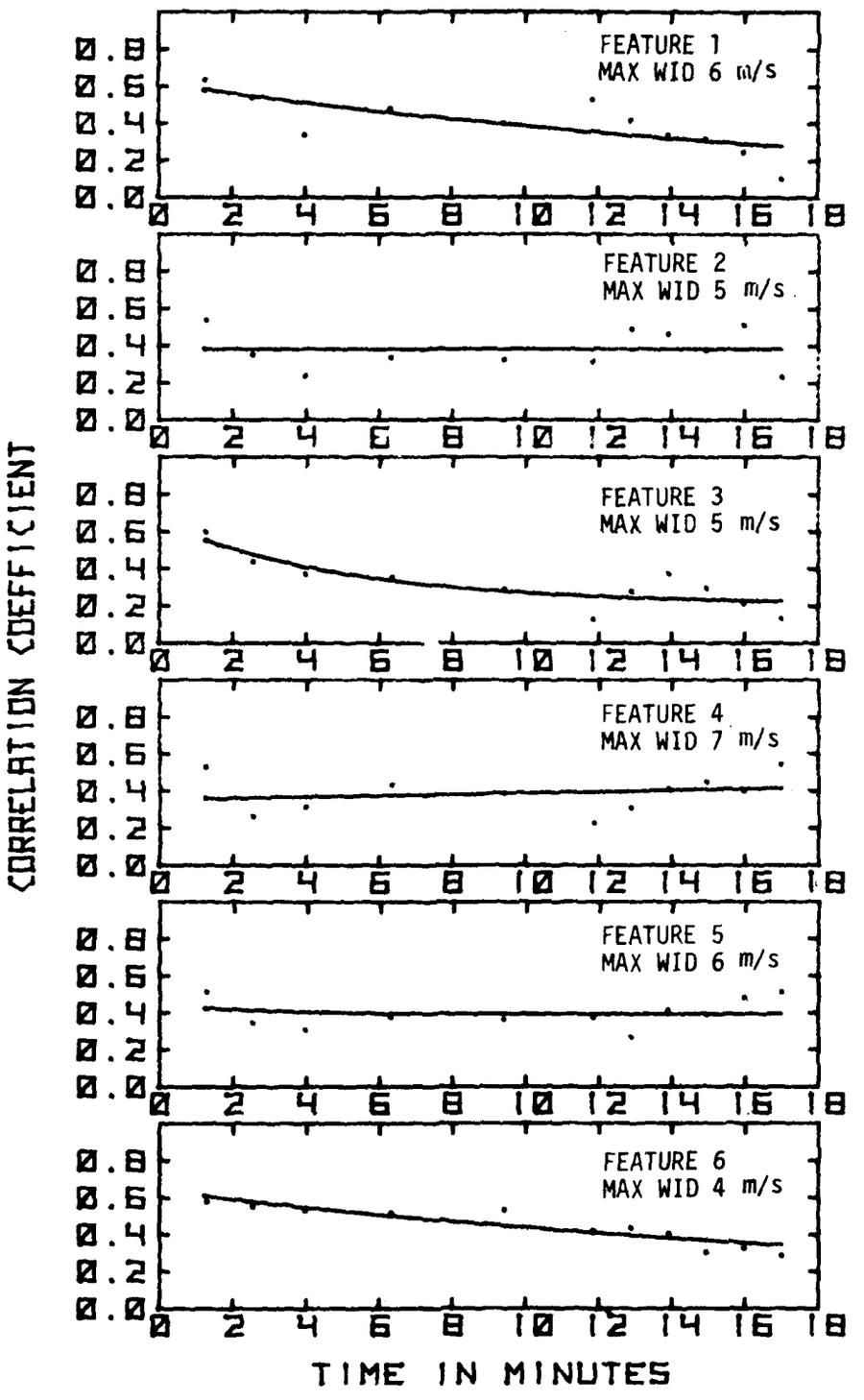

Figure 16(a)(iii) Spectrum width correlation evolution of June 17, 1980 storm at 0.8° elevation.

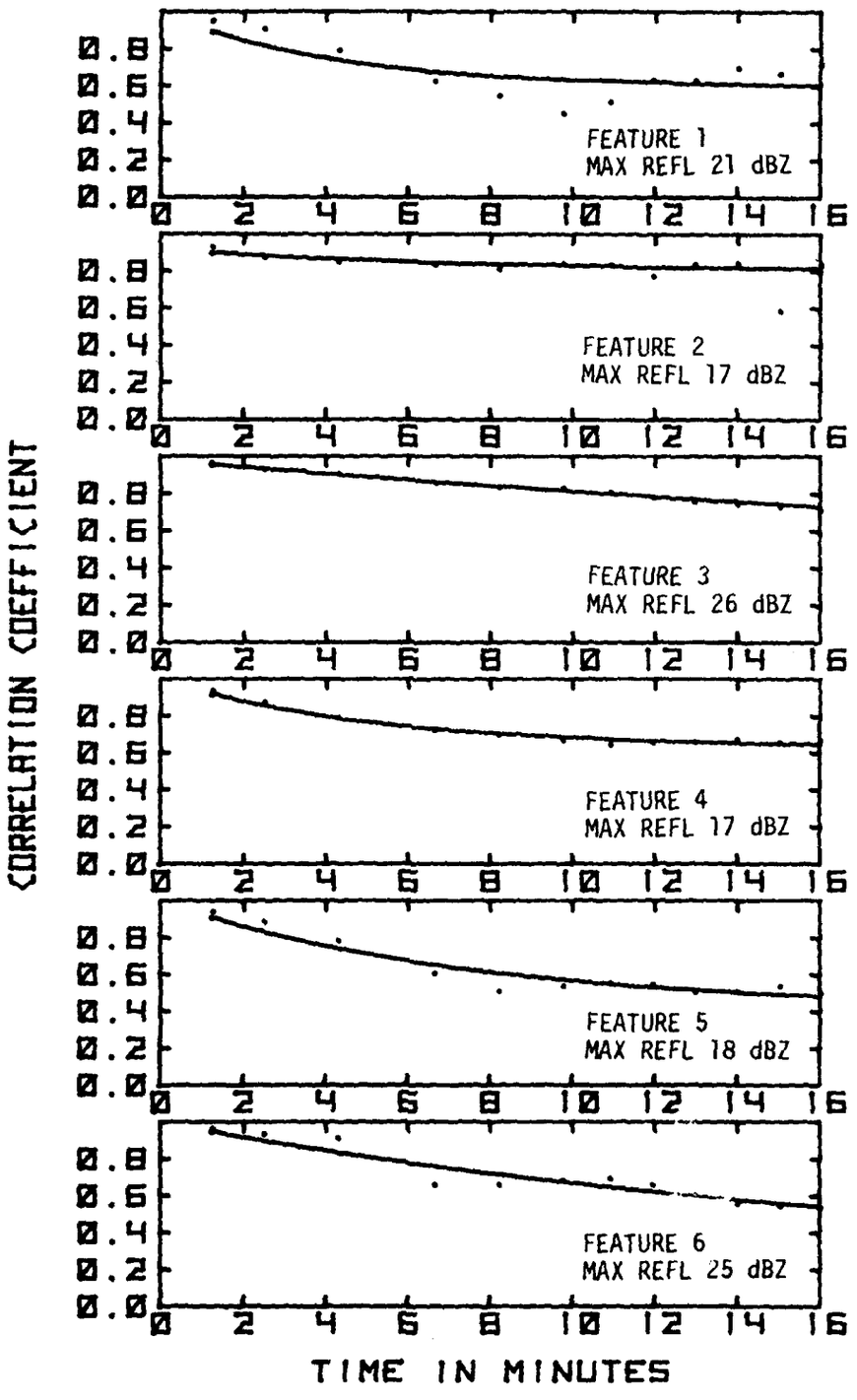

Figure 16(b)(i) Reflectivity correlation evolution of June 17, 1980 storm at 1.8° elevation.

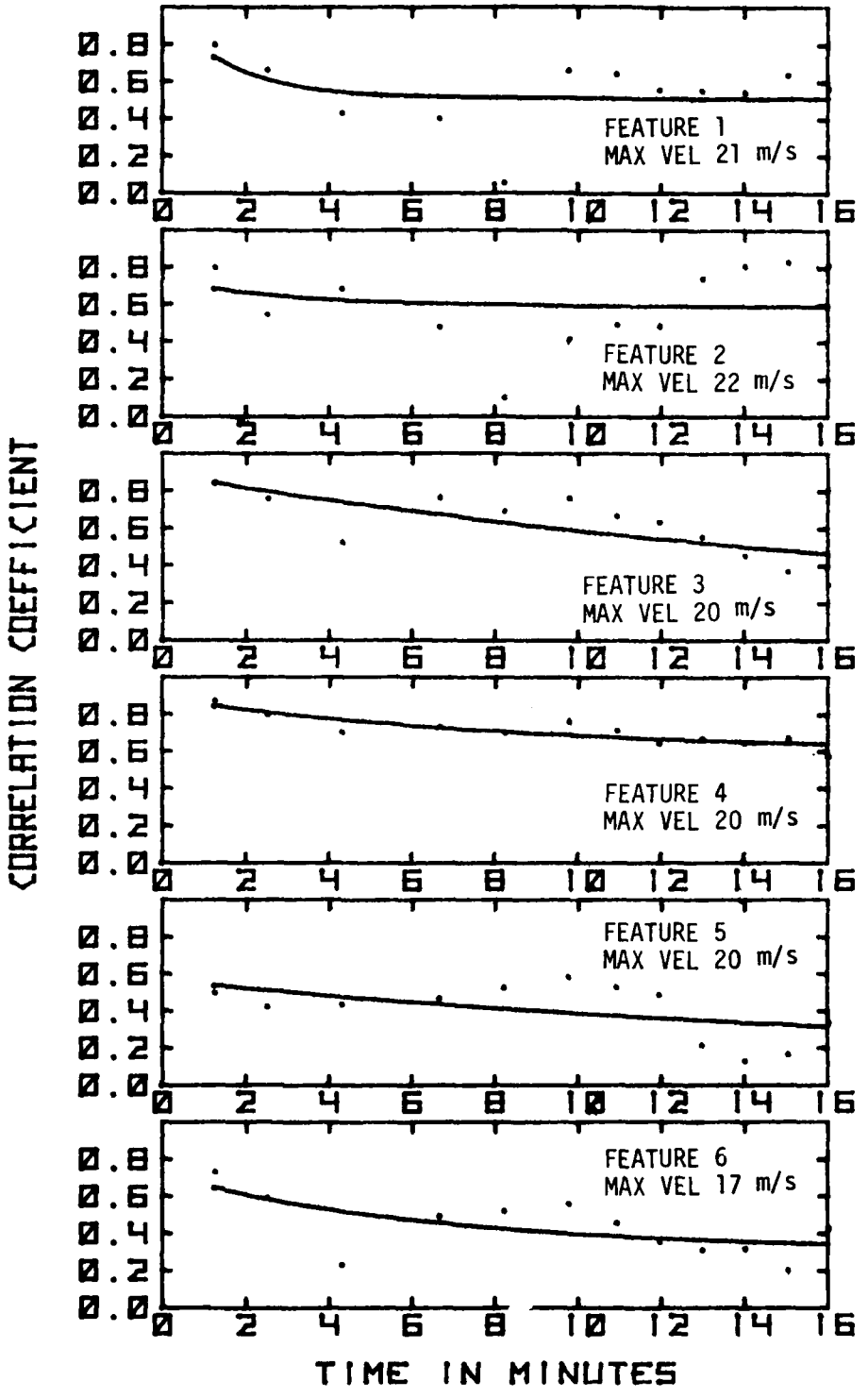

Figure 16(b)(ii) Velocity correlation evolution of June 17, 1980 storm at 1.8° elevation

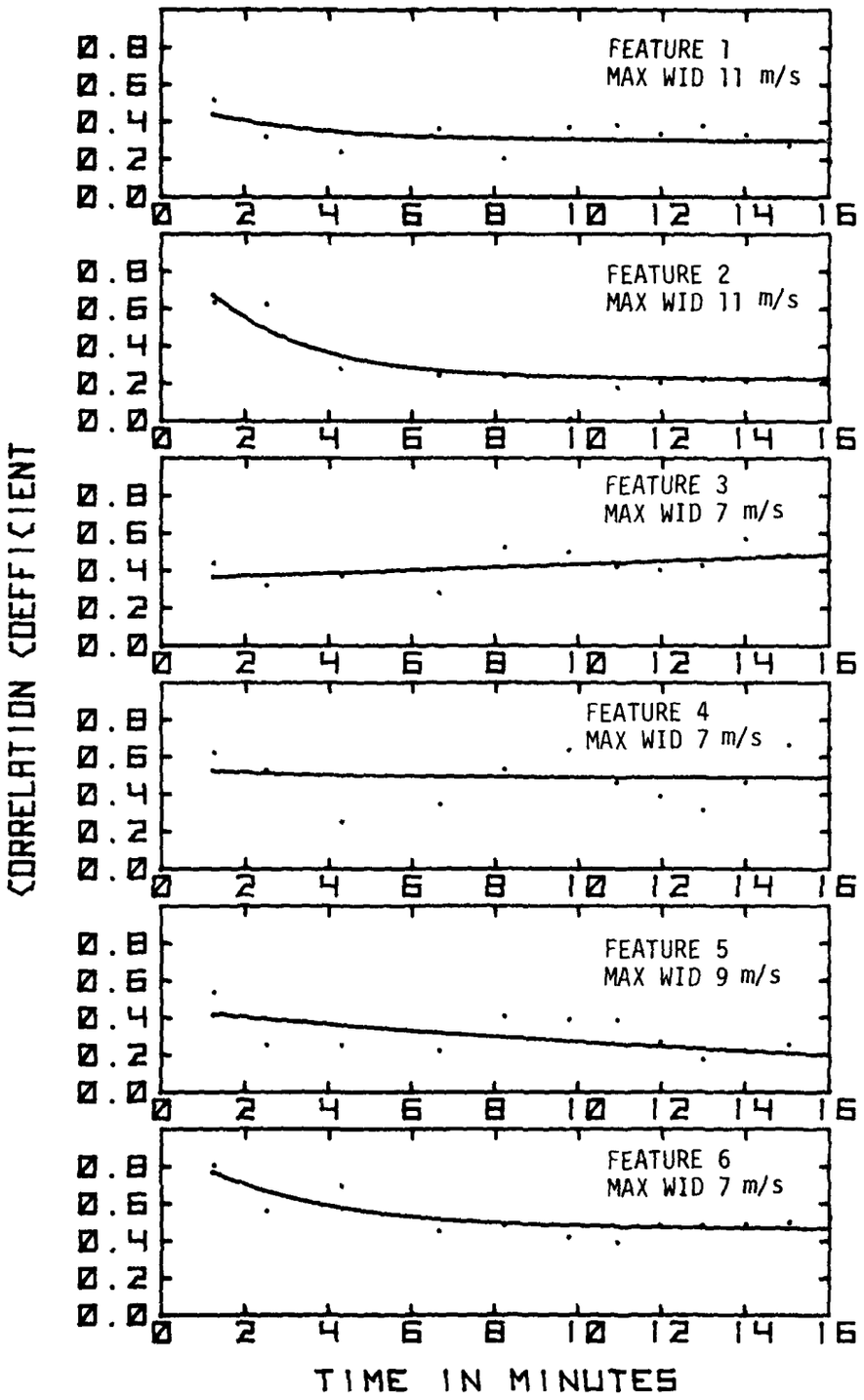

Figure 16(b)(iii) Spectrum width correlation evolution of June 17, 1980 storm at 1.8° elevation.

nearly uniform correlation away from origin and greatly reduced scatter of individual points in comparison to Fig.17(a)(iv).

Correlation method alone appears to have a disadvantage in tracking and estimating the lifetimes of small features in a large uniform field. One way to minimize this problem is to assume feature boundaries well outside the flat portion of the field. However, this may result in feature sizes that are very large, resulting in loss of resolution and large computational requirements. Also, since larger features tend to persist longer, very large features are not likely to resolve the question of whether the data update rate should be 5 minutes or 2.5 minutes; they would probably always last much longer than 5 minutes.

Correlation results for the 4° elevation scan through the April 3, 1981, storm are shown in Fig.17(b). In Figs.(i), (ii), and (iii) of this set the evolution of five features in the reflectivity, velocity and width fields respectively are shown. Again, because of the different feature sizes in the three fields, the three sets of graphs are to be considered independently. An extra set of six features in the velocity field alone are represented in Fig.17(b)(iv). Each of the graphs in the set in Fig.17(b) indicates a lifetime longer than 5 minutes.

4.4 Summary and Conclusion

A computer-based procedure has been evolved for reducing the raw data and subjecting them to correlation analysis with facility for feature tracking. The results among a number of observations regarding the behavior of correlation evolution, show clearly that within the storms studied, no feature would have undergone sharp changes to the point of being unrecognizable within a time scale of 5 minutes, provided that all the three moment fields of the storm are under observation.

5. Concluding Remarks

5.1 Summary of Findings

The lifetimes of the significant features in several central Oklahoma storms have been studied in this report using photo-interpretation and computer-aided time-lapse correlation. The motivation for this study was to generate data which would help decide whether an update rate of once in five minutes would be adequate for aviation weather surveillance using NEXRAD, or whether it would be necessary to renew information every 2.5 minutes so that if there are fast transient phenomena, they would not be missed by falling between scan cycles.

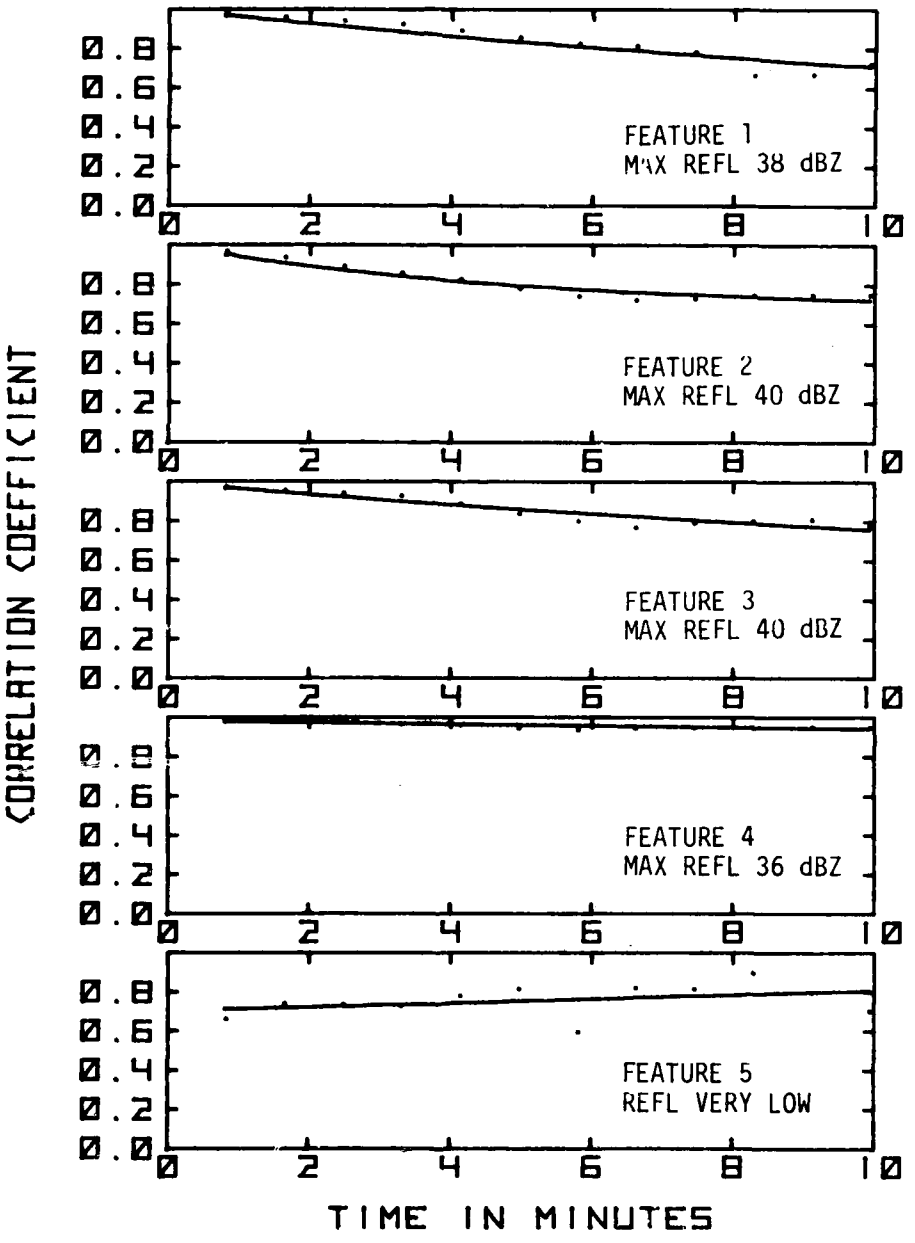

Figure 17(a)(i) Reflectivity correlation evolution of April 3, 1981 storm at 0.4° elevation.

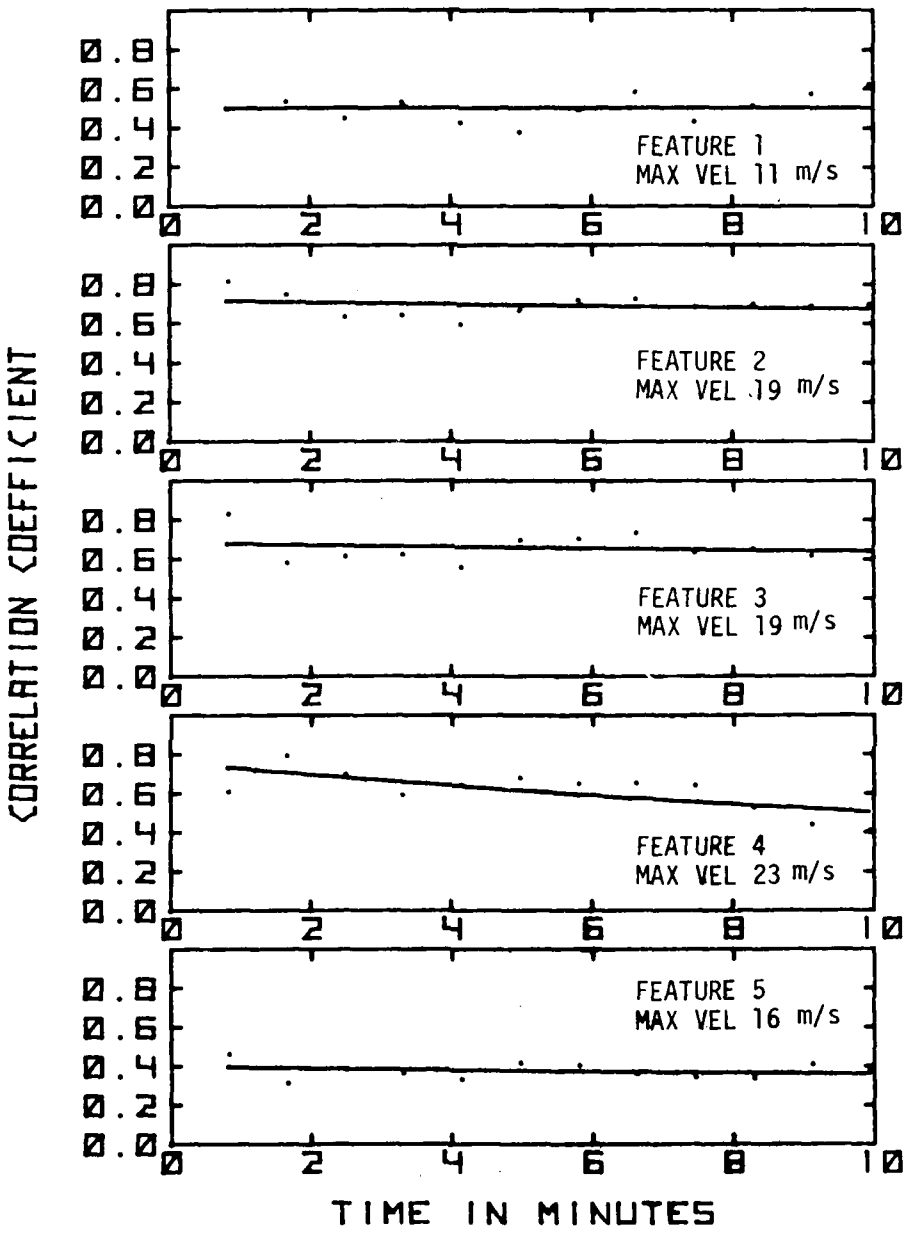

Figure 17(a)(ii) Velocity correlation evolution of April 3, 1981 storm at 0.4° elevation.

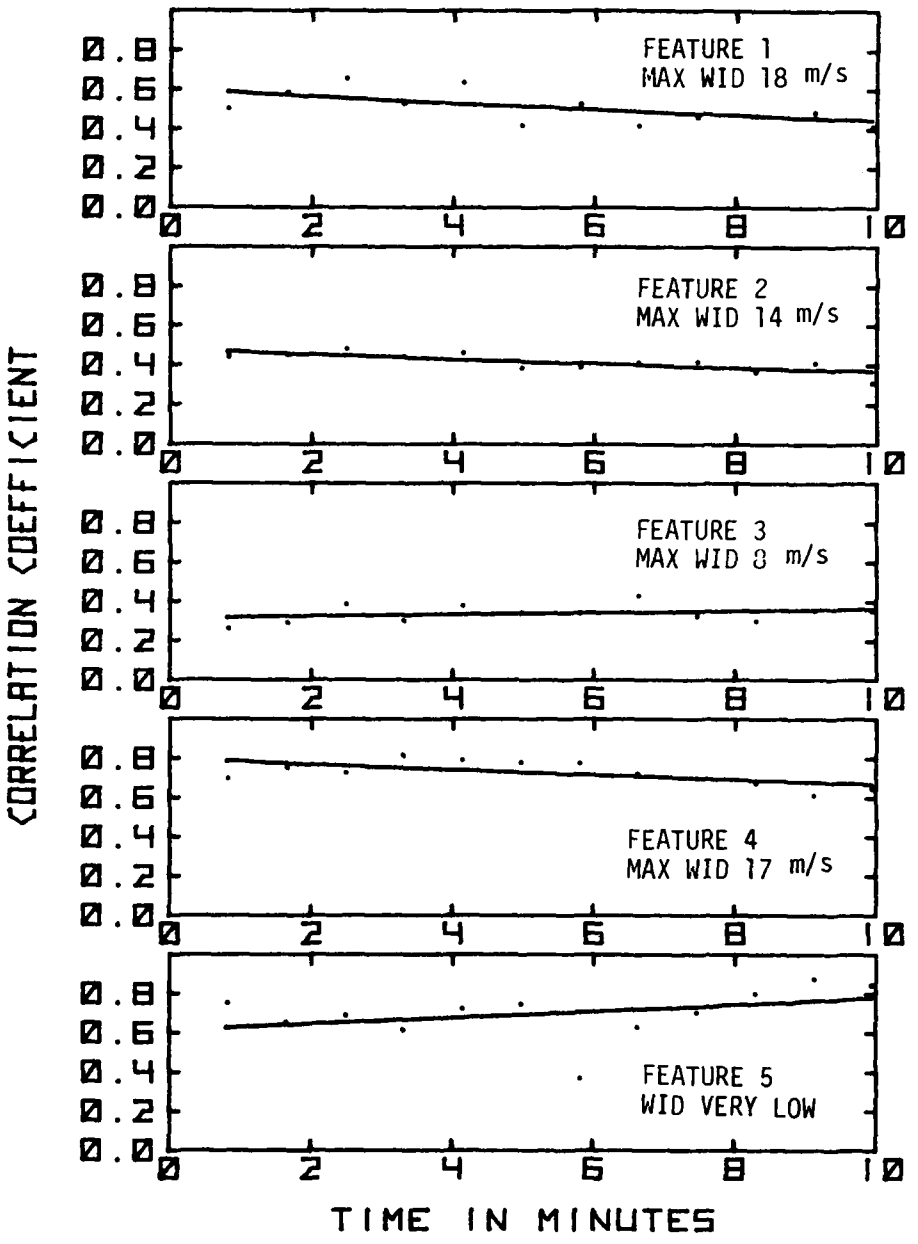

Figure 17(a)(iii) Spectrum width correlation evolution of April 3, 1981 storm at 0.4° elevation.

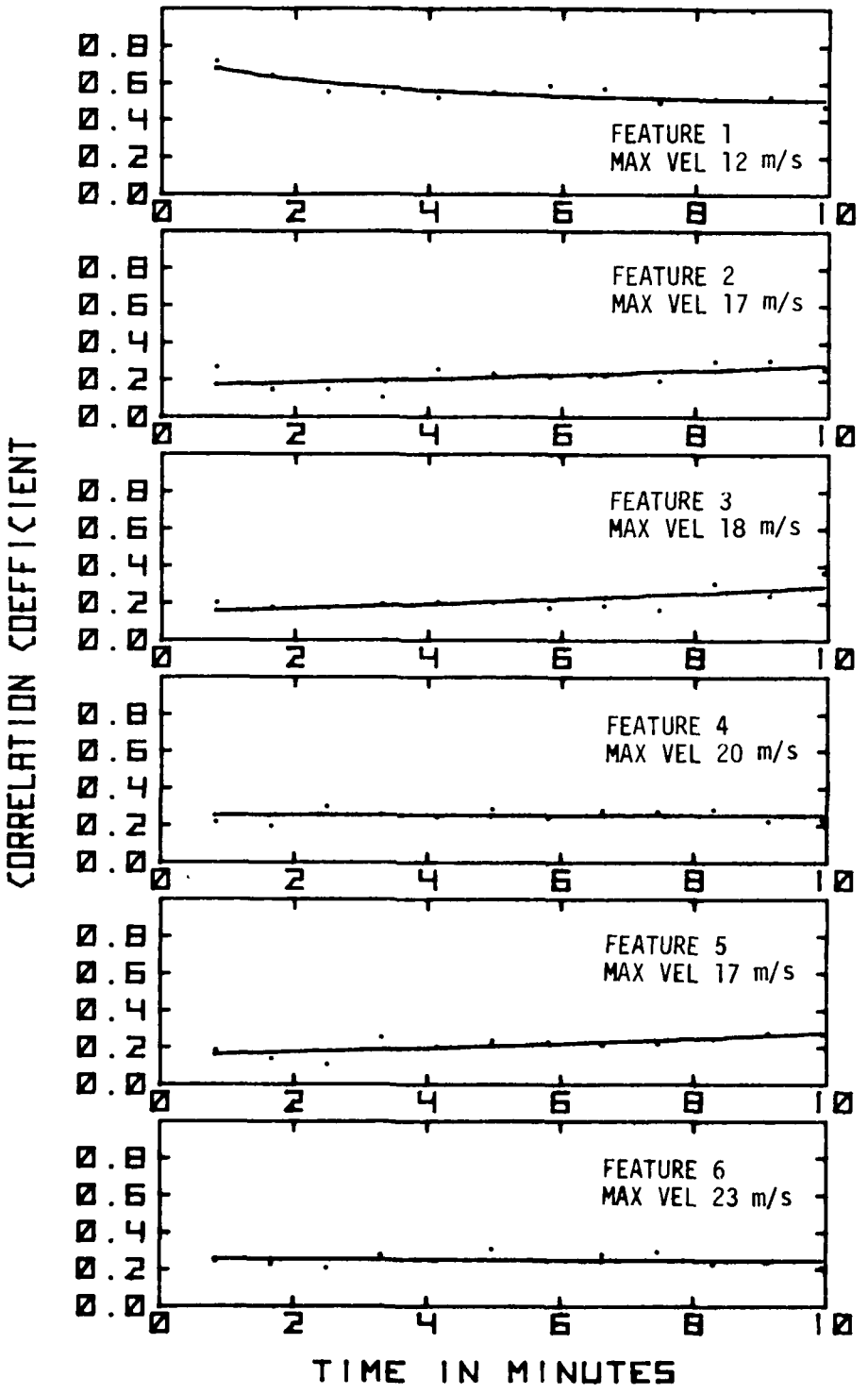

Figure 17(a)(iv) Velocity correlation evolution of six extra features in April 3, 1981 storm at 0.4° elevation.

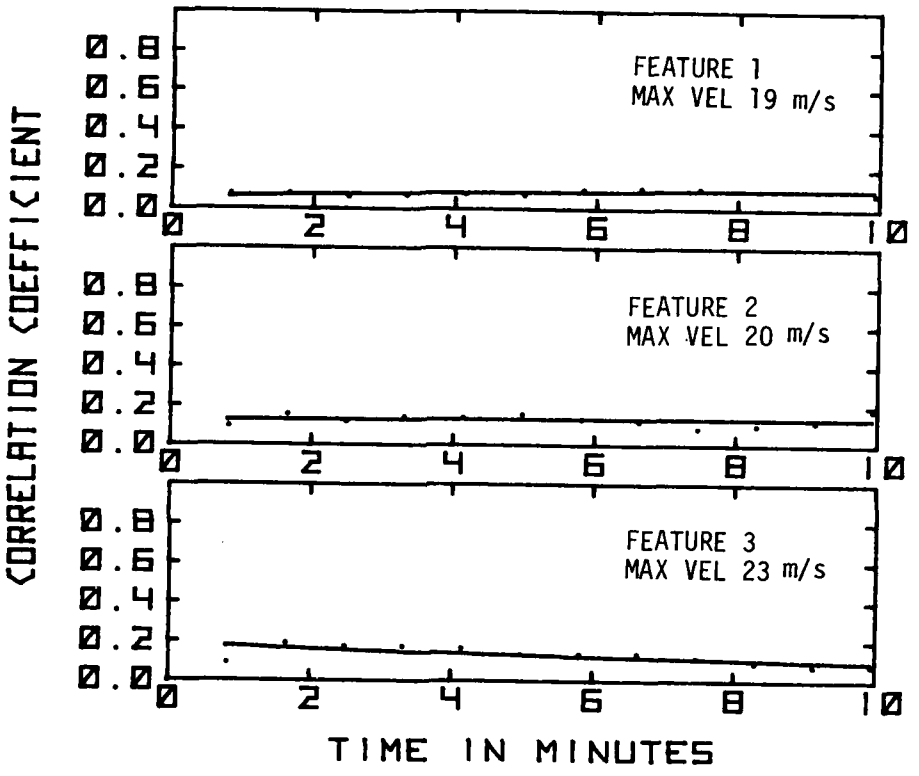

Figure 17(a)(v) Velocity correlation evolution of three large features (9 km x 25°) in April 3, 1981 storm at 0.4° elevation.

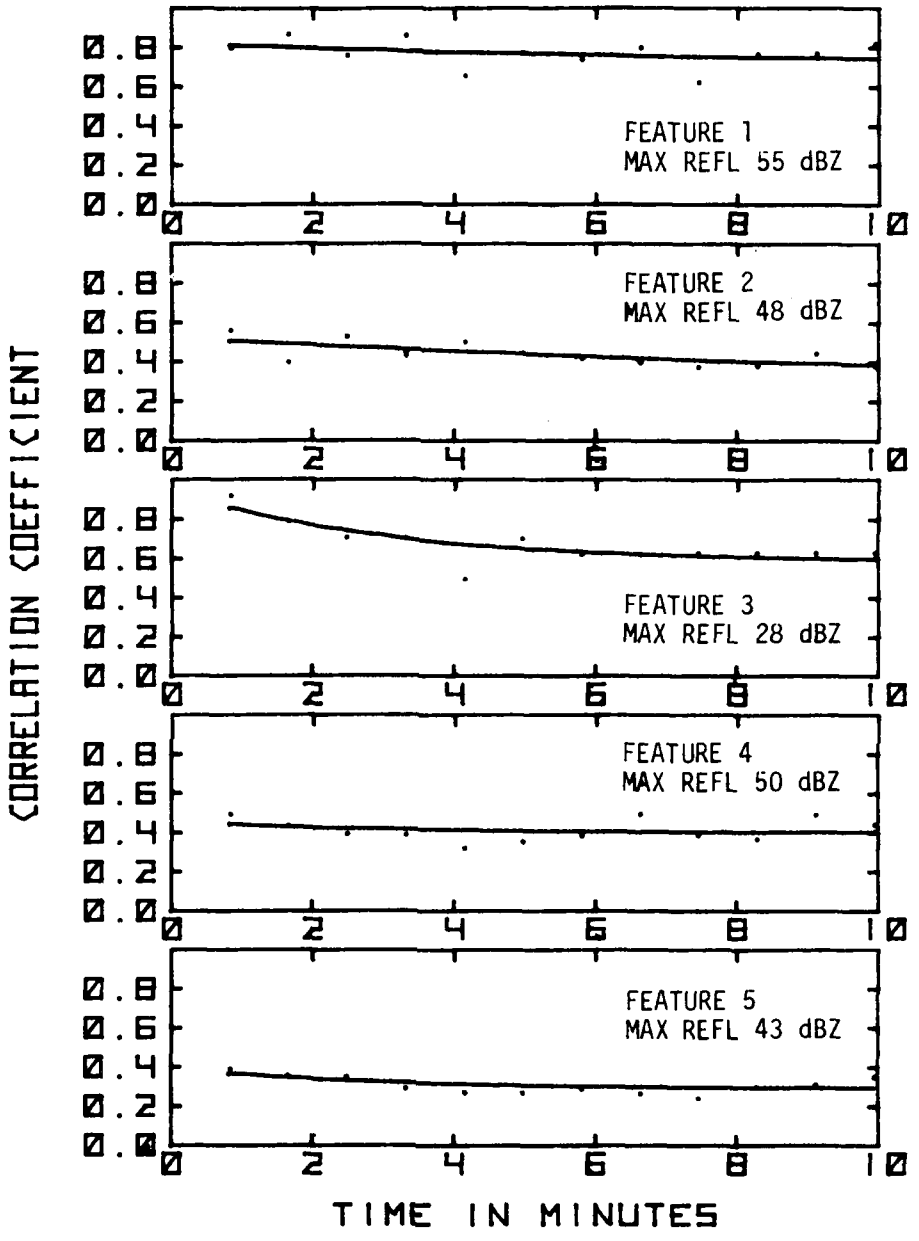

Figure 17(b)(i) Reflectivity correlation evolution of April 3, 1981 storm at 4.0° elevation.

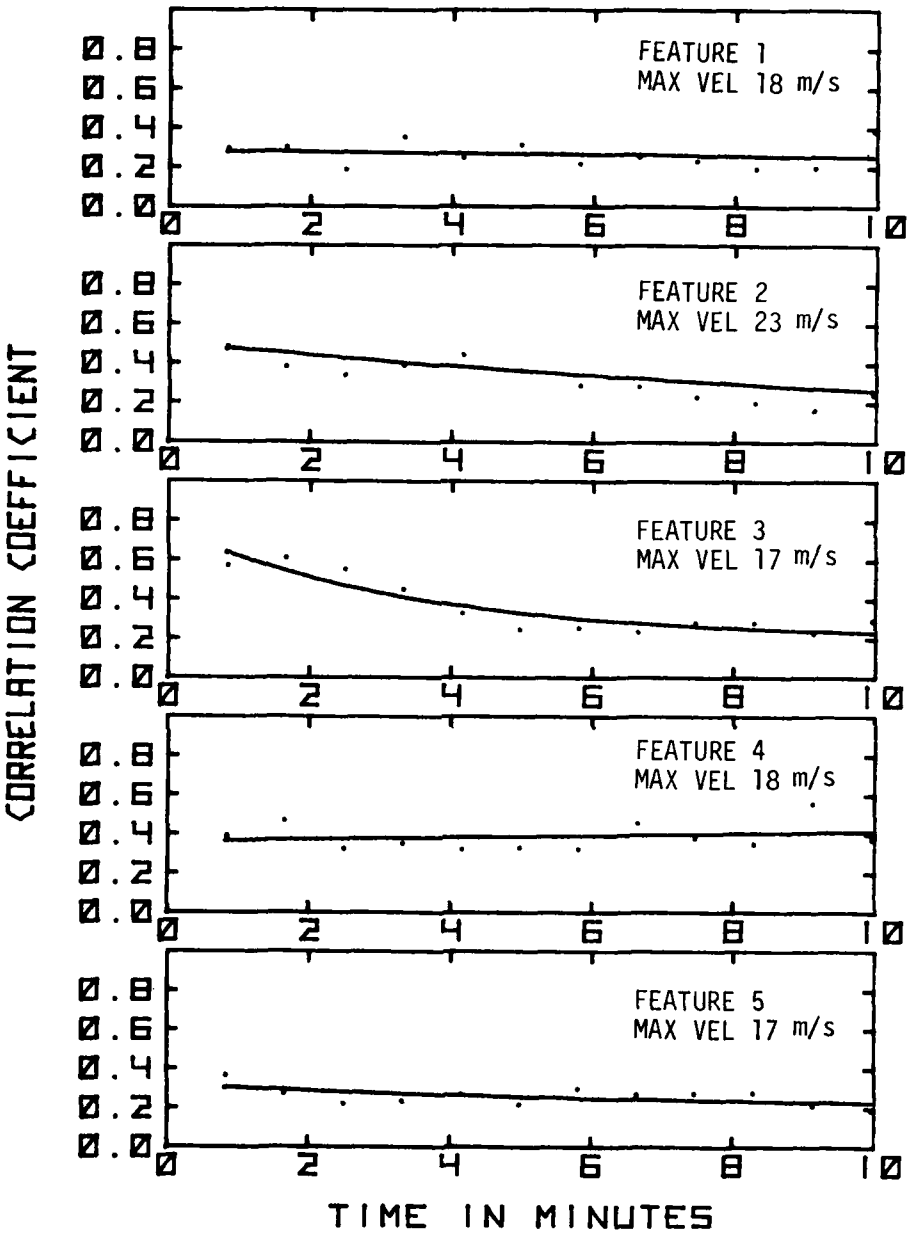

Figure 17(b)(ii) Velocity correlation evolution of April 3, 1981 storm at 4.0° elevation.

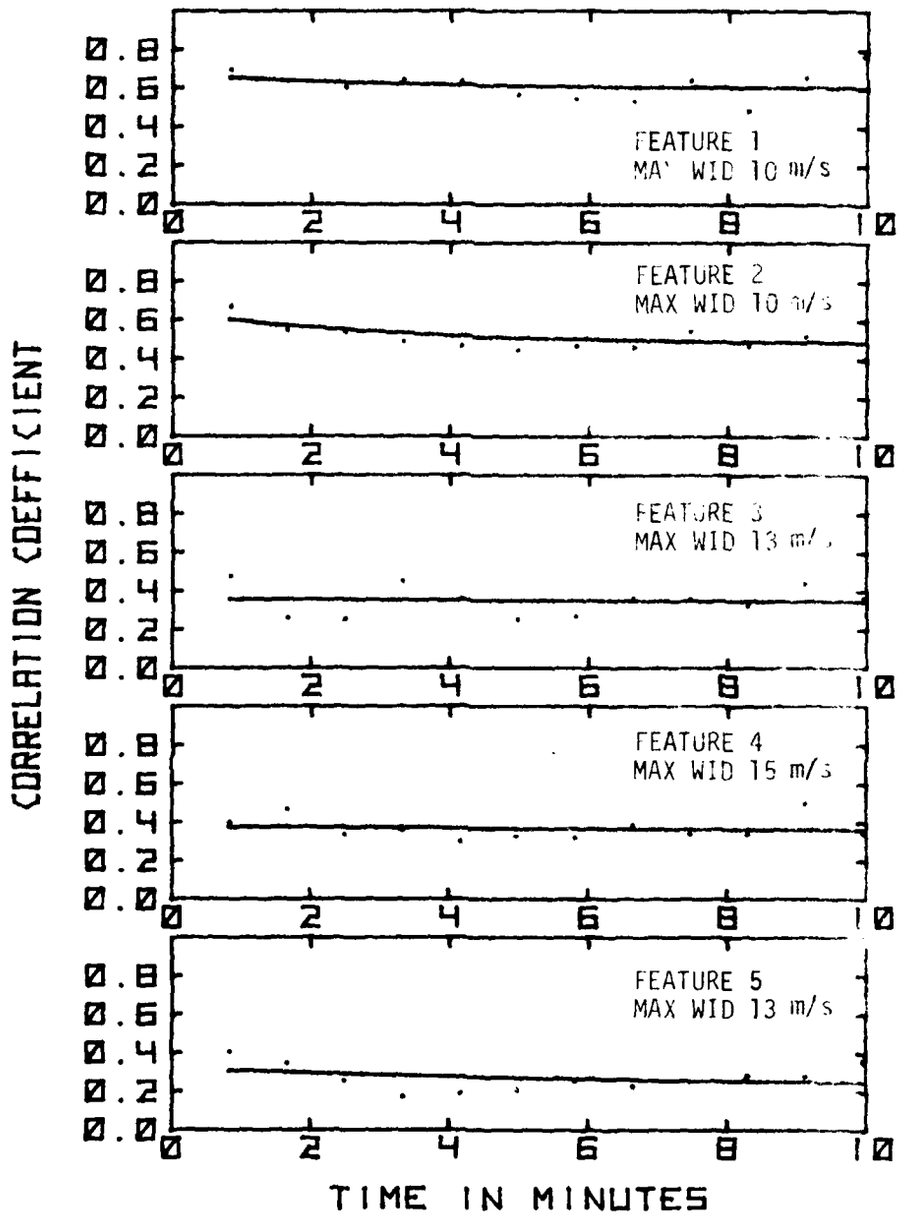

Figure 17(b)(iii) Spectrum width correlation evolution of April 8, 1981 at 4.0° elevation.

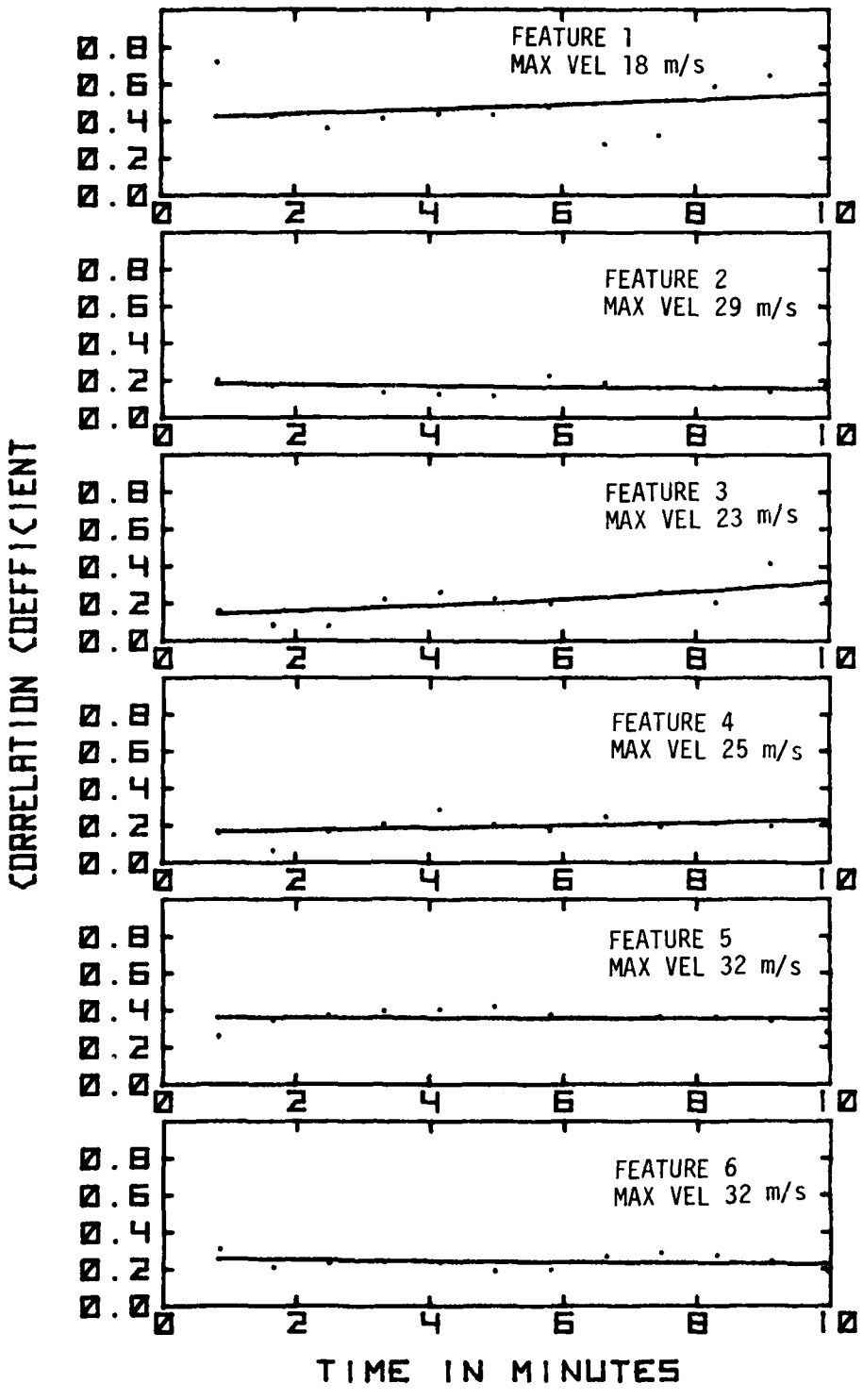

Figure 17(b)(iv) *Velocity correlation evolution of six extra features in April 3, 1981 storm at 4.0° elevation.*

Storm data from 1980 and 1981 Spring Programs have been used in this study and a scan interval less than 2.5 minutes has been used for each storm.

The clear observation from both the photo-interpretive and correlation studies is that among the storms studied, there is no significant or potentially hazardous change in any feature that could be detected by a 2.5-minute cycle, but would be missed by a 5-minute cycle. There are isolated scan levels and moment fields in which certain features appear to grow or decay within time scales faster than 5 minutes. However, if observations from several scan levels and all the three moment fields (reflectivity, radial velocity, and Doppler spectrum width) are properly combined, then this study provides overwhelming evidence that a simple, monotonic 5-minute scan should be adequate for NEXRAD air weather surveillance application.

5.2 Limitations of the Study and Suggestions for Further Work

To conclude beyond all reasonable doubt that ultrafast convective phenomena are so rare as not to affect NEXRAD scan strategy, one would have to study a large number of storms over an extended period of time. This report is based on data from five storms taken during two spring seasons, those of 1980 and 1981. While the assumption is that these storms are quite representative, there is always a finite probability that the set is atypical. Thus, further data collection, processing and interpretation to corroborate the findings in this report are in order.

Most of the data used in this study were collected during the period when the storm had already stabilized. This has been due to the very nature of the data collection process; since it is too expensive to operate the radar all the time, data are obtained only during storm periods, and in the absence of accurate forecasting for small-scale phenomena, the radar is usually switched on only when the existence of a storm system has been already reported. Alternatively, a system may form outside the radar range and when it moves into the range, the storm cells are usually well-formed. Thus, the explosive growth and, less importantly, the rapid decay periods of the storms have not been considered. This is a limitation of this study. Very sharp rainfall rate gradients have been predicted by certain models [23] but do not appear to have been substantiated by observations.

However, there is reason to believe that the conclusions of this report would not be changed very much if and when data on the explosive growth periods are included in the study. Experience has shown that large jumps in reflectivity

usually occur over pre-existing cells of detectable strength. Furthermore, if such growth of precipitation is to occur, it must be preceded by vigorous dynamical processes in the cells which should be detectable in the velocity and/or Doppler spectrum width fields, if not the reflectivity field.

A disadvantage of the computer-based correlation method employed in this report is its limitation in tracking small parts of fields that have large, nearly uniform parameter values. A relatively straightforward way of softening this drawback, without involving the use of alternative or additional attributes, is to perform some from of filtering/smoothing operation on the data field before subjecting it to correlation. Such filtering must be selective so as to reduce the very high frequency components of the field and thereby minimize the spike of the autocorrelation at the origin without affecting the gradients of larger scale. Certain filtering schemes have been used before in studying lifetimes [15], but specific algorithms that are effective and efficient for the current application will constitute a worthwhile extension.

Another simplification implicitly assumed in the correlation procedure used in this report is that features undergo only translational motion. Other systematic motions such as rotation, shear, etc., have not been taken into account. However, their inclusion in the algorithm would not alter the final conclusion since the lifetime estimate using translation only is conservative. This is because at present the unaccounted for rigid body motions aid the decay of the correlation coefficient caused by internal changes within the feature. Thus isolating these rigid body displacements would reduce the decay rate and hence increase the computed lifetime of storm features.

References

[1] Annual Review of Aircraft Accident Data: U.S. Air Carrier Operations (1976). NTSB Report No. NTSB-ARC-78-1.

[2] Annual Review of Aircraft Accident Data: U.S. Air Carrier Operations (1977). NTSB Report No. NTSB-ARC-78-2.

[3] Annual Review of Aircraft Accident Data: U.S. Air Carrier Operations (1978). NTSB Report No. NTSB-ARC-80-1.

[4] Briefs of Fatal Accidents Involving Weather as a Cause/Factor, U.S. General Aviation (1976). NTSB Report No. NTSB-AMM-78-5.

[5] Briefs of Fatal Accidents Involving Weather as a Cause/Factor, U.S. General Aviation (1977). NTSB Report No. NTSB-AMM-78-16.

[6] Briefs of Fatal Accidents Involving Weather as a Cause/Factor, U.S. General Aviation (1978). NTSB Report No. NTSB-AMM-80-5.

[7] W. Frost and D.W. Camp, "Summary of aviation weather research and development needs identified through the annual workshops on meteorological and environmental inputs to aviation systems". Obtainable from D.W. Camp, Space Science Lab., NASA Marshall Space Flight Center, AL 35812.

[8] R.J. Doviak, D.S. Zrnic' and D.S. Sirmans, "Doppler weather radar", Proc. IEEE, vol. 67, No. 11, pp 1522-1553, Nov. 1979.

[9] D.S. Zrnic', "Estimation of spectral moments for weather echoes", IEEE Trans. Electron., vol. GE-17, No. 4, pp. 113-128, October, 1979.

[10] D.S. Zrnic' and R. J. Doviak, "Effective antenna patterns of scanning radars", IEEE Trans. Aerosp. Electron, Syst., vol. AES-12, pp 551-555, September, 1976.

[11] H.L. Groginsky and K. Glover, "Weather radar canceller design", Preprints, 19th Conf. on Radar Meteorology, Amer. Meteorol. Soc., Boston, Mass., pp. 192-201, Apr., 1980.

[12] D.S. Zrnic' and S. Hamidi, "Considerations for the design of ground clutter cancelers for weather radar", U.S. Dept. of Transportation, Report No. DOT/FAA/RD-81/72, February 1981.

[13] R. H. Blackmer, Jr., "The lifetime of small precipitation echoes". Material prepared in connection with M.I.T.'s weather radar research, a project sponsored by Signal Corps Engineering Laboratories under Contract No. DA-36-039-SC 64472.

[14] R.E. Rinehart, "Internal storm motions from a single non-Doppler weather radar", National Center for Atmospheric Research, Boulder, Colorado, Technical Note NCAR/TN-146+STR, October, 1979.

[15] J.W. Wilson, "Movement and predictability of radar echoes", National Severe Storms Laboratory Tech. Memo. IERTM-NSSL-28, November, 1966.

[16] E. Kessler, III and J.A. Russo, Jr., "Statistical properties of weather radar echoes", Proceedings of the Tenth Weather Radar Conference, Washington, D.C., April 22-25, 1963, pp 25-33.

[17] G.A. Smythe, "Correlation of Doppler radar velocities and reflectivities with application to retrieving the transverse wind, M.S. Dissertation, University of Oklahoma, 1981.

[18] 1980 Spring Program Summary, NOAA Technical Memo ERL NSSL-91, R.J. Doviak, Editor., April, 1981, 128 p.

[19] D.S. Zrnic' and P.R. Mahapatra, "Lifetimes of atmospheric features hazardous to aircraft navigation: A study conducted to determine scanning strategies for air traffic radars", Interim report submitted to FAA, April, 1981.

[20] Next Generation Weather Radar System (NEXRAD) Request for Proposal SA-82-TPB-0010, U.S. Dept. of Commerce, NOAA, National Weather Service, August, 1981.

[21] J.H. Renick, "Radar reflectivity profiles of individual cells in a persistent multicellular Alberta hailstorm", Seventh conf. on Severe Local Storms, American Meteorological Society, 1971.

[22] L. Stevenson, P. Bloor and P. Remfer, "Impact of NEXRAD user requirements - Summary", DOT-TSC-VV-81-1.

[23] M.K. Yau, "A two-cylinder model of cumulus cells and its application in computing cumulus transports", Journal of the Atmospheric Sciences, vol. 37, pp 2470-2485, November, 1980.